Lawrence Berkeley National Laboratory
Recent Work

Title
CONTROLLED THERMONUCLEAR RESEARCH SEMIANNUAL REPORT. January through June 1963

Permalink
https://escholarship.org/uc/item/72m3j57x

Author
Lawrence Berkeley National Laboratory

Publication Date
1963-07-01

eScholarship.org Powered by the California Digital Library
University of California

UCRL-10852

University of California

Ernest O. Lawrence Radiation Laboratory

CONTROLLED THERMONUCLEAR RESEARCH SEMIANNUAL REPORT

January through June 1963

BERKELEY AND LIVERMORE, CALIFORNIA

TWO-WEEK LOAN COPY

This is a Library Circulating Copy which may be borrowed for two weeks. For a personal retention copy, call Tech. Info. Division, Ext. 5545

DISCLAIMER

This document was prepared as an account of work sponsored by the United States Government. While this document is believed to contain correct information, neither the United States Government nor any agency thereof, nor the Regents of the University of California, nor any of their employees, makes any warranty, express or implied, or assumes any legal responsibility for the accuracy, completeness, or usefulness of any information, apparatus, product, or process disclosed, or represents that its use would not infringe privately owned rights. Reference herein to any specific commercial product, process, or service by its trade name, trademark, manufacturer, or otherwise, does not necessarily constitute or imply its endorsement, recommendation, or favoring by the United States Government or any agency thereof, or the Regents of the University of California. The views and opinions of authors expressed herein do not necessarily state or reflect those of the United States Government or any agency thereof or the Regents of the University of California.

UCRL-10852

University of California

Ernest O. Lawrence Radiation Laboratory

CONTROLLED THERMONUCLEAR RESEARCH SEMIANNUAL REPORT

January through June 1963

BERKELEY AND LIVERMORE, CALIFORNIA

TWO-WEEK LOAN COPY

This is a Library Circulating Copy which may be borrowed for two weeks. For a personal retention copy, call Tech. Info. Division, Ext. 5545

Research and Development

UCRL-10852
UC-20 Controlled Thermonuclear Processes
TID-4500 (19th Ed.)

UNIVERSITY OF CALIFORNIA

Lawrence Radiation Laboratory
Berkeley, California

Contract No. W-7405-eng-48

CONTROLLED THERMONUCLEAR RESEARCH SEMIANNUAL REPORT

January through June 1963

July 22, 1963

Printed in USA. Price $2.75. Available from the
Office of Technical Services
U. S. Department of Commerce
Washington 25, D.C.

CONTROLLED THERMONUCLEAR RESEARCH SEMIANNUAL REPORT

January through June 1963

Contents

---

* Preceding semiannual reports: UCRL-10607, UCRL-10294

CONTROLLED THERMONUCLEAR RESEARCH SEMIANNUAL REPORT

January through June 1963

Lawrence Radiation Laboratory
University of California
Berkeley and Livermore, California

July 22, 1963

INTRODUCTION

C. M. Van Atta

Some of the more significant results and conclusions of the past six months in controlled thermonuclear research are briefly described below. The continued success of the finite-Larmor-orbit and finite-conductivity theories of plasma behavior in providing explanations of experimental results and guidance for new plasma experiments is most encouraging.

Considerable progress has been made toward completion of new experimental facilities and in modifying existing facilities to meet the need for the attainment of higher plasma temperature and longer confinement time.

Toy Top

In the multiple-compression experiments it was reported previously that neutron production is observed for about 250 microseconds, with the maximum occurring a few microseconds before the maximum in the magnetic field and the rate falling off with a 1/e time constant of 50 to 70 μsec. From observation of the signals on arrays of probes detecting charged particles escaping axially beyond the magnetic mirror and energetic neutral particles ejected radially in the median plane of the final compression stage, it is concluded that the decay of the plasma is predominantly caused by charge exchange on contaminants and not by instabilities. This is a most encouraging result.

Neutral yield curves have been completed for the compression cycle on the assumption of the presence of background neutron gas at various pressures. The results are in good agreement with the experimental yield curve and indicate that the residual gas molecular density is in the range of about 2 to 5×10^{11} cm^{-3}.

A vigorous effort is now under way to determine the sources of contaminants and to reduce or delay their effects on the plasma. Operations are soon to be shifted to the larger 2X facility, in which the better vacuum design and greater aperture are expected to contribute to a reduction and delay of the contaminants.

Alice

Plasma oscillation of frequency close to the ion precessional frequency had previously been reported in the Alice energetic neutral atom injection facility with beam intensity up to about 60 mA, residual gas pressure of about 10^{-8} torr, and density of energetic (20-keV) captured ions of about 10^{8} cm^{-3}. These oscillations are believed to be of the stable type predicted by the finite-orbit theory. When the particle beam is turned off two modes of plasma decay are observed, one in which the frequency of the oscillations decreases as the plasma density decreases, and the other in which the frequency remains constant as the plasma decays. These two modes are now believed to correspond to two branches of the curve for stable oscillations predicted by the theory.

Analysis of the buildup and decay of the Alice plasma leads to the conclusion that not more than 20% of the beam particles captured as ions are ionized by collisions with residual gas molecules, the remaining 80% or more being ionized from highly excited states by the Lorentz $\overline{v} \times \overline{B}$ force.

Since the residual gas pressure of 10^{-8} torr is still about ten times as high as would permit exponential buildup of the plasma to much higher density, the Alice facility is now undergoing major changes which should reduce the base pressure to 10^{-9} torr. If this is indeed the case, the density of captured energetic ions should then increase to 10^{9} ions/cm^{3} or more, at which--according to the finite-orbit theory--the plasma density should be above the predicted range of flute instability and into the upper stable regime.

Table Top

In the slow magnetic compression experiments in the Table Top machine the field configuration has been changed from the simple mirror field, with field intensity maximum at the ends and minimum at the median plane, to one in which there is a secondary maximum in the median plane. The ratio of the magnetic field strength at the central plane to that at the field minimum was about 1.26 at the axis and 1.06 at the chamber wall. At low plasma density the rotational instabilities in the two lobes of the field were found to be entirely uncorrelated. However, as the density was increased approaching the stable regime, the incidence of correlated behavior (indicating a degree of coupling across the central mirror) was observed to occur in an increasing proportion of the observed events.

Astron

The Astron electron accelerator has continued in operation with increased pulsed beam current of about 120 amperes at 4.1 MeV. The self-consistent solution for the E layer previously reported has been modified to allow not only the current density, but also the axial derivative of the density, to go to zero at the end of the E layer. This modification is also consistent with programming the currents in the field coils in such a way that the field due to the E layer is entirely contained within the present array of field coils as the E layer is built up, so that no additional end coils are required. All the necessary power supplies for energizing the field coils are scheduled for delivery within the next few weeks, and construction is proceeding so that injection of electrons in experiments directed toward the buildup of the E layer are expected to begin some time during the coming fall.

Levitron

In the operation of the Levitron the development of a low-amplitude instability mode, beginning about 200 μsec after the start of the cycle, was previously reported. Some characteristics of this instability have since been determined by carrying out correlation probe measurements along and across the helical magnetic field lines. The observations reveal a high correlation along the field lines, with correlations in radial direction as well. The wave frequency is low compared with that of Alfvén waves, and the wavelength rather short. These observations help to define the character of the instability but as yet do not permit a specific classification.

Bumpy Torus

The injection section of the Bumpy Torus has been set up with a 150-keV electron gun. The performance of the split-magnet section in guiding the injected electrons into the interior of the torus, where they spill out in both directions of the toroidal field from the split magnet, has been observed and is found to be substantially as predicted.

Homopolar V

The stilbene crystal and pulse-discriminator circuit for observing fast neutrons (> 1 MeV) in the presence of x rays has been completed and used to determine the time history of neutrons from the Homopolar V device. During the first few microseconds after application of the voltage there is a large burst of neutrons due to bombardment of the central electrode, which is normally at negative potential. This initial burst saturates the electronics of the discriminator circuit so that observations cannot be made during the first few microseconds of the discharge. However, after recovery of the detector circuit, neutrons are observed for at least 150 μsec after initiation of the discharge, indicating that energetic deuterons are confined for at least that length of time.

The Homopolar Gun

This is a single-ended rotating-plasma device in which the plasma is produced in the tapered field region near a magnetic mirror and is eventually to be ejected into a region of lower magnetic field along the field lines. This device has been operated initially with a second mirror to stop and confine the plasma. After some modification necessitated by some unexpected features of behavior, the device has been performing qualitatively as intended. A version of the homopolar gun is being made for use on the Alice machine to provide an initial pulse of dense plasma of high purity to be injected into the Alice machine from one end as a target for ionizing the atoms of the energetic neutral beam.

Sheet Pinch

In a tubular sheet pinch device (Triax) designed specifically to permit end-on viewing of the plasma cylinder, the development of the tearing mode of instability predicted by the finite-conductivity theory has been demonstrated. End-on photographs taken with a Kerr-cell framing camera show the bunching of the plasma cylinder into a multiplicity of strands initially parallel with the axis of the tube and then later twisted into a spiral form. A detailed experimental study of the tearing mode of instability can now be carried out and the results compared with theoretical predictions.

I. PYROTRON (MAGNETIC MIRROR PROGRAM)

1. INTRODUCTION AND SUMMARY

Richard F. Post

During the period covered by this report additional experimental and theoretical insight was gained concerning the plasma confined in the Alice experiment, and a significant conclusion was reached, regarding charge-exchange losses in the multistage experiment. Some informative experiments with modified mirror fields were performed in the Table Top facility, and a further extension of the finite-orbit theory was made and employed in the interpretation of the Alice results.

In the multistage experiment exhaustive measurements were made of the radial dependence of the time-resolved flux of ions escaping axially from the compressed plasma column. The results of these measurements confirmed the previously reported elimination of gross transverse plasma drift, but also provided important quantitative data on the rate of any type of plasma transport across the field. It was shown that any fine-scale transport that may occur is too slow to account for the limited neutron-emission time. However, on the basis of these and other measurements it was further shown that the previously unexplained decrease in neutron emission is entirely explainable in terms of charge-exchange losses as a result of evolution of neutral gas by bombardment of the chamber walls. The loss process is apparently maintained by a cascade involving the charge-exchanged particles themselves. Since the particle-surface interaction studies by Hunt in the Alice program have shown ways to avoid such cascades, there is reason to believe that charge-exchange losses in the multistage experiment can in the near future be eliminated as an important loss mechanism. Some other aspects of the probe measurements in the multistage experiment may also be very important in understanding mirror confinement: Although the present plasma configuration, together with the use of insulating chamber walls, does not permit finite-orbit stabilization effects to be effective on the $m = 1$ (transverse drift) mode, higher modes should be stabilized. Indeed it is found that modes of orders less than 4 do not develop appreciably during the time of observation, even though the theoretical growth rate of such modes is expected to be shorter than the confinement time. However, there is evidence that high-order fluting may develop in the low-density region at the plasma boundary. This apparently does not lead to appreciable transport across the field, but nevertheless is apparently followed by loss of these particles out of the end of the machine. It is tempting to ascribe these particular losses to velocity-space instabilities occurring in the rarefied (and anisotropic) outer regions of the plasma, but there is as yet little direct experimental evidence to support this interpretation.

In the Alice experiment additional data were obtained on plasma losses and the previously reported low-frequency plasma oscillations. There seems to be little reason to doubt that the observed oscillations result from finite-orbit effects in the plasma. The general variations of frequency with density, together with the observation of a "critical" density regime where instability-induced plasma losses occur, seem to agree with the theory.

Furthermore, conditions have been found under which density "jumps" occur and under which at the same time the enhanced plasma losses are substantially reduced or perhaps even completely eliminated. Even these effects seem understandable in terms of finite-orbit effects. In sum, the continued evidence for agreement between the experiments and the theory suggests that the theory may point out the way to steer through the "instability maze" during the buildup phase of the Alice plasma so that substantially higher densities can be reached. The technological developments required for this--namely, improved ion beam collimation and vacuum pumping--have now been largely achieved through the recent changes in the Alice facility, and we look forward to the coming experiments with uncommon interest.

Significant experiments which give an insight into the anatomy of interchange instabilities were performed in the Table Top facility. By improving the vacuum pumping conditions in the central chamber and by operating in the "hot ion" mode it was possible to show that the presence or absence of a "background" plasma has a pronounced influence on the stability of the compressed column against the $m = 1$ mode. This result is not in disagreement with theory, which shows that the boundary conditions immediately surrounding the plasma are very important in determining its stability for $m = 1$, although relatively unimportant for higher modes. In this connection, the improved vacuum conditions permitted the following significant observation: Under the best vacuum conditions, an $m = 1$ instability can be initiated, leading to a rapid spiraling motion of the plasma column out to the vicinity of the wall. At this point the plasma column takes up the regular rotation previously reported. However, under the improved vacuum conditions the charge-exchange lifetime of the ions becomes very long (probably approaching 1 second). This has permitted the observation of an unusual circumstance: the plasma column is seen to rotate for as long as half a second, slowly abrading itself at the wall. The only possible interpretation of this behavior is that under these conditions, even though the column is in rapid gross rotation, the transport of plasma particles from the interior of the column out to its surface must proceed exceedingly slowly. This experimental observation may be related to finite-orbit effects, operating to stabilize the plasma against high-order instabilities. The sharp boundary of the plasma (observed) may also be a contributing factor to improve the effectiveness of the stabilization. In effect, the plasma acts as though endowed with a sort of "surface tension" so that it moves as a coherent whole, even in the nonlinear limit represented by the gross rotations that we observe.

In other experiments in Table Top a modified mirror field was used, where the central field was reshaped in order to make the field curvature convex toward the axis, thus moving the concave (destabilizing) regions out to the ends. Although it was now somewhat more difficult to trigger the rotating instability, interesting effects were observed. It was found that under "high-density" conditions the rotation was correlated over the entire length—indicating effective conduction along the field lines. At somewhat lower densities, however, rotating forms at the two ends were observed which were uncorrelated in rotation frequency, showing that the columns were effectively decoupled. Under these latter conditions coherence of the individual plasma columns was still observed, showing that end conduction cannot here play an important role in stabilizing modes higher than $m = 1$.

2. MULTISTAGE HIGH-COMPRESSION EXPERIMENTS

Frederic H. Coensgen, William F. Cummins, Robert E. Ellis, William E. Nexsen, Jr., and Arthur E. Sherman

A. Toy Top III S

Introduction

During this report period the reaction history has been the focal point of the investigations in Toy Top III S. As parametric variations of the operation have not produced dramatic or even consistently detectable changes in the reaction history, it has been necessary to improve existing measurements and to develop new ones. Notably, the signal-to-background ratio of the prompt-neutron detector has been improved, complex probe arrays have been developed and used to study the plasma flux escaping from the far mirror, and a neutral (fast atom) detector has been installed at the wall in the midplane of the containment region.

At present it appears that charge exchange is the principal process that limits the reaction rate and results in the rather short half-life of the hot deuterium plasma. Not only are the observations consistent with charge exchange, but also no other single process can account for so many of the observations, including the neutral signals. The existence of other processes is not ruled out; we argue only that they are not the dominant factor leading to the rapid dissipation of the hot deuterium plasma. The major considerations are discussed below.

Plasma Drift and Hydromagnetic Instabilities

We have previously reported the elimination of the transverse plasma drift in the Toy Top experiments.[1] The improved behavior was observed after the azimuthal symmetry of the field had been improved by an order of magnitude and the radius of curvature of the magnetic field lines has been increased by a factor of 5 or more. However, as finite ion orbit effects are not predicted to stabilize the $m = 1$ mode, the improvement is attributed solely to the improved symmetry. Some indication of the precision necessary in magnet construction can be gained by reviewing the results of the rather extensive measurements of the fields produced by the three magnet systems that have been used. In the first system, in which the plasma drift was consistently toward the low field region, the asymmetry at all longitudinal positions was 2 to 5% across a 22-cm diameter. At the position of maximum distortion, the largest magnetic contour lying within the vacuum chamber had a mean diameter of 8.5 cm. Randomly directed drifts were observed in a second system (the 6-inch system), in which the wide magnet conductors were replaced

---

1. Frederic H. Coensgen, William F. Cummins, William E. Nexsen, Jr., Arthur E. Sherman, and Robert E. Ellis, in Controlled Thermonuclear Research Semiannual Report, UCRL-10607, January 16, 1963.

by five eight-turn magnets constructed of 5/8-in. conductor. The radial asymmetries in this set were less than 0.5% except for axial positions near the leads, where they were as large as 2% in a 15-cm diameter. The largest closed magnetic contour lying within the vacuum system was 3.5 cm in diameter. In the present 9-inch system the radial asymmetries are everywhere less than 0.5% for a 22-cm diameter, the contours are circular within 3 mm at a radius of 11.4 cm, and the magnetic axis does not deviate more than 2 mm from the mechanical axis.

As the plasma is apparently lost in 250 to 300 μsec, the absence of plasma at the wall indicates only that the transverse plasma drift is less than 3×10^4 cm/sec. Two probe arrays have been used to study the plasma flux that escapes from the far mirror, in an effort to detect slower drifts and to study transverse diffusion. The first array contained 21 probes across a diameter and could be rotated to any azimuthal position. The second array consisted of probes on 0.5-in. centers arranged in five columns of six probes each. This 30-channel probe array could be rotated about the magnetic axis when the system was under vacuum. Its radial position could be changed only by remounting the array. The spatial and temporal dependence of the escaping plasma was far more complex than expected. However, on the basis of these probe studies we make the following tentative conclusions.

(a) The upper limit of coherent transverse drift velocity (m = 1 flute instability) is 10^4 cm/sec.
(b) Low-order flute modes m = 2, 3, and 4 do not develop appreciably during compression.
(c) Flute-like disturbances at the plasma boundary with wavelengths of the order of 2 in. corresponding to $m \approx 10$ are found under conditions where m = 4 and higher orders should be strongly suppressed by the finite ion orbit effects.[2] The experimental evidence is unsufficient to identify this observed signal with a plasma flute, but it is certain that some plasma does diffuse across the boundary and is subsequently lost from the end of the mirror system.
(d) The transverse diffusion is insufficient to account for the observed decay of the reaction rate.

It should be noted that during the first 60 to 80 μsec the contained plasma is in contact with a plasma stream from the injectors, and at all times there is an observed plasma flux out of the end of the containment region.

Velocity-Space Instabilities

One of the notable features of the prompt-neutron signal is the break in the rise of the counting rate. The break occurs between 60 and 70 μsec, which is considerably earlier than the peak of the compression at 105 μsec (times measured from start of compression field). The break is suggestive of a loss mechanism such as a velocity-space instability that has a sudden onset. However, the invariance of the reaction history for different magnetic compression ratios indicates that if velocity-space instabilities are the

---

2. M. N. Rosenbluth, N. A. Krall, and N. Rostoker, Nuclear Fusion, 1962 Supplement, Part 1, p. 143.

primary cause of the reaction rate decay then they do not have a sudden onset at some point in the compression cycle but rather must be present from the beginning of the cycle. Theoretically this is inconsistent with the Harris instability.[3]

Ion-Ion Scattering

Ion-ion scattering of the trapped D^+ is easily ruled out as the principal loss mechanism. First, the decay rate is faster than would be expected; second, it does not change as the density of the trapped plasma is changed; and third, the orienting effect of the compression field still exceeds the randomizing effect of the collisions at the time the reaction rate is rapidly decreasing. The last two arguments also apply to scattering of the D^+ ions by impurity ions, although the evidence is not as conclusive.

The density of the trapped plasma and of the impurity ions can be varied by a factor of 3 by changing the injector potential and by a factor of 2 by changing the injector position. In the latter case the distance between the injectors and the containment chamber was increased by 10 feet, which essentially doubled that distance. The time dependence, with the long injection chamber, of any interaction of the trapped plasma and the late plasma stream should be different from that observed with the short injection chamber. As the reaction history is not sensitive to these changes we believe that neither slow impurities nor late plasma from the injectors can be a major factor in the decay of the reaction rate.

Energy Transfer to Electrons

The energy transfer rate to the electrons becomes appreciable only if the electron temperature remains of the order of 10 eV. In previous experiments the electron temperature was found to be of the order of 100 eV at the end of the compression, and ion energy was found to increase nearly as predicted. Furthermore, energy transport should show an unobserved density dependence. For these reasons, energy loss to the electrons, though probably occurring, does not appear to be the major factor contributing to the decay of the reaction rate.

Charge Exchange

On first considerations this process is as easy to rule out as ion-ion scattering. The mean life against charge exchange with the background gas is of the order of 1 msec. If charge exchange with neutrals from the source were the dominant effect there should be a marked difference in the reaction history between the short and long injection chambers. The differences would arise from the fact that the ions are collimated by the magnetic guide field while the neutrals are unaffected by it. Thus the ratio of ion density to neutral density would be significantly changed.

---

3. W. E. Drummond, M. N. Rosenbluth, and M. L. Johnson, Bull. Am. Phys. Soc. II 6, 185 (1961).

However, there are two positive pieces of evidence that charge exchange occurs to some extent. First, neutrals are detected at the walls, and second, the ion probes beyond the far mirror detect a slow ion signal which is present only if a trapped plasma is present. A third consideration is that all the features of the reaction history are consistent with charge exchange, provided a mechanism for injection of large quantities of neutrals is operative independent of the injector potential and position. The evolution of gas from the vacuum chamber walls, first by ion bombardment and subsequently by neutral bombardment, appears to be just such a mechanism. Only a fraction of a monolayer is required to account for the observed effects. Indeed, the principal features of the dependence of the reaction history upon the rise time and magnitude of the compression field are consistent with a simple model in which the neutral density is quickly increased to 2 to 7×10^{-5} Torr and remains constant throughout the cycle. By further extension of the model at least a qualitative agreement can be obtained between the observed time dependence of the neutral signal for various conditions and that predicted on the basis of charge exchange. The late increase in the neutral signal appears to be due to that fraction of the slow ions which are trapped long enough in the rising compression field to gain sufficient energy so as to be detected when they later escape by charge exchange. Thus the late rise in the neutral signal appears earlier as the magnitude of the compression field is raised or as the rise time is decreased.

Evolution of gas from the walls near the transition between the 18-in. and 9-in. sections is given further support from the observation of intense plasma bombardment of this section during the injection phase of the cycle. We have attempted to reduce this bombardment by tapering the long injection guide field so that the field lines always curve away from the plasma. Baffles were also introduced so that the limiting aperture was moved further from the compression chamber. Although the wall bombardment was reduced it was far from eliminated. From the observed shift in the time of the maximum reaction rate the neutral density was not changed by more than a factor of two.

B. 2X Construction

The remaining expenditures necessary for initial operation of the 2X facility constitute about 10% of the total cost. Labor costs comprise most of the remaining expense, as only miscellaneous small parts and a small amount of cable are needed.

On the basis of the present rate of progress we expect to begin pulsed operation in October.

The detailed report of the construction is covered in the electrical and mechanical engineering sections of this report.

C. Future Program

Toy Top III S

The energy analyzer is being installed on the system to determine for the current conditions the ion energy distribution after compression. Upon completion of the energy determinations the facility will continue to be used to develop new diagnostic methods. A plasma camera, a low-energy ion analyzer, and a movable neutral detector are now under development. Additional probe instrumentation for further studying the transverse plasma diffusion is nearly completed.

Initial 2X Operation

Final design of the pulsed magnet field was delayed until we had a better understanding of the decay of the hot deuterium plasma in Toy Top III S. As discussed in Section A above, it appears that charge exchange is presently the limiting factor, therefore the diameter of the 2X compression chamber will be 18 in. This size is set by the maximum diameter of non-conducting vacuum chamber available. The large-diameter chamber is chosen to accommodate various pumping devices, which should prevent an increase in the neutral density at the time of injection. The approximate specifications of 2X are as follows: i. d. = 18 in., distance between mirrors = 10 ft, injection field = 500 to 1000 gauss, mirror ratio ≈ 1.5. In order to evaluate the effect of the increased size and the new trapping conditions, the initial operation of 2X will duplicate as closely as possible the present III S operation. Improved wall conditions, improved injection, etc., will be introduced later.

Many of the measurements that have not been made on the Toy Top plasma are being studied and instrumented for 2X. Among these are determination of electron temperature, and measurements by means of neutral atomic beam probes and laser beam probes.

3. TABLE TOP III

Stability Studies with Improved Vacuum Conditions and with a Modified Magnetic Mirror Field

Walton A. Perkins and William L. Barr

To improve the pumping speed and reduce the number of secondary neutral atoms produced by hot neutrals striking the wall in the containment region, a stainless steel liner that could be cooled with liquid nitrogen (LN) was placed inside the central chamber. This allowed LN cooling and molybdenum gettering of the inner wall over the entire 15-ft length of the machine.

Most of the experiments were performed under hot ion injection conditions.[1] An electron multiplier (in the midplane, radially 2.5 ft from axis)

---

1. W. A. Perkins and R. F. Post, Observation of Plasma Instability with Rotational Effects in a Mirror Machine (UCRL-7302, March 1963), Phys. Fluids (to be published).

was used as a neutral-particle detector. The main signal detected by the electron multiplier was proved not to be due to ultraviolet light. This was shown by comparing the time variation of its signal with that of a light detector (photomultiplier) and by putting a 10-mil LiF cover in front of the electron multiplier to exclude particles. With this cover, only the "source spike" signal persisted. Electron multiplier signals and capacity probe signals are shown in Fig. I-1 for three conditions. The source is fired 0.2 msec after initiation of the scope trace, and a source spike is seen on the electron multiplier signal at this time. In the top set of traces taken at high base pressure (10^{-7} torr) the plasma is quiescent and no rotational fine structure is seen on either the signals of the capacity probe or those of the electron multiplier. The middle and bottom sets of traces were taken under the better vacuum conditions outlined above (base pressure $\approx 10^{-9}$ torr). In the middle and bottom sets, the capacity probe and neutral-particle detector both indicate the off-axis rotation of the column. As determined by the capacity probe, the column is positively charged in the middle set and negatively charged in the bottom set of Fig. I-1. Because of collimation, the electron multiplier can detect only neutrals formed near the horizontal plane that passes through the axis. In most cases of a "hot ion" plasma (positively charged column), the electron multiplier detects the plasma twice per revolution as the column passes through the plane of the detector. In some cases of a positively charged column and in all cases of negatively charged column the electron multiplier's fine structure peaks once per revolution. By careful studies of the time sequence of the signal of the electron multiplier relative to the signals of capacity probes, it was shown that this fine structure is caused by the hypercycloidal motion of the ions in the crossed electric and magnetic fields. The electron multiplier is energy-sensitive, so the peak signal occurs when the ion's velocity vector is pointing toward the detector near that time in its hypercycloidal motion when it has its peak energy. As the ion temperature decreases the particle motion changes from one that is nearly circular to a hypercycloid motion with fairly sharp cusps. Therefore, the two positions from which the high-energy neutrals are sent to the detector merge into one with decrease in ion energy.

With the better vacuum conditions in the central region, this instability (with the rotating column) would persist for hundreds of milliseconds as the column slowly abraded itself at the wall (see Fig. I. 2). The lower pictures show the fine structure on a fast sweep of the scope. The top dual beam trace gives an integrated signal whereas the bottom signal is differentiated (which occurs is established by setting the terminating RC of the capacity probes).

These signals show that the column of the left trace is positively charged whereas the column of the right trace is negatively charged.

For a given source voltage the plasma would pass from stable to occasionally unstable to very unstable as the vacuum was improved. At very high injected densities (three sources discharging at 6 to 8 kV) this effect was harder to show, but with a molybdenum-gettered central chamber, gas from the source burst could be pumped out in a few milliseconds and then the instability with the characteristic rotation would appear. This means that a high density of gas is necessary in the stabilizing mechanism[1] either

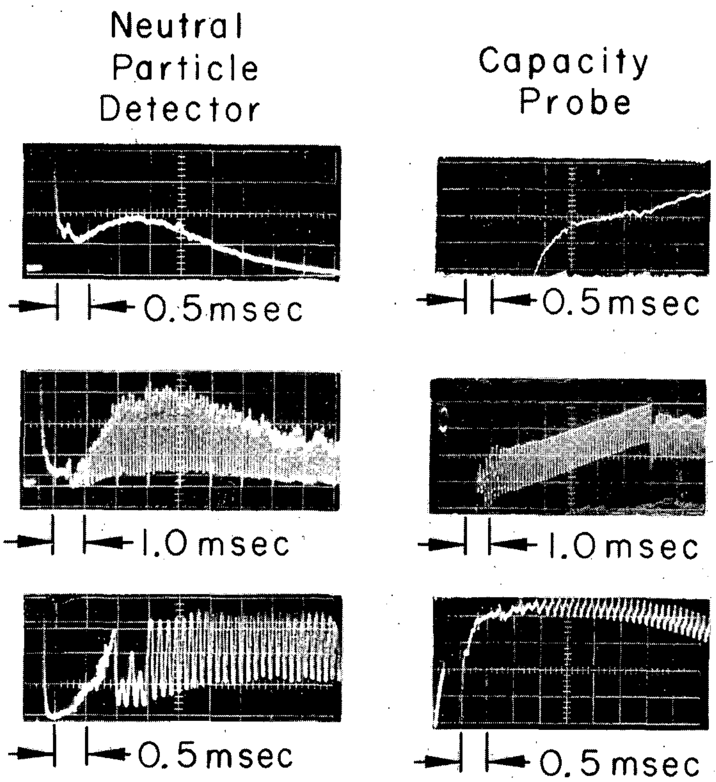

ZN-3904

Fig. I-1. Neutral-particle detector (electron multiplier) and capacity probe signals for "hot ion" injection conditions. Top set for quiescent plasma, middle and bottom sets for unstable cases with rotation of positively and negatively charged columns respectively. For this figure the polarity of all the signals is inverted.

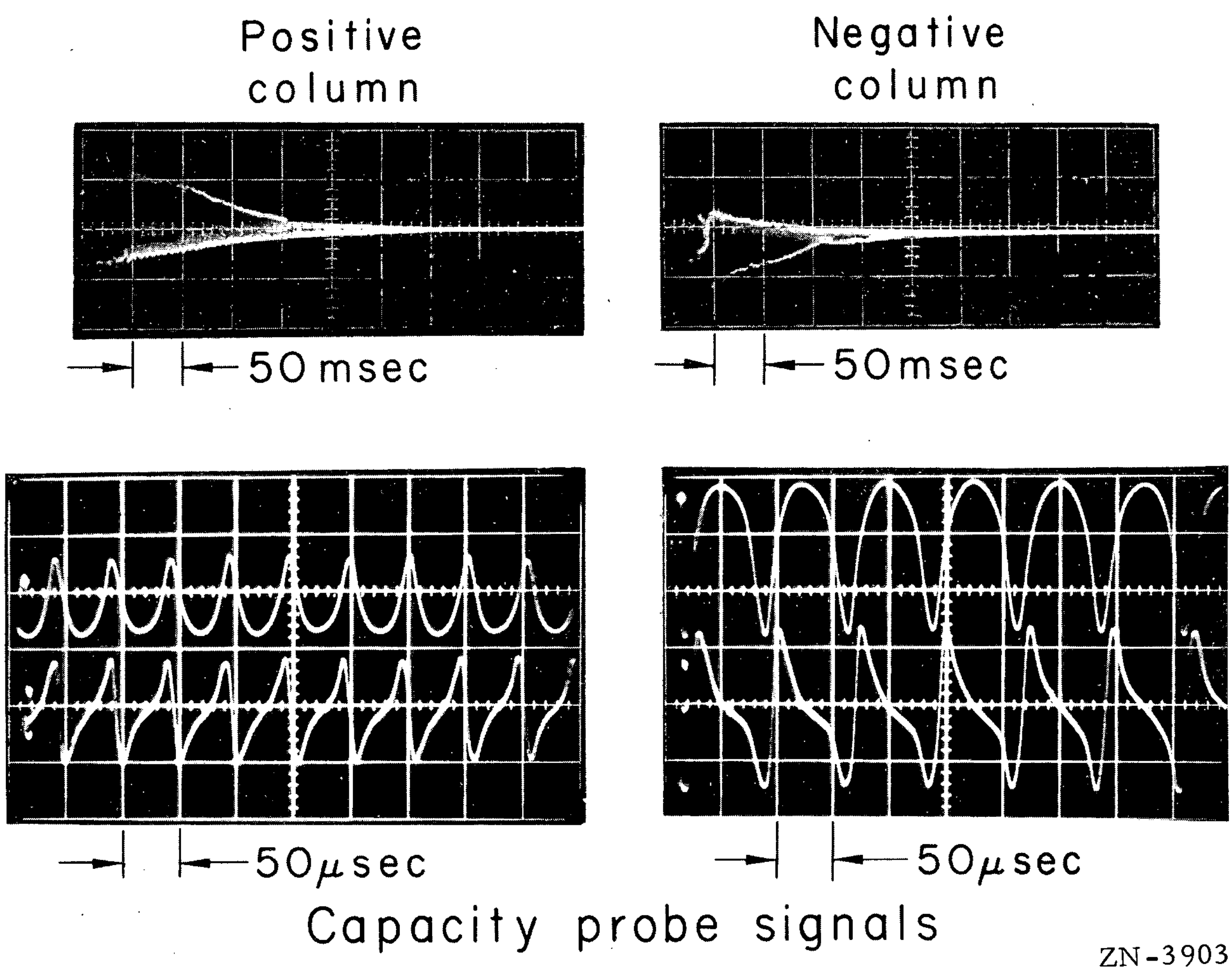

Fig. I-2. Capacity probe signals for long-lasting positively and negatively charged columns. The bottom traces show the fine structure on a fast sweep speed of the scope for two different probes. The RC time constants of the probes were set (relative to the rotation period) so that the signal of the upper trace would be integrated while the signal of the bottom trace would be differentiated.

(a) as a source of cold plasma or (b) as a scatterer which can neutralize or dissipate a flute.

In another experiment the magnetic field geometry was modified by adding a weak mirror in the midplane. The resulting field lines, as calculated by a 7090 computer code, are shown in Fig. I-3. The purpose of this experiment was twofold: (a) to obtain a direct experimental determination if the instability occurs because the plasma is contained by magnetic field lines that bend concavely toward the axis as predicted for the interchange instability, (b) to see if anything can be learned about the conduction of plasma along field lines, through a weak mirror.

Capacity probes and scintillation detectors were placed near the walls in the midplane and in each weak-field region about 11 cm east and west of the midplane (see Fig. I-3). Stainless steel cups were put around the capacity probes to ensure that they did not pick up a signal from an adjacent region.

Capacity probe signals are shown in Fig. I-4 for the three regions. In the top set the field geometry was the same as that of a simple mirror machine with no bump in the center. For this geometry the signals from the east, west, and central regions always correlated (i.e., the rotating column was straight and connected throughout the region). The middle and bottom sets were for the field geometry shown in Fig. I-3. In the middle set the rotations are correlated in the weak-field regions and center while for the bottom set the rotations are uncorrelated in the weak-field regions with no appreciable signal in the central (midplane) region. Relative to the east and west probe signals, the signal of the central capacity probe was always larger when the three signals correlated. This indicates that the column is connected through the midplane for these cases. At low injected density the signals in the two weak-field regions are never correlated. No signal was detected in the central region. At high injected density (as high as possible but still remaining in the unstable region) the signals would correlate part of the time (see Fig. I-4, middle set and Fig. I-5, right-hand set). Similar results were obtained with the scintillator probes as shown in Fig. I-5. For high injected density a light monitor in the midplane indicated a density of roughly 10^9 cm^{-3} near axis in the midplane.

Varying the position of one of the capacity probes showed that the peak instability signal occurred in the weak-field region. The results of these experiments with the magnetic field configuration of Fig. I-3 are consistent with the picture that instability is caused by the field lines' bending concavely toward the axis. At present we have drawn no definite conclusion concerning the effect of conduction along the field lines on the rotation of connected and separated columns.

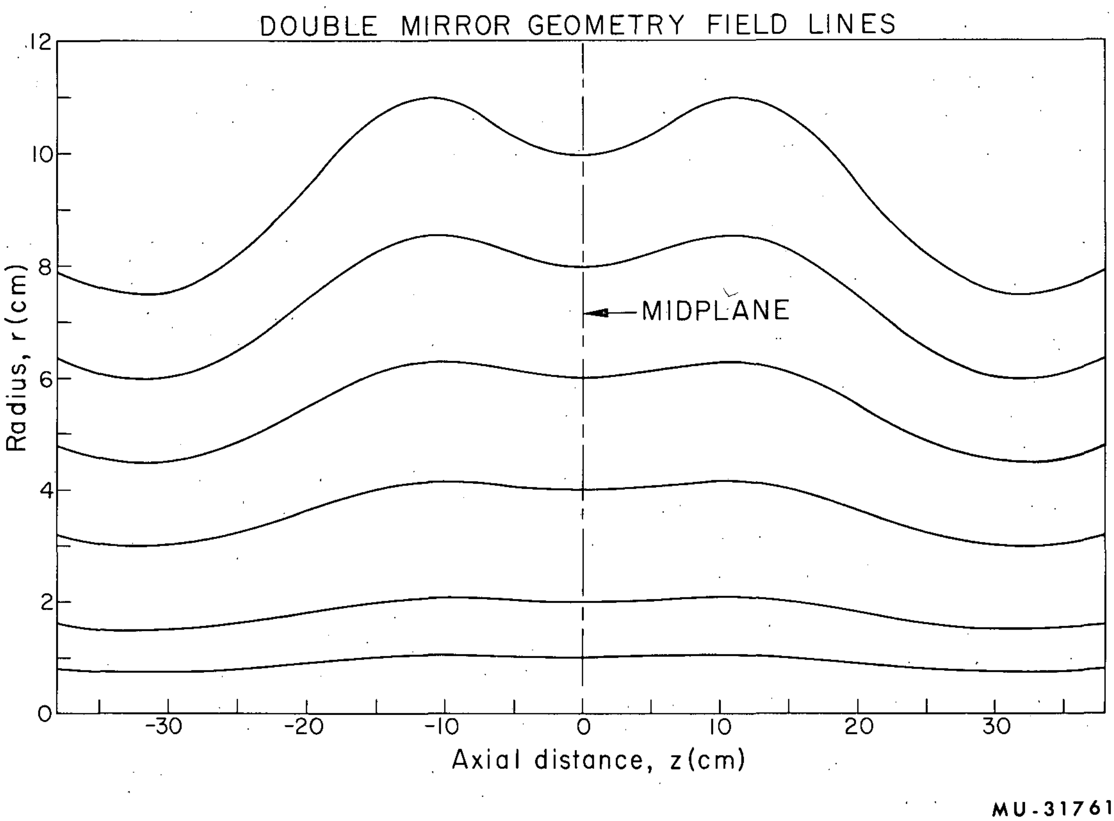

Fig. I-3. Calculated magnetic field lines for mirror machine with an extra small mirror in the midplane. The mirror ratio in the midplane was 1.06 on axis and increased to 1.25 near the walls of the chamber. The mirror ratio for the outside mirrors was 1.9 on axis and increased to 2.2 on the outermost flux lines.

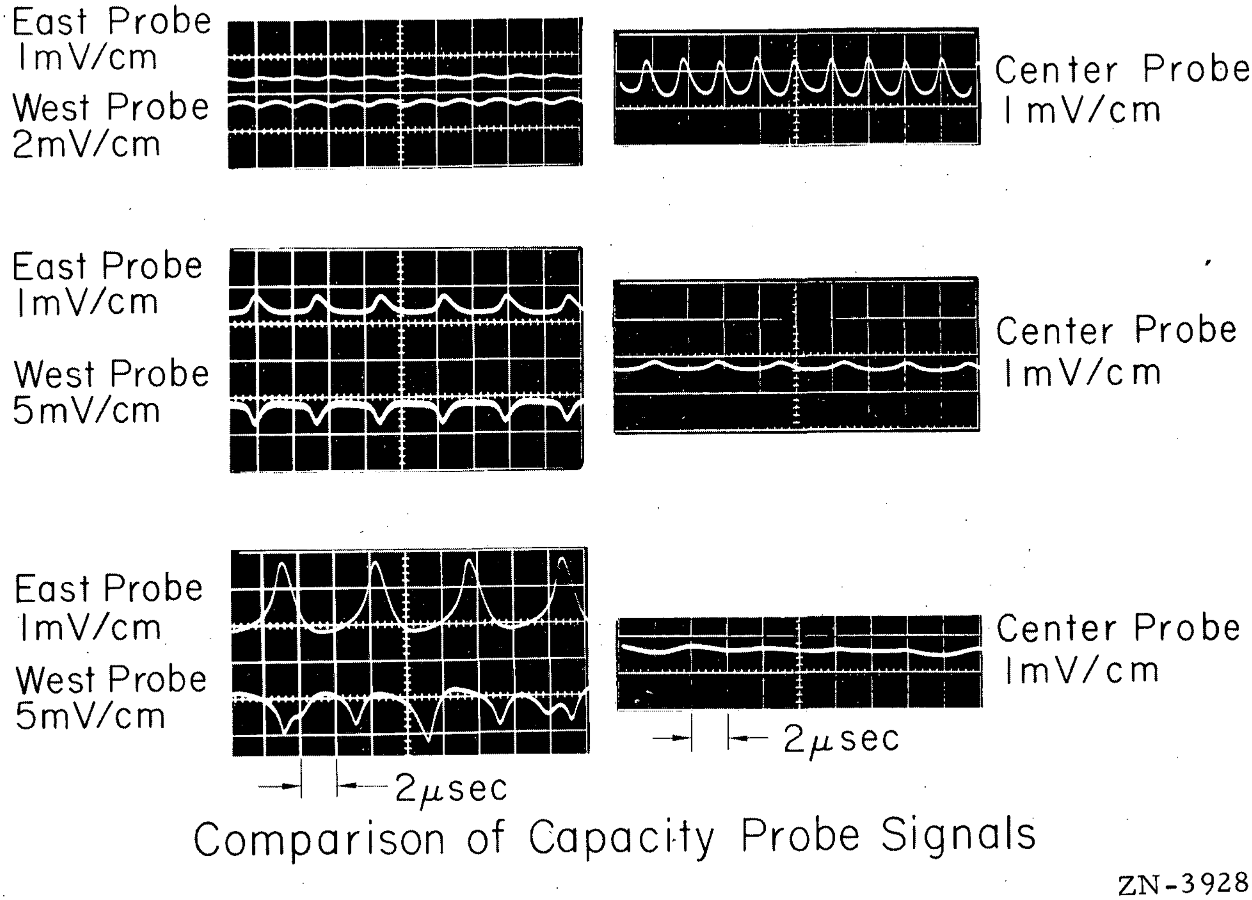

Fig. I-4. Capacity probe signal for a probe in the midplane and probes 11 cm east and west of the midplane. (East probe had 1/4 in. longer cap than west probe, thereby reducing its signal.) Top set is for ordinary mirror machine, middle and bottom sets for the field geometry of Fig. I-3. Polarity of east and center probe signals is inverted.

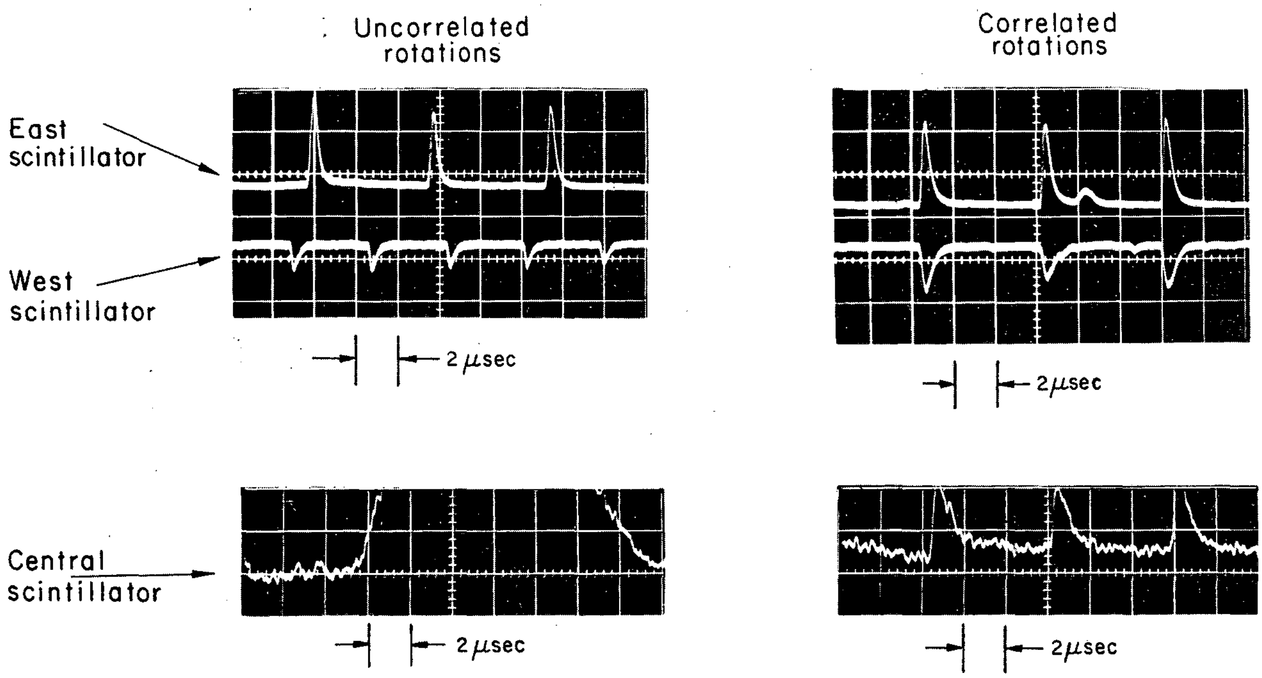

ZN-3927

Fig. I-5. Scintillation probe signals for a probe in the midplane and probes 11 cm east and west of midplane. Magnetic field geometry is that of Fig. I-3. Polarity of east and central scintillator probe signals is inverted.

4. ALICE (ENERGETIC NEUTRAL-ATOM INJECTION)

A. Alice Plasma Experiments

Charles C. Damm, James H. Foote, Archer H. Futch, Jr., Andrew L. Gardner, Frank J. Gordon, Angus L. Hunt, and James F. Steinhaus

Introduction

During the first part of this period the observations of plasma behavior in Alice were continued. The range of operating conditions was the same as described in the preceding semiannual report.[1] The major objective of the experiments during this periods of operation was the study of the low-frequency plasma oscillations. The additional results obtained strengthen the interpretation of these oscillations in terms of the finite-orbit stabilization theory as extended to the low-density regime by Post.[1] The results of these measurements and the interpretation have been published.[2]

Plasma Density

Unusual density variations have been observed which are also generally understandable in terms of the finite-orbit stabilization theory. An example is given in Fig. I-6, where it is seen that as the magnetic field reaches 25 kG the plasma density, as evidenced by the signal on a fast-atom detector, increases to a higher level. At the same time the ion current to the radial plasma limiter (which is an insulated plate at a radius of r = 12 cm) decreases. The magnitude of the decrease is of the right order to account for the particles which then contribute to the increased density and leave the plasma by charge-exchange scattering. In some cases, the density does not fluctuate as greatly at the higher level as in Fig. I-6. Often the density increases to the higher level and remains relatively constant for times like 1 second, until turnoff of the injected beam.

The variation of density with injected beam intensity is shown in Fig. I-7, again at 25 kG field. The density is seen to generally limit at about 4×10^{7} ions/cm^{3}, as in the example of Fig. I-6. The density increases are depicted by the dashed lines. The solid curve A is the expected density on the basis of the measured vacuum and Lorentz-force trapping. The vacuum is assumed to consist of a constant hydrogen equivalent pressure of 1.5×10^{-9} torr, together with an increase with beam of 1.3×10^{-10} torr/mA. The Lorentz trapping fraction is taken to be 3.7×10^{-5} on the basis of our measurements of excited-state populations, together with the known magnetic field gradients. For comparison, curve B is the average density expected from gas collisional ionization alone.

The observed density transitions can be tentatively described in terms of the finite-orbit theory. With respect only to the m=1 mode, the theory predicts

1. Charles C. Damm, James H. Foote, Archer H. Futch, Frank J. Gordon, Angus L. Hunt, and James F. Steinhaus, in Controlled Thermonuclear Research Semiannual Report, UCRL-10607, Jan. 1963, p. 15.

2. C. C. Damm, J. H. Foote, A. H. Futch, and R. F. Post, Phys. Rev. Letters 10, 323 (1963).

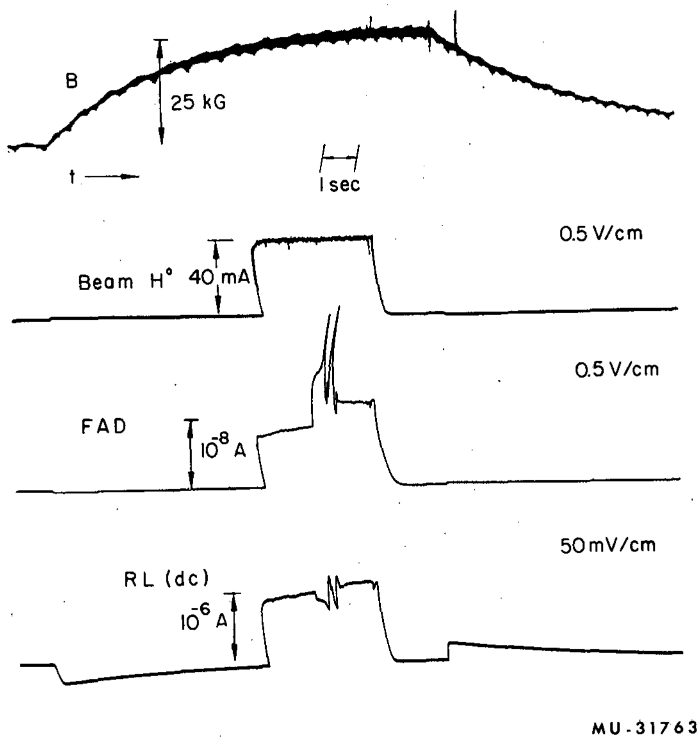

Fig. I-6. Density fluctuations in the Alice plasma. The fast-atom detector signal (FAD) is proportional to plasma density. The current to the radial plasma limiter (RL) varies with plasma density.

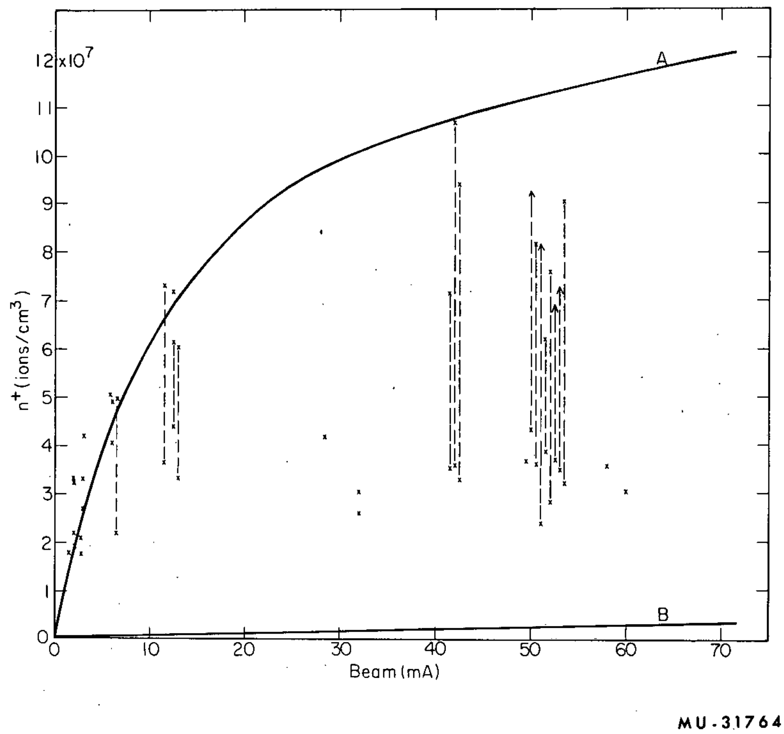

Fig. I-7. Variation of density with injected beam intensity. Curve A is the expected density based on Lorentz-force trapping; curve B is based on gas collisional ionization alone.

two stable density regions separated by an unstable gap (see Fig. 2 of reference 2). Our model of the behavior is that the density increases until it arrives at the edge of the unstable region. Radial particle losses then hold it there until, for some reason, the transition to the upper stable branch occurs. At the higher density the oscillation frequency is predicted to be of the order of 15% higher, and such an increase is observed. The reason for the density transition in our case may be related to the onset of very strong emission at the ion gyrofrequency coincident with the transition. However, cause and effect are by no means clear yet. Although the upper measured densities agree fairly well with the expected values, the uncertainties in both are about a factor of two. Therefore we cannot yet say that losses of this magnitude due to instabilities do not exist.

Radio-Frequency Activity

The signals at the ion gyrofrequency received on a single-turn loop antenna have now been detected by a broad-band receiver as well as by a frequency-spectrum analyzer. The emission is observed to vary from bursts of a few milliseconds' duration to continuous, and in general the continuous emission is more intense than the bursts. The rf activity varies with the magnetic field and with the plasma density. At fields below 12.5 kG, signals are always observed, becoming weaker and more intermittent in general as the density is decreased. Often but not always the rf bursts correlate with fluctuations in density. At 12.5 kG strong and continuous emission is observed, correlated with large density changes. Up to 15 kG intermittent activity is observed, again correlating sometimes with density changes. Between 15 and 25 kG a very quiet region exists with only a few occasional bursts. At 25 kG the large and continuous emission again appears, as mentioned, coincident with the large density changes. The presence of strong rf during periods of maximum density suggests that no large ion losses are associated with the activity. This is reinforced by the occasional observation of rf for times like 0.5 sec during the charge-exchange-dominated decay (after beam turnoff).

A new antenna capable of resolving field components of the rf emission is under construction. It is expected that this will elucidate the structure of the oscillations and shed some light on the cause.

Plasma Potential Measurements

The circuitry for the lithium ion beam source and detector has been modified so that the average plasma potential vs time can be displayed directly on an oscilloscope. The scope trace showing Li^+ accelerating voltage as a function of time is brightened for a short period as the transmitted ion current reaches half of full value. The accelerating voltage is saw-toothed at 1 kc/sec, so that the resolution time for the plasma potential is 1 msec. An example of the potential measurement correlating with other plasma properties is shown in Fig. I-8. Studies of these correlations were not completed because of failure of the Li^+ ion source. The defects have been remedied and measurements will continue in the next period of operation.

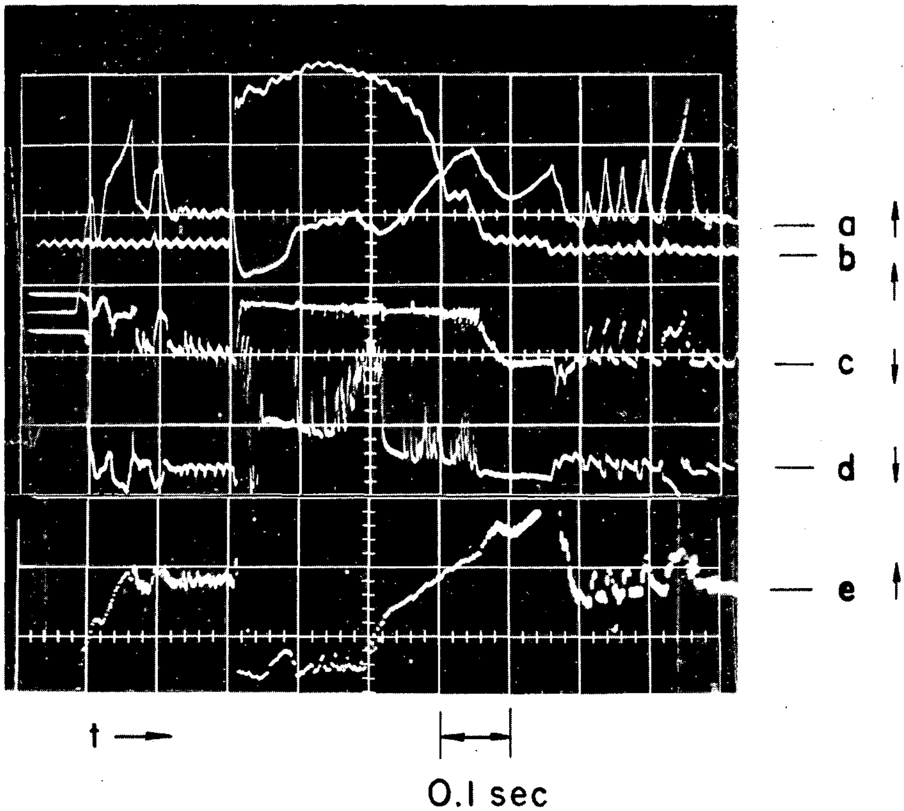

ZN-3926

Fig. I-8. Correlations of signals at B = 12.5 kG: (a) fast-atom detector, (b) radio-frequency signal, (c) amplitude of low-frequency oscillation (inverted), (d) frequency of low-frequency oscillations (inverted), (e) plasma potential.

Rebuilding of Alice

The changes and repairs to the Alice machine started late in February have been completed and operation is to be resumed soon. Adjustable beam collimators have been added to the injector line in order to control the edges of the beam and reduce the pressure rise in the trapping chamber during injection. A new getter pump has also been added to the injector line to help control gas flow. The water-vapor curtain to reduce molecular streaming from the neutralizer cell has been relocated, for greater effectiveness, more nearly midway between the neutralizer and trapping chamber. Based on the encouraging results of our surface bombardment studies, a titanium target has been installed in the beam termination pump in an effort to bury the beam directly. If the pressure in the burial chamber can be reduced, the beam tube can be enlarged and more beam can be transmitted from the source. All in all, these changes are expected to reduce the pressure in the trapping region, with the consequent possibility of reaching higher plasma densities.

B. Further Calculations on Finite-Orbit Effects

Richard F. Post

It has been found possible to extend the finite-orbit theory calculations to a limit beyond that covered in calculations already reported.[1] The extension permits consideration of unstable wavelengths that are comparable in size to the orbit radii. It is based on the observation that in a perturbation electric field that can be represented by plane waves of wave number k, the "effective" electric field giving the correct $\vec{E}\times\vec{B}$ drift velocity for a particle guiding center is simply

$$\vec{E}^1 = J_o(ka)\,\vec{E}, \tag{1}$$

where $\vec{E}$ is the field at the guiding center, J_o is the zero-order Bessel function of the first order, and a is the orbit radius. By use of this expansion, and a similar one involving the transformation of guiding center density to particle density, the following dispersion equation for the plasma frequency is found (in the plane case):

$$\omega^2\left\{J_o^2(k_xa) + b^2\right\} - \omega\omega_c\left\{\left(\frac{k_o}{k_x}\right)\left[1 - J_o^2(k_xa)\right] + \left(\frac{k_xg}{\omega_c^2}\right)\left[J_o^2(k_xa) + b^2\right] + gk_o = 0. \tag{2}$$

This equation reduces to that found by Rosenbluth et al.[2] for the case $b^2 \to 0$, $k_xa \ll 1$. Making the approximate conversion to the mirror machine case as discussed previously, one can obtain a "universal" frequency plot vs

1. Richard F. Post, in Controlled Thermonuclear Research Semiannual Report, UCRL-10607, Jan. 1963, p. 25.

2. M. N. Rosenbluth, N. A. Krall, and N. Rostoker, in Nuclear Fusion, 1963 Supplement, Part I, 143 (1961).

a plasma "density" parameter which reduces to the one previously given in the limit $k_x a << 1$. The allowed values of $k_x a$, consisting of a discrete spectrum, are of course to be determined by the periodic boundary conditions. This result (omitting the arguments in J_o) is

$$\frac{\omega\pm}{\omega_B} = \frac{1}{2}\left[1 + \tilde{x}\right]\left\{1 \pm \sqrt{1 - \frac{4}{[1 - J_o^2]} \frac{\tilde{x}}{(1 + \tilde{x})^2}}\right., \tag{3}$$

where ω_B is the precession frequency for the mode wavelength considered and the "density" parameter $\tilde{x}$ is defined through

$$\tilde{x} = \left\{\frac{2[1 - J_o^2]}{k_x^2 a^2}\right\} x$$

and

$$x = \frac{k_o P}{[J_o^2 + b^2]} .$$

Equation (3) is plotted in Fig. I-9 for various values of the parameter $[1 - J_o^2]$. It can be readily shown that the condition for stability is

$$\frac{x}{[1 + x]^2} < \frac{[1 - J_o^2]}{4}, \qquad \text{stable}, \tag{4}$$

from which follows

$$\tilde{x} < \frac{1 - |J_o|}{1 + J_o}, \qquad \text{stable},$$

or

$$\tilde{x} > \frac{1 + |J_o|}{1 - J_o}, \qquad \text{stable}.$$

The values of $k_x a$ for $J_o = 0$ are seen to be always stable. From these expressions stability criteria of the same form as the one given in the preceding semiannual report can be derived for the appropriate limits, $k_x a << 1$.

The maximum growth rate of instability in the unstable density gaps can be readily evaluated, and is given by

$$\frac{\nu_{max}}{\omega_B} = \frac{|J_o|}{1 - J_o^2} . \tag{5}$$

The dispersion equation (2) can be written in a form which is almost identical to one derived by Mikhailovsky,[3] differing only in terms that are unimportant in the cases presently considered ($b^2 > 1$). It is not understood why any difference should exist, but it can probably be traced to the very different methods of analysis used in the two cases. It should be noted that Eqs. (2) and (3) predict that, in addition to the m = 1 unstable gap apparently now observed, higher-order gaps should also appear as the density is increased. However, as the wavelength becomes comparable to the orbit radius, other effects--such as the steepness of the density gradient--will probably dominate, and likely invalidate any conclusions deduced from these equations. The analysis presented here has nevertheless proved its worth in interpreting the regime in which the Alice experiments are presently carried out.

3. A. B. Mikhailovsky, Zh. Eksperim. i. Teor. Fiz. 43, 509 (1962); Translation: Soviet Phys. JETP 16, 364 (1963).

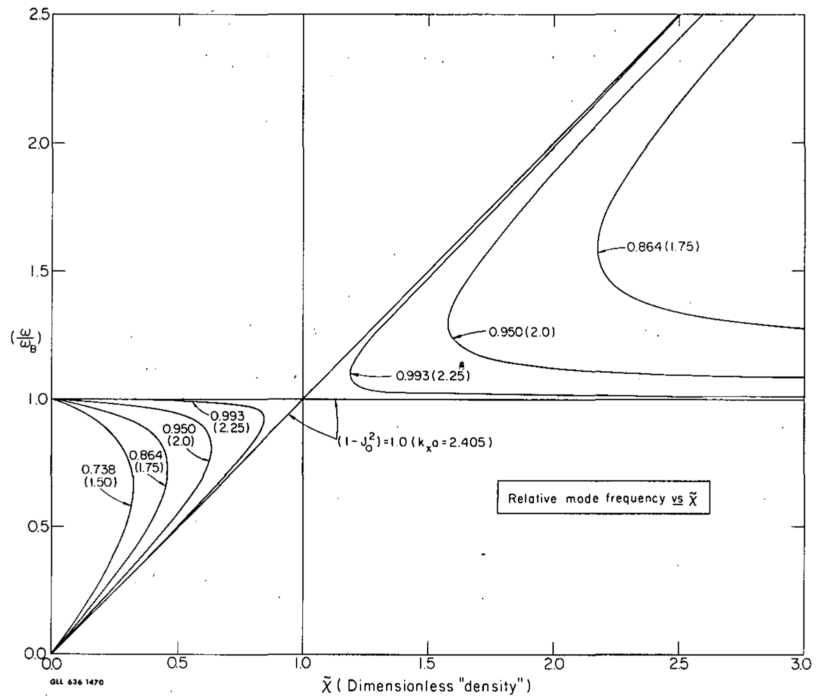

MU-31765

Fig. I-9. Relative mode frequency vs $\tilde{x}$.

C. Ion Source Development

Frank J. Gordon

One ion source during this period ran for more than 50 hours. At termination, output of atomic hydrogen to the trapping chamber was still more than 50 mA (power equivalent). Termination resulted from widening of the carbon exit slit caused by corrosive action of the hydrogen arc.

Development has begun of the 40-keV ion source mentioned in the preceding report. Thirteen runs have been made during which mechanical and electrical flaws have been corrected. To date 13 mA (power equivalent) has been collected on a 1.75-in.-diameter target 6 ft from the source.

D. Cold Plasma For Beam Trapping

James F. Steinhaus and Norman L. Oleson*

After development of a gating system for rapid turnoff of the Alice beam, the occluded-gas cold plasma source (P-3) was briefly tried in Alice during February. Because of termination of the operation of Alice only a few pulses were obtained. The results were (a) an apparent trapping of about 15% of the atom beam owing to the presence of cold plasma, although rapid charge-exchange losses resulted; (b) very large bursts of ultraviolet light from the cold plasma, which invalidated information on the fast-atom detector so that neither the hot plasma density nor the neutral particle density in the cold plasma could be measured; (c) low-frequency oscillations in Alice disappeared as a result of the firing of the gun; it remains to be seen if this was simply due to pressure bursts associated with the pulse.

The pulse line used in firing the cold plasma gun was modified to include two additional portable 200-μsec sections, making a pulse line capable of generating square-wave pulses up to 600 μsec long. Electron temperatures, pressure rises, and plasma densities were measured for the longer pulses. Initial electron temperatures were found to be about 3 eV in a new source washer, dropping sharply to about 0.6 eV in 200 μsec. A source with a somewhat depleted supply of H_2 in its washer (about 1000 shots) had an initial electron temperature about 5 time as high. The temperatures remained constant after 200 μsec. Microwave measurements indicate that maximum densities were not affected by the pulse length. To obtain a better idea of the number of neutral particles coming from the gun, the plasma column is being passed through diaphragm partitions in the vacuum chamber and the pressure rise measured on both sides.

---

* U. S. Naval Postgraduate School, Monterey, California.

A. L. Gardner made some preliminary measurements of the phase shift of a 25-Gc wave that is reflected from the plasma at well beyond cutoff density.[1] These measurements have verified that the cold plasma density does indeed maintain a reasonably constant value during the square pulse of current to the source, and they have given order-of-magnitude confirmation of the peak density estimate from cutoff measurements of about 2 to 3×10^{14} electrons/cm^3.

The triplex source is currently being tested. This is an assembly of three conventional occluded-gas Ti washer-type sources operating in parallel. The purpose of this particular arrangement is to provide a larger volume of cold plasma, 2.5 to 3 in. in diameter (instead of 0.75 to 1.0 in. for a single source). Preliminary measurements indicate the electron density is at least as large as that obtained by a single gun operating at 1/3 the arc current. It was interesting to note that the pressure remained at the same value in the triplex arrangement as for an individually fired source (with the same total arc current).

Because of the presence of neutrals and heavy ions, such as those of Ti, in the cold plasma source, injection around a "corner" through a baffled pipe containing a magnetic guide field is being considered. This scheme has been used with Ti washer sources by Eubank and Wilkerson at Princeton,[2] who found it possible under certain conditions of input density and bending of magnetic field to achieve a tenfold reduction in plasma contaminants of atomic mass > 3. A theoretical treatment of the plasma stability for such a plan, using finite-orbit criteria of Rosenbluth, Krall, and Rostoker,[3] has been considered by L. S. Hall at our Laboratory. The equipment is expected to be tested in the present P-3 facility.

William L. Barr, who assisted in taking spectroscopic data, is also collaborating with us in the analysis of various characteristics of the cold plasma gun obtained over the past several years. A report is in preparation.[4]

---

1. S. Takeda and M. Roux, J. Phys. Soc. Japan 16, 95 (1961).

2. H. P. Eubank and T. D. Wilkerson, Phys. Fluids 4, 1407 (1961); also private communication.

3. M. N. Rosenbluth, N. A. Krall, and N. Rostoker, Nuclear Fusion, 1962 Supplement, Part I, p. 143.

4. James F. Steinhaus, Norman L. Oleson, and William L. Barr, Investigation of a Plasma from an Occluded-Gas Cold Plasma Source, UCRL-7097, in preparation.

E. Alice Diagnostics

James H. Foote and Archer H. Futch, Jr.

Radial Profile Detector

During the next Alice running period, we hope to obtain useful data with a new diagnostic device called the radial profile detector. Its main purpose is to give information on the trapped ion density as a function of radius. This detector will collect the ions resulting from charge-exchange collisions of the trapped fast ions with the background gas. The slow ions produced by these collisions should be quickly scattered out the mirrors of the machine. The radial distribution of these escaping particles should therefore be a measure of the trapped-ion radial distribution.

Figure I-10 shows the main features of the radial profile detector. Seventeen detector plates are uniformly positioned along a radial line between $r = 0$ (z axis) and $r = 11$ cm. Each plate extends about 0.5 cm radially and is 1 cm^2 in area. This series of collector plates is placed just outside one mirror of the Alice machine. Through use of two sets of ring-shaped sliding vacuum seals with differential pumping between, the detectors can be rotated to any desired azimuthal position and can be retracted to a position 51.5 cm from the mirrors.

There are three high-transmission tungsten grids in front of the collector plates. The outer one is permanently grounded and the inner grid will be biased negative with respect to the plates so as to suppress secondary-electron emission from the plates. The multigrid method, we hope, will enable us to differentiate between the ions and electrons escaping from the plasma. An appropriate variable biasing arrangement may give information on the energy distribution of the escaping ions (and electrons) and thus possibly give additional information on the plasma potential.

We plan to display the signals from the 17 collector plates on an oscilloscope directly as a radial distribution. The low-magnitude currents collected by the plates will charge capacitors. A mechanical sampling switch[1] will sample all channels periodically. In this way, the magnitude, shape, and time variation of the ion-density radial profile can be examined.

CsI(Tl) Scintillation Counter

A CsI(Tl) scintillation counter for counting fast neutral atoms from charge-exchange reactions and other radiation from the Alice plasma has been installed at the midplane of the Alice machine. The scintillation counter, located approximately 7.5 feet from the axis, is connected to one of the radial ports by a liquid-nitrogen-cooled tube. Magnetic shielding of the photomultiplier tube has been provided. A transistorized preamplifier has been designed by the Electronic Counting Group. The scintillation counter with the transistorized preamplifier has been checked for resolution and low noise with the pulse-height analyzer.

1. The switch to be used is mSCAN High Speed Sampling Switch, produced by Fifth Dimension, Inc., Princeton, New Jersey.

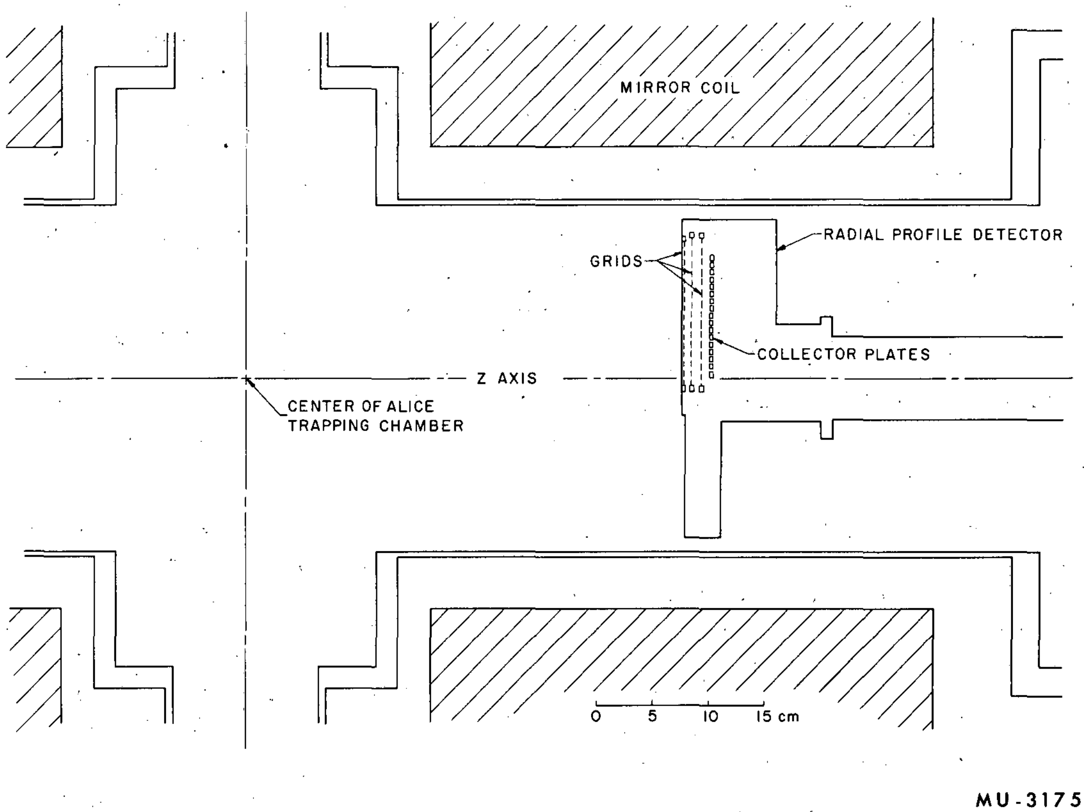

Fig. I-10. Schematic of Alice central region with radial profile detector in position.

A scintillation counter of this type will be a valuable addition to the diagnostic equipment for Alice. This counter would be useful for such measurements as the following.

1. As a fast atom detector it would have certain advantages over the present detector, which measures the secondary electrons emitted from a metal target by fast atoms. Calibrating errors would be eliminated, since individual fast atoms would be detected. Errors due to photoelectron emission would also be eliminated.

2. The sensitivity of the counter allows the beam of particles to be collimated so that all particles arrive from a small region of the plasma. Present design allows the plasma to be scanned radially from 0 to 5 cm.

3. It may be possible to determine the electron temperature from x rays emitted by the plasma. Provisions have been made for inserting foils of different materials and thickness. These foils would stop fast atoms and only partially absorb x rays. The temperature of the electrons would be determined from the absorption of the x rays.

4. A significant change in the energy of the trapped ions in the plasma would be detected by a change in the pulse-height spectrum of fast atoms resulting from charge exchange.

Semiconductor Detectors

Semiconductor detectors are being investigated for possible use as particle detectors for Alice and also for the Lorentz ionization experiment. Their small size and insensitivity to magnetic field make them particularly useful as detectors to determine the axial extent of the plasma in Alice. For this purpose a series of four surface barrier detectors will be located at the vacuum chamber walls, one at the midplane and the other three along a line parallel to the axis of the machine. These detectors will operate at approximately liquid nitrogen temperature. Automatic shielding of the sensitive gold surface will prevent this surface from being coated with molybdenum during evaporation of the getters. At present the energy resolution and noise characteristic of the detectors are being investigated as a function of temperature.

F. Lorentz Ionization Experiments

Archer H. Futch, Jr., and Charles C. Damm

In a previous progress report, tentative data were presented on the Lorentz ionization of hydrogen atoms produced by charge exchange on lithium vapor (UCRL-10607, p. 30). This preliminary result indicated a strong dependence on the vapor pressure in the neutralizer. For a constant ionizing field, the fraction ionized increased as the vapor pressure was varied from 1 to 10μ of Hg.

During the period covered by this report, the background gas pressure between the lithium neutralizer and the ionizing field has been reduced. Recent measurements still indicate a dependence on the lithium pressure in the region from 1 to approximately 10 μ. As the lithium pressure was increased above 10 μ, the fraction ionized was found to be essentially constant over the pressure range from 10 to 25 μ of Hg. The foregoing results suggest that at low vapor pressures the excited neutral atoms are produced by charge exchange both with lithium vapor and with the background gas. As the lithium vapor pressure is increased, the fraction of the excited neutrals produced by charge exchange on the background gas decreases, becoming negligible at 10 μ lithium pressure.

Figure I-11 shows results obtained recently with both a lithium neutralizer and a water vapor neutralizer. Curves a and b of Fig. I-11 show the fraction of excited neutral atoms in a 35-keV D^0 beam which is ionized by the electric field at distances of 217 cm and 100 cm, respectively, from the neutralizer. The neutral beam was produced by charge exchange on water vapor. A comparison of curves a and b shows a relatively small decay in the population of the excited atoms in traveling the additional distance of 117 cm to the ionizing field, indicating lifetimes of the order of microseconds. Mean radiative lifetimes for these excited levels are expected to be in this range.[1]

Curve d of Fig. I-11 shows the excited-state population that results when the hydrogen atoms are produced by charge exchange on lithium vapor. Comparing curve a with curve d indicates an increase in the excited-state populations by approximately a factor of 3 when lithium is used instead of water as the neutralizing vapor.

The dependence of the excited-state population on the velocity of the beam atoms has also been investigated. Measurements indicate less than 15% variation over a range of velocities corresponding to atomic hydrogen energies from 15 keV to 42 keV. The dependence on velocity is indicated in Fig. I-11 by comparing curves b and c.

Additional information on the experimental arrangement and recent results are given in a separate report.[2]

---

1. J. R. Hiskes, Nuclear Fusion **2**, 38 (1962).

2. Archer H. Futch and Charles C. Damm, Enhancement of the Excited-State Population in a Hydrogen Atom Beam, (UCRL-7344-T, May 3, 1963), Nuclear Fusion (to be published).

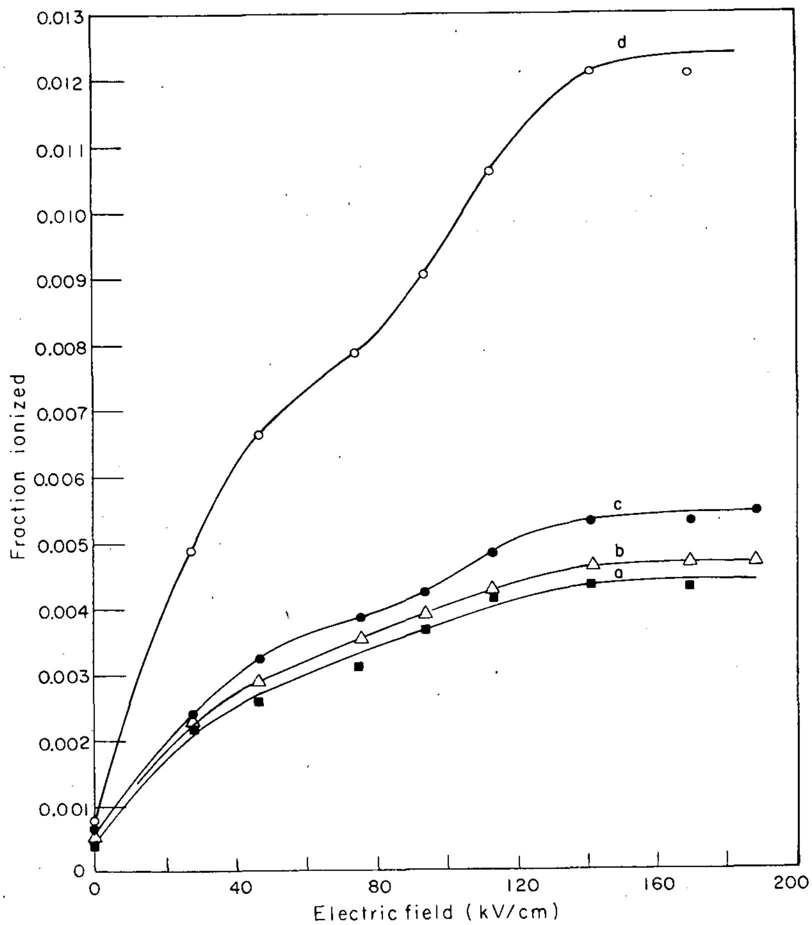

MU-31766

Fig. I-11. Fraction of neutral beam ionized versus the electric field. (a) 35-keV D^o, distance, L, between neutralizer and ionizing field is 217 cm, (b) 35-keV D^o, L = 100 cm, (c) 42-keV H^o, L = 100 cm. The neutral beams for curves a, b, and c were produced by charge exchange on water vapor. (d) 35-keV D^o, produced by charge exchange on lithium vapor, L = 217 cm.

G. Vacuum and Surface Studies

Angus L. Hunt and Charles C. Damm

Surface Bombardment Studies

The bombardment of representative wall materials with 15-keV deuterons has continued with the study of titanium and molybdenum targets in the apparatus described in previous reports. The comparative study of 5-mil-thick foils of titanium and molybdenum at temperatures from 150°K to 900°K has emphasized the importance of the solubility of the incident particle in the target or wall material as a function of temperature, and has supplemented our concept of the interaction mechanism of energetic charged or neutral atoms with metallic surfaces. Our previous results suggested that clean metallic surfaces below 110°K would provide satisfactory walls for some high-purity plasma experiments. It was postulated that under continued bombardment the increasing particle concentration within the target material resulted in diffusion to the surface and molecular desorption. Cooling the target reduced the diffusion rate and provided effective entrapment of the incident particles in a nonequilibrium concentration in the metal. The study of molybdenum and titanium with widely differing solubilities for deuterium showed that the incident particle can be retained in the metal surface from room temperature to as high as 350°C if the solubility for deuterium is sufficiently high and if the solubility limits are not exceeded. The solubility phenomenon, as exemplified by titanium, might make it possible to perform some high-purity plasma experiments at relatively high temperature, providing a method can be found to eliminate the thermal desorption of gases from surfaces adjacent to the high-temperature region and the diffusion of less soluble residual gases from the hot titanium.

Vacuum Gauge Development

Two commercial vacuum gauges of the magnetron type were investigated for use in Alice in the variable return flux of less than 3 kilogauss. For the pressures between 10^{-9} and 10^{-8} torr, stable and linear operation was found for field changes of about 500 gauss for some applied electric potential difference to the gauges. Although the stability and linearity of the gauges depended on the location and magnitude of external loading capacitors, the results were sufficiently encouraging for installation of one gauge in Alice for calibration and further examination.

H. Microwave Measurements for Alice

Andrew L. Gardner

The feasibility of microwave measurements of electron density in Alice is being studied. The chamber size and electron density are presently in the proper range for cavity-type measurements, but the various conductors within the chamber seriously affect the modes of oscillation. An experimental search revealed no natural resonances that were well suited to this application. The difficulty of providing an appropriate liner for such measurements precludes its further consideration at present.

Evaluations are being made of the possibility of transmission measurements at K band or possibly at X band.

Bench tests have shown the utility of a simple null method of measuring small phase shifts in which the only nonpassive circuitry, besides the power for the CW klystron, is provided by standard oscilloscope components. The signal phase is compared with a variable reference phase reflected from a varactor. At 24 Gc the circuitry was sufficiently stable to allow resolution of about 10^{-3} radian (corresponding to $n_e = 1.5 \times 10^8$ over a 20-cm path) with a response time of about 10^{-2} sec. The long-time stability over periods of a few minutes was also of this order without any special precautions to stabilize the klystron.

II. ASTRON PROGRAM

1. INTRODUCTION

Nicholas C. Christofilos

The Astron accelerator became operational up to its full energy of 4 MeV during this report period. One accelerating unit will be added later which will increase the energy to 4.7 MeV.

The beam current is limited to 120 A, mostly because of defects in the electron gun. A new gun is now being assembled. The operation of the accelerator is discussed in more detail in Sec. II. 2.

The completion of the Astron facility has been very much expedited following the successful operation of the accelerator.

The power supplies for all the Astron tank coils have been ordered. The cables connecting the Astron coils to 128 power supplies are now being installed. The mechanical assembly is almost complete. It is expected that by this fall the installation will be completed.

The initial phase of the experimental program is aimed at investigating the buildup of the E layer, to learn to bypass or avoid coupling of the injected electron bunches with the microwave modes of the cavity or with ion plasma waves. The slowing-down process as the electrons pass through the resistor region will be studied in detail. The procedure of building up the E layer is described in detail in a separate report[1] and is discussed briefly in Sec. II. 3 of this report. The two basic methods to avoid coupling with plasma frequency or microwave modes of the tank are

(a) changing the thickness of the E layer by changing the atomic number of the neutralizing gas,
(b) changing the transit time the electrons in the E layer require to oscillate back and forth between their mirror points, by changing the mirror ratio during the buildup phase.

During these experiments the E layer will be monitored through a variety of diagnostic instruments. The position and thickness of the E layer will be observed visually through three television cameras, one located in the center and one at each end. The current distribution of the E layer will be monitored through a number of Hall current probes. The behavior of the injected bunches as they pass through the resistor region will be observed by viewing the induced current in the resistors. Finally, any kind of noise or oscillations up to 3000 Mc will be observed through special, very fast scopes.

1. N. Christofilos, Proposed Current Distribution of the Astron E Layer, Lawrence Radiation Laboratory Report UCID-4577, June 4, 1963.

2. ASTRON ELECTRON ACCELERATOR

Ross E. Hester, William A. S. Lamb, Daryl D. Reagan,
William A. Sherwood, Ross L. Spoerlein, and Robert E. Wright

The Astron accelerator, consisting of the electron gun and six accelerator units, was put into operation in mid-February.

Peak currents of 150 amperes have been produced, but the amplitude of the current pulse is not constant in time. The average current during the 0.3-μsec pulse is 120 A. Most of the operation has continued to be at 5 pulses per second. The beam can be focused to less than 1 in. in diameter. The beam diameter has been determined by collecting the current on segmented targets or by melting holes in 8-mil-thick lead foils placed immediately in front of the aperture of a Faraday cup.

The beam energy has been determined to be 4 MeV ± 100 keV. This has been determined by a calorimetric measurement using a deep watercooled Faraday cup. Another method of determining the beam energy is to add up the voltages measured on the precision resistor strings attached to each core monitor loop. The resistor strings were calibrated by turning off accelerator units and individual cores until the threshold for the photodisintegration of deuterium at 2.26 MeV was established. This measurement was accomplished by bombarding a tantalum target placed immediately in front of a bottle of heavy water. A BF^3 counter was used to count the neutrons.

Work is continuing that should improve accelerator operation. Some preliminary experiments have been started to study predicted beam oscillations when the beam is injected through a 0.25-mil Mylar foil into a gas-filled tank. The pressure ranges of interest are 1 to 10 mm Hg, and the foils have demonstrated their ability to withstand such pressures for reasonable lengths of time before failing from radiation damage.

Figure II-1 is an overhead view of the Astron accelerator as it appeared when first put into operation.

3. CURRENT DISTRIBUTION OF THE E LAYER

N. Christofilos

The first goal of the Astron program is to demonstrate the feasibility of the E layer, namely to establish a layer of rotating electrons up to the point where the self field of the E layer is equal and opposite to the external magnetic field.

The Astron experimental model consists of a long cylindrical tank, as shown in Fig. II-2. A solenoid (11) is located outside the tanks from one end of the machine to the other.

This solenoid or tank coil is divided into a center section, 64 feet long, and two end coils. The center section consists of 128 coils connected--in pairs located symmetrically with respect to the symmetry plane, A-A'--to 64 power supplies. The power supplies are controlled independently so that any desired field distribution can be obtained.

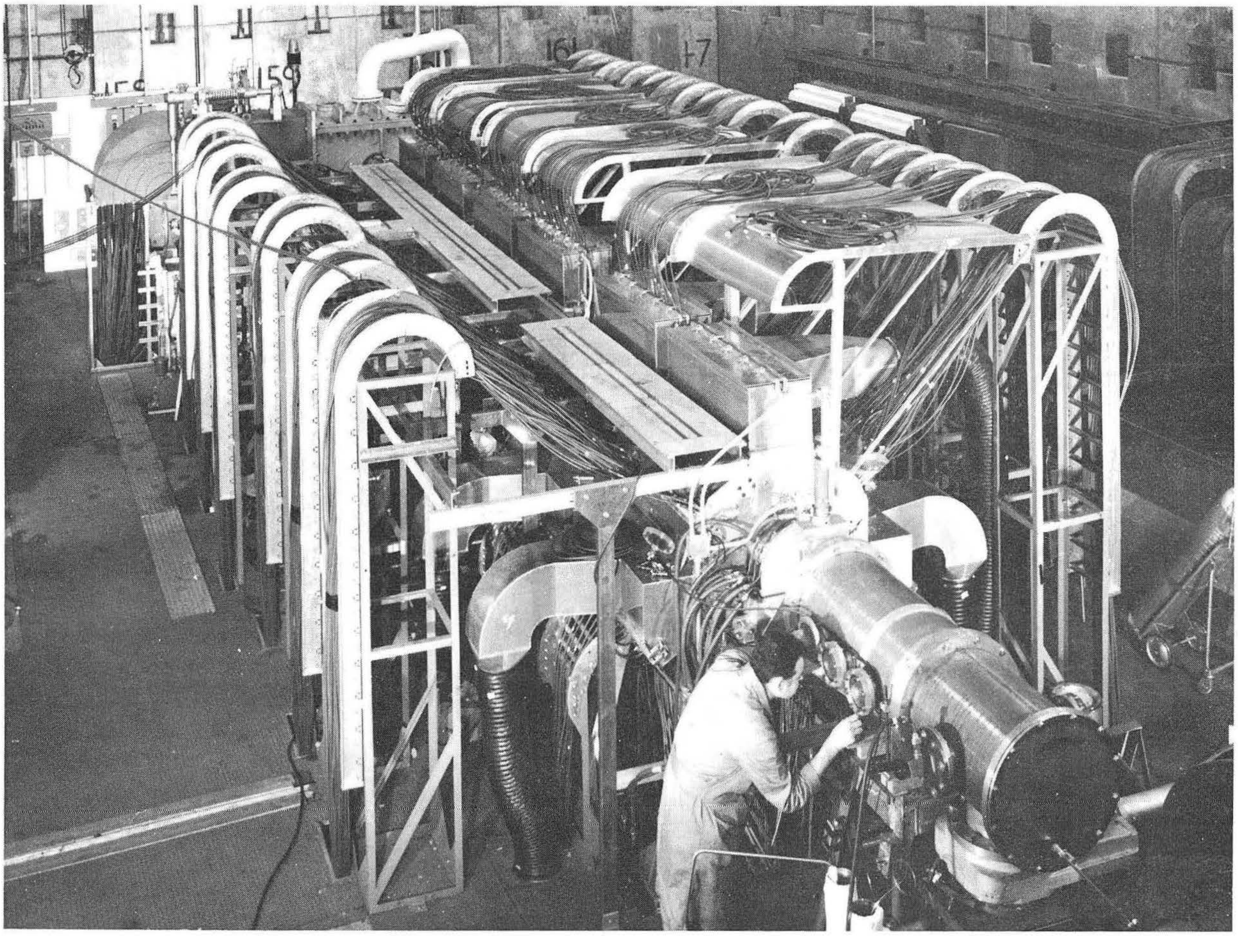

ZN-3929

Fig. II-1. Astron electron accelerator. An overhead view of the Astron accelerator as it appeared when first put into operation.

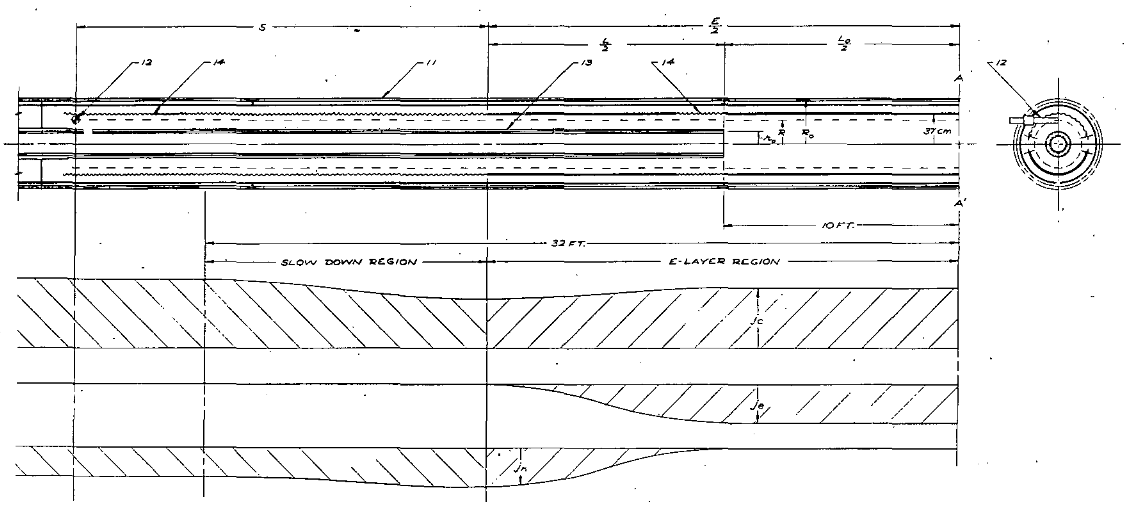

MU-31767

Fig. II-2. Astron tank layout.

The electrons are injected through an injector tube (12) at a radius R. A section of the tank, of length S (Fig. II-2), is the resistor region where the slowing down of the injected electrons is effected, whereas the balance of length E is the space where the E layer can be established. A cantilever (13) protrudes through the resistor region and part of the E layer region. The diameter of the cantilever is 41 cm. In the resistor region, thin wire resistors (14) are disposed, between the wall of the tank and the cylinder of radius R, the electrons are injected, forming a cylindrical surface of 37 cm radius.

A beam of high-energy electrons (4 to 5 MeV) at 100 to 200 A is injected periodically. This beam is injected for 0.2 to 0.3 μsec, 10 to 30 times per second. The injected electrons form a bunch of a few thousand amperes moving away from the injector.

The tank coil current is constant over the injector tube, its value being determined by electron energy and the desired Larmor radius R. A few feet away from the injection point the current in the tank coils starts decreasing to form a mirror field. As the electron bunch moves through the resistor region, falling in the mirror field, it loses energy through only currents induced in the resistors. The total incremental energy loss is approximately equal to the relative depth of the mirror field. During the slow-down phase, though, it is desirable to maintain the electron bunch radius constant; therefore another set of coils is required, located in the cantilever, which provides additional magnetic flux to maintain the so-called betatron condition. The current distribution in both the tank and cantilever coils in the resistor region has been described.[1]

The power supplies for both the tank and cantilever coils are divided in two groups. In each group the current-control circuits for cantilever and tank coils power supplies are interlocked so that any change in the current of the tank coils automatically changes the current in the cantilever coils in accordance with the betatron conditions.

Each of the groups is provided with dual controls, thus allowing a setup of two predetermined mirror shapes, the first meeting the condition required at the very start of the buildup phase of the E layer, the second setup meeting the requirements of a fully established E layer. During the buildup phase the current of the tank coils is gradually changed so that the initial current distribution is changing, thus gradually approaching the current distribution required by the fully established E layer. The current distribution of the tank coils depends on the current distribution in the E layer. A basic requirement that must be met by any equilibrium solution of the E layer current distribution is that the magnetic flux created by the rotating electrons must emerge through its surface without any leak through the open ends. This condition is necessary for two reasons:

(a) The betatron condition must be maintained if the E layer radius is to be kept constant along its length.

---

1. N. Christofilos, Astron Electron Injection, Lawrence Radiation Laboratory Report UCRL-5617-T, June 22, 1959.

(b) Any leakage flux would have been linked with newly injected electrons before they reach the end of the E layer, causing a continuous recession of the mirror points, and thus extending the length of the E layer with each injected electron bunch.

If a given E layer current distribution is not meeting this requirement external coils are required at each end to neutralize the flux leaking through the end. One equilibrium solution was worked out by Heckrotte and Neil.[2] The current distribution is proportional to sin (kz), where $z = 0$ at one end of the E layer. This solution required a continuous current distribution in two end walls located at each end of the E layer. However, an annular slot is required in each wall to allow for injection of the electrons. Through this slot the flux is leaking out. Thus, from the practical point of view it appeared difficult to confine the E layer flux within its prescribed length. Besides, it was desirable at this time to avoid end coils so that the length of the resistor region could be varied in order to study in detail the slow-down process.

Therefore a new solution was sought that does not require end coils. This condition can be met by any solution whereby the radial component of the E layer field as well as its vector potential is zero at each end.

An E layer current distribution that meets this requirement is

$$j = \sum_{n=1}^{\infty} c_n \left[1 - \cos(nkz)\right]. \qquad (1)$$

The solution of the Maxwell's equation determines the current distribution in tank and cantilever coils. The solution giving the vector potential in the three regions--namely, in the volume enclosed by the E layer, the space between the tank coil and the E layer, and outside the tank coils--is discussed in detail in a separate report.[3]

In all the previously proposed E layer current distributions, the external magnetic field far from the ends as well as the vector potential at each end remained unchanged during the buildup of the E layer. Hence at $\zeta = 1$,[4] where the vector potential far from the ends becomes zero, the azimuthal mechanical momentum of the electrons becomes one-half the total momentum. It is desirable to provide the possibility, though, of changing the value of the azimuthal momentum, especially in order to avoid the so-called B_θ instability. In order to increase the azimuthal mechanical momentum far from the ends of the E layer we must reduce the vector potential at injection. This can be accomplished by an internal coil located on the cantilevers which is energized with a current opposite in direction to the current of the external or tank coils.

---

2. V. K. Neil and Warren Heckrotte, A Self-Consistent Distribution of Electrons in the Astron E-Layer, Lawrence Radiation Laboratory Report UCRL-6942, May 21, 1962.

3. N. Christofilos, Proposed Current Distribution of the Astron E-layer, Lawrence Radiation Laboratory Report UCID-4577, June 4, 1963.

4. ζ is the loading factor of E layer, defined as the ratio of the self-field to the tank-coil field at the symmetry plane, near the axis of symmetry.

Let B_n, r_o be respectively the field inside this coil and its radius. This coil runs along the machine, starting beyond the injection point of the electrons in the machine and terminating at the end of the cantilever (Fig. II-2). The current distribution in this coil is uniform in the resistor region and thereafter is tapered as $[1 + \cos(kz)]$, as shown in the lower part of Fig. II-2. Thus, the flux linked by the electrons upon their injection in the E layer is reduced by a factor $(1 - \alpha)$, where

$$\alpha = B_n r_o^2 / B_o R^2, \tag{2}$$

$$B_o = 1700 \sqrt{\gamma_i^2 - 1} / R, \tag{3}$$

and γ_i the electron energy, upon injection in the E-layer region, expressed in rest mass units. Then an elementary calculation yields

$$(p_\theta / p_o) = (1 + \alpha)/2. \tag{4}$$

The flux of the internal coil, or "negative flux coil," varies during the buildup proportionally to the loading factor ζ. It is contemplated in the Astron experiments to vary α from zero up to 0.4, thus the mechanical momentum will vary between 0.5 and 0.7. In order to maintain the betatron condition it is necessary now to change the external magnetic field far from the ends during the buildup phase, thus

$$B_c = B_o(1 + \alpha). \tag{5}$$

The allowed values of "α" depend on the radius of the E layer and the tank coil respectively. In the Astron model the radius of the tank coil is 56 cm.

Then the value of α for a given value of the E layer radius (R) can be varied within the limits indicated in the table.

R(cm)	α
27	0.22 - 0.32
30	0.28 - 0.36
33	0.39 - 0.42

The above values of α are the maximum values at $\zeta = 1$. During the buildup phase, α must be increased from zero to a maximum value within the limits shown in the Table. The value of ζ is proportional to the E layer current, which will be monitored during the buildup phase through a Hall current probe placed at the axis of the E layer tank, at the symmetry plane. The current in the negative flux coil is then manually changed to follow the E layer current. Since the range of incremental values of α for a given E layer radius is more than ± 10%, the manual adjustment appears to be feasible and from the practical point of view.

The E layer current distribution discussed briefly in this section and in more detail in reference 3 is a solution in the thin-layer approximation. Since the E layer will be several centimeters thick, there will be departures from the proposed solution. However, the proposed E-layer current distribution is considered as a starting point to provide guidance in specifying an initial set of magnetic field parameters and the current distribution in the coils during the buildup phase. It is expected that monitoring the E layer radius near each end and at the symmetry plane will determine more precisely the field distribution during the buildup phase.

A key feature of the proposed current distribution is that the end of the E layer is very smoothly tapered while the mirror points at each end are spread along 25% of its total length. Therefore no harmful end effects are presently expected.

The electron energy distribution in the E layer at steady state is continuous from the injection energy down to a minimum energy at which large-angle scattering can remove the electrons from their organized motion. Therefore during the buildup phase the first injected electron bunch must have lost all its energy by the time the last bunch is injected. However, during the buildup phase the inverse betatron effect is absorbing half of the energy of the first injected electron bunch by the time field reversal ($\zeta = 1$) is reached. This energy loss represents the energy stored in the magnetic field of the E layer. The other half of the energy must be removed by scattering. As soon as the desirable degree of field reversal is reached ($\zeta \approx 1.02$ to 1.05) the number of electrons in the E layer must remain constant. Thereafter the electrons are injected at a rate equal to the rate at which electrons are lost by scattering. Since the number of electrons as well as the current remains constant, the betatron loss disappears, thus the electrons lose energy at half as great a rate as during the buildup phase. Consequently, as soon as the desired value of ζ is reached either the injection rate must be reduced by 50% or the gas pressure must be enhanced by a factor of two.

Preliminary investigation of the self-consistency of the described solution of the E layer current distribution indicates that the solution is self-consistent provided that the energy density population is decreasing slightly with decreasing energy. The scattering loss, though, increases slightly with decreasing energy, thus the electron population per unit energy is depleted faster as the electron energy decreases.

More accurate calculations on the self-consistency of the proposed current distribution are being carried out by Warren Heckrotte and Kelvin Neil.

The calculations on the self-consistency of the solution must be carried out, though, for several values of ζ in order to determine the required energy distribution during the buildup phase. At this time it has been assumed that the ratio of the width of the energy spectrum to the injection energy is equal to the loading factor ζ.

The frequency of the axial oscillations of the first injected bunch of electrons is 0.5 to 1 Mc if $\alpha = 0$ at injection. This frequency, however, corresponds to an axial velocity of 0.05 to 0.1 c, which may be too small to avoid coupling either with cavity microwave modes or with the neutralizing ions' plasma frequency. Therefore the parameter α will have to be slightly negative at the beginning of the buildup phase to provide a mirror field to enhance the axial momentum of the electrons.

The plasma frequency of the neutralizing ions can be varied within a limited range by changing the atomic number of the neutralizing gas, thus varying the scattering angle for the same energy loss. Thus, the transverse temperature of the E layer as a function of the electron energy can be controlled, which in turn controls the thickness of the E layer and hence its density as a function of ζ. It is expected, however, that changing the parameter α, which in turn changes the frequency of the axial oscillation--i.e., the transit time an electron requires to travel a round trip from one mirror point at one end to the other mirror point at the other end and back—will be adequate to avoid resonant coupling either with the cavity modes or with the ion plasma frequency.

III. LIVERMORE PINCH PROGRAM

Dale H. Birdsall, Stirling A. Colgate, Harold P. Furth,
Charles W. Hartman, Richard H. Munger, and Ross L. Spoerlein

1. LEVITRON

Operation

Immediately following the period of the preceding progress report, the levitron was shut down for major repairs. The rough vacuum seal of the copper shells had deteriorated because of a progressive chemical reaction between Silastic silicone rubber and copper. Following a repair of this seal by a combination of nickel plating and surface priming, the torus was reassembled with simplified coils. The original operation had demonstrated conclusively that the short-rise-time fields ($\approx$ 100 μsec) were unnecessary, and that good "coupling" (inductive plasma current) could be achieved with fields rising in several milliseconds. Since study of the phenomena limiting the confinement time remains the primary scientific objective, the complexity associated with the fast fields became superfluous, and the new coils were designed to facilitate the slow-field operation. Several months later, with a vacuum of 3 to 5×10^{-7} mm Hg, a D_2 pressure of 3.10^{-2} μ, and a B_z rise time of 3 msec, the limiting inverse-pinch coupling time of 2 msec was explored. The general characteristics of the discharge were the same as previously reported, and the analysis of the instability was pursued.

Instability Studies

As previously reported, the levitron is subject to a low-level magnetic disturbance ($|B_r| \approx 5$ gauss out of $|B| \approx 5000$ gauss). This disturbance is so small relative to instabilities in conventional pinches that it might be ignored, were it not that the time of onset (200 μsec after pinch initiation) coincides with a sudden loss of plasma containment and with a discontinuous change in sign for $d\sigma/dt$. In view of these correlations, the magnetic disturbance is believed to be closely related to the basic containment-loss problem in the levitron.

The amplitude of the disturbance is correlated with the "stress" in the magnetic field, i.e., with the amount of magnetic energy that can be released by relaxation toward the vacuum field. This feature is consistent with either $J_{\parallel}$-induced or β-induced instabilities. If the first alternative is relevant, the use of nonohmic heating, either as an auxiliary or exclusively, should cure the present instability. On the other hand, if we find that the β rather than the $J_{\parallel}$ is important, we may demonstrate a basic stability property: a large shear does not suffice to compensate for a strong negative gradient in absolute magnetic field, at least not at low temperatures. In view of the decisive importance of settling this question, our major research effort has been along these lines.

The frequency spectrum of the magnetic disturbances is peaked for autocorrelation times of 5 to 20 μsec. The frequency increases with the amplitude of the disturbance. Various spatial autocorrelation measurements were made, which are illustrated in part in Fig. III-1. Three B_r probes were placed near the tube wall in Ports 1, L, and R, and B_r was studied for a regime where magnetic field lines passed through Ports 1 and L (top and side ports, 90° apart in minor azimuth, 30 cm apart along the major azimuth). The correlation 42 cm along field was found fair, while the two probles L and R, located 6.5 cm apart across field, showed anticorrelation (180° apart in phase) more commonly than correlation. Thus it appears that the disturbances are of the flut type, with $\lambda_{\parallel}/2 \approx 40$ cm and $\lambda_{\perp}/2 \approx 6$ cm. By means of various RC filters, it was found that the lower-frequency components have longer wavelengths. Two multiloop B_r probes were also used in Ports 1 and L to study correlation simultaneously along field and across field in the radial direction. The radial correlation within each probe was always found good all through the principal current layer (≈ 5 cm). Correlation studies along field indicated that waves for which the surface "$\bar{k} \cdot \bar{B}_o = 0$" lay within the current layer (i.e., flutes aligned with field lines lying inside the current layer) showed the usual good correlation of B_r along radius. This result is highly significant, since for infinite-conductivity hydromagnetic disturbances B_r must have a null at $\bar{k} \cdot \bar{B}_o = 0$. It is concluded that the observed disturbances are either finite-resistivity instabilities, or else waves excited by some other mechanism, but violating infinite-conductivity topology.

Of the known finite-resistivity modes (see Section IV) the tearing mode seemed a possible candidate, though the magnitude of the vacuum-field component in the levitron made this somewhat unlikely. To settle the matter an initial-B_z, B_θ-pinch configuration was set up such that the plasma-current shear everywhere reduced but nowhere reversed the vacuum shear. This configuration, which is absolutely stable against the tearing mode, was still found to exhibit the usual instability. Thus only the rippling ($J_{\parallel} \times \nabla\sigma$-driven) and gravitational (β-driven) instabilities remain as possibilities among the known finite-resistivity modes.

As shown in Fig. III-1, Langmuir-probe floating-potential measurements were also made. The correlation along field between Ports 1 and R was good, and simultaneously no cross-field correlation to Port 2 was observed. The probes measure mean values up to 200 to 300 volts as they are moved radially into the current layer, and fluctuations typically of order 20 volts, with autocorrelation times of 20 μsec. Correlations between two probes at different radii were found good. The lack of cross-field correlation, if genuine, is interesting, since it implies either (a) tangential electric fields sufficient to account directly for radial plasma velocities of order 3×10^4 to 10^5 cm/sec; or else (b) the possibility of thermal fluctuations sufficient to allow rippling mode.

Injection

Because of the obvious possibility that the observed instability may be associated with $J_{\parallel}/J \gg 1$ or $J_{\parallel} > neV_t$, there has always existed the need for introducing an already ionized and, if possible, heated plasma into the levitron, independent of the usual formation by a large $J_{\parallel}$. The hollow-cathode source of Fig. III-2 was designed and tested with the concept in mind

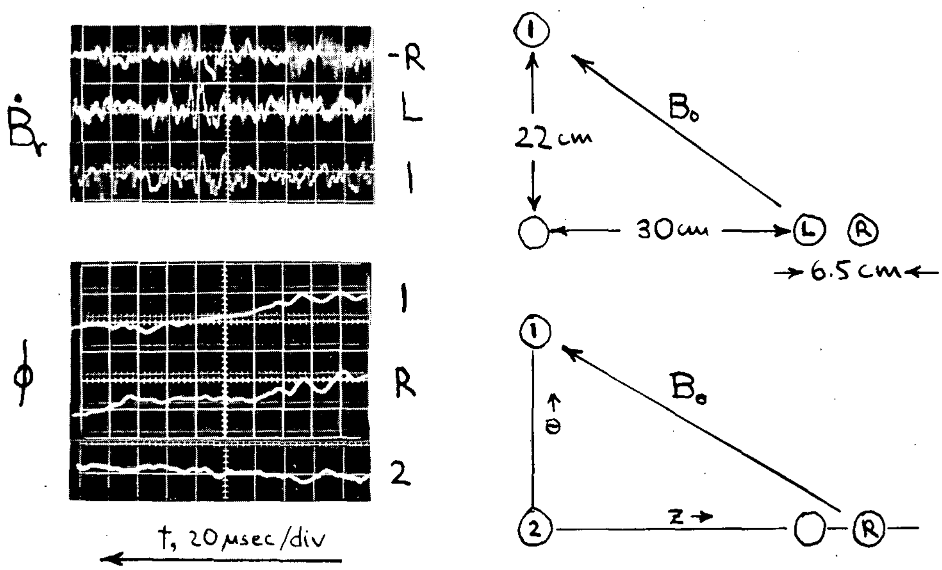

MU-31549

Fig. III-1. Levitron probe correlation.

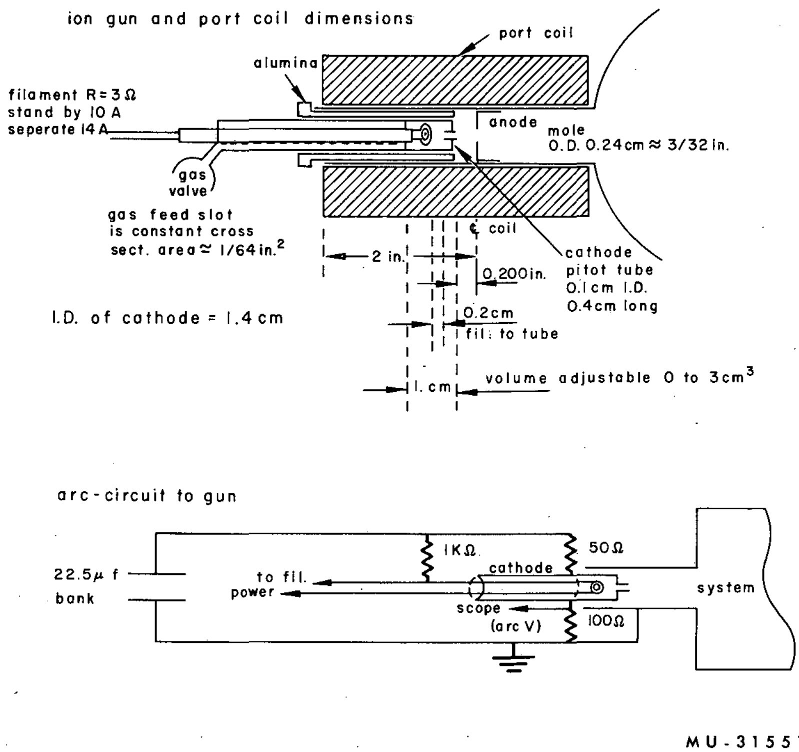

Fig. III-2. (Top) Ion gun assembly. (Bottom) Monitoring circuit and voltage divider for ion gun.

that plasma injected quasistatically on a local bundle of "diverted" lines of force (Fig. III-3) would "turn the corner" before striking the hard core, and drift onto a toroidal flux surface (containing helical field lines). A Langmuir probe plot of the gun output is shown in Fig. III-3. B_z and B_θ are raised slowly and simultaneously to minimize $E_{\parallel}$. Since the drift time on this surface before reaching diverter lines that return back through the wall is very long (several milliseconds), there is ample time in a rising field for the surface to be moved radially inward away from the diverter field. In this fashion a consecutive series of flux surfaces may be loaded with plasma and carried into the confinement volume. This sequence of events has been confirmed experimentally by observing the radial distribution of the plasma with Langmuir probes at various locations around the torus. The maximum plasma density near the hard core reached several times 10^{11} per cm^3, and the position of the maximum density as a function of time and radius agreed qualitatively with the time of loading of the initial flux surface. The spreading in minor azimuth is very rapid (less than 1/4 major turn), as would be expected from the large shear. In addition it was reassuring to confirm experimentally that a pure toroidal field (B_z only) exhibits no confinement, presumably because of rapid drift to the walls. An effort to make quantitative measurements was frustrated by the nonreproducibility of the source and its inability to operate longer than 1 msec. The latter limit causes at least 50% of the gas to be injected in neutral form, so that density measurements as a function of time, which might give confinement data, are uncertain because of additional ionization. These initial results will be pursued with an improved source.

2. LINEAR HARD-CORE PINCH

Experimentation with the inverse pinch formed by a rising B_θ has continued to demonstrate the destabilizing effects of the cathode. Correlation of the sheath drop and fluctuating fields in the current layer is shown by Fig. III-4. To obtain the traces shown, the plasma floating potentials V_{sheath} (relative to the cathode) was measured with a Langmuir probe positioned in the current layer. At the same time, fluctuations in B_r and E_θ were monitored with a magnetic probe and dual floating Langmuir probe (5 mm spacing) located in the current layer midway between the electrodes. Similar correlations are observed for all pressures less than 100 μD_2, although at higher pressure the frequency of fluctuations decreases. The FeI line was monitored with a monochromator viewing the cathode.

Azimuthal correlation of B_r signals obtained from magnetic probes positioned around current layer midway between electrodes have shown the general filamentary character of the discharge. At low pressure filaments have been identified which are anchored at the cathode and change pitch with B_z as pinch current increases.

The dominance of electrode effects is now fairly well understood, and it appears to preclude a careful study of fine-scale hydromagnetic instabilities arising from finite resistivity. A report has been presented.[1]

---

1. Charles Hartman, Electrode Sheath Effects in Pulsed High-Current Discharges (UCRL-7357, June 13, 1963), in Proceedings of the Sixth International Conference on Ionization Phenomena in Gases.

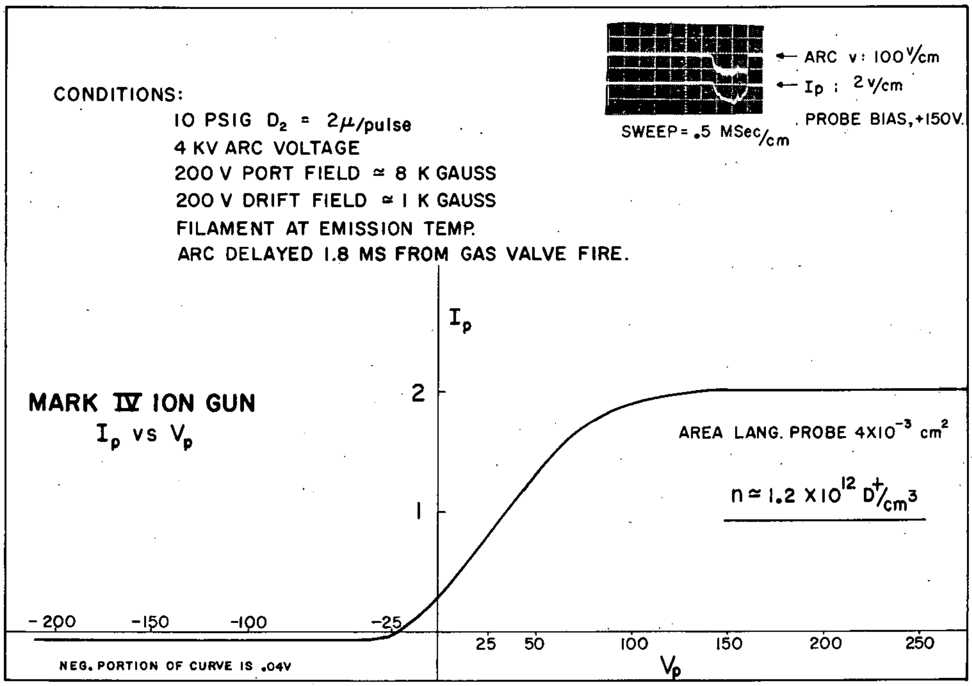

Fig. III-3. Langmuir-probe curve of ion gun output.

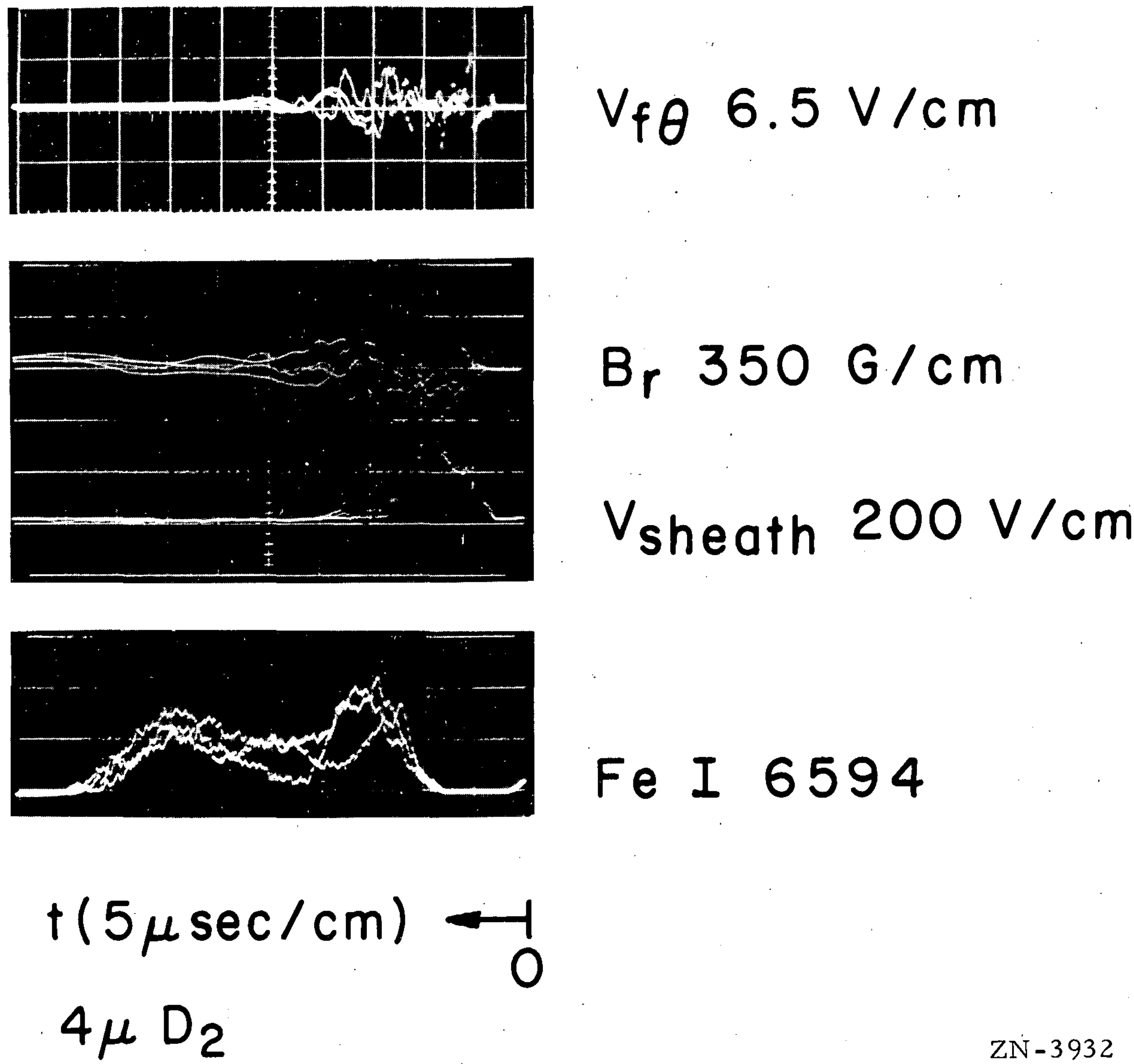

Fig. III-4. Sheath potential correlation. $V_{f\theta}$ is the floating potential graident in the θ direction.

Alfvén Wave Studies

Because of the cathode instability mechanisms outlined above, and in the search for a more general knowledge of wave propagation in pinches, the launching, propagation, and attenuation of torsional Alfvén waves have been studied in the linear hard-core pinch. One quantity of considerable interest with respect to instability growth is the damping of an Alfvén wave due to magnetic shear. However, before successful measurements of the latter quantity, we have discovered a "fast" mode of propagation that apparently depends upon the parallel component of the kinetic energy of the electrons injected from the launcher.

Fig. III-5 shows the pinch tube with the launcher and radial magnetic probes which extend to the flux surface corresponding to the launcher. The launcher consists of a central electrode (1/8-in. stainless steel) backed up by a 1/2-in.-diameter insulating disk of quartz. In operation a pinch is first made in the pinch tube by the sudden reduction to zero of an initial vacuum B_θ field in the presence of a uniform B_z of 2 kG. The discharge is initiated not only by the induced voltage from B_θ, but also by the simultaneous firing of the multiple spark triggers in the cathode. Approximately 35 μsec after the pinch, when $B_\theta = 0$, a fast 1-μF 5-kV capacitor is discharged ($t/4 = 0.5$ μsec) between the launcher center electrode and the cathode. Since the cathode, outer wall, and anode are equipotential at this time, some current flows along a tube of force to the anode from the launcher. This current, in the form of either a wave or a prompt electron stream, is observed by the multiple sets of B_r probes. Figure III-6 shows the maximum probe signals in the "unwrapped" θ-z cylindrical surface for an initial gas filling of 2 μ argon and 10 μ deuterium. The spatial behavior is that of a current filament of radius ≤ 2 cm and axial decay length of approx 40 cm for 10 μ D_2 and of approx 20 cm for 2 μ A. Figure III-7 shows the propagation velocity in each gas and the signals from which these data were taken. The probes 20 cm from the launcher show both an initial early rise and a later slow component for each gas. That the maximum of the D_2 early signal occurs before I_{max} in the launcher suggests a phenomenon based not upon the magnetic pressure of the launcher, but more likely on $\dot{B}$. If the initial launcher current consisted of electrons emitted across a sheath potential of 100 to 300 eV then the total kinetic energy of these electrons was more than adequate to give rise to the observed fields of 40 to 80 gauss. The decay length of the fast component in argon is ≤ 10 cm, which is consistent with the larger scattering cross section. To qualitatively check the electron-stream concept, a screen of 5 × 10 cm dimension was interposed between the probe sets at 20 and 40 cm, and a wave attenuation of less than the screen opacity of 30% was observed for both fast and slow components. A torsional hydromagnetic wave should not propagate through the screen, therefore other phenomena must be invoked.

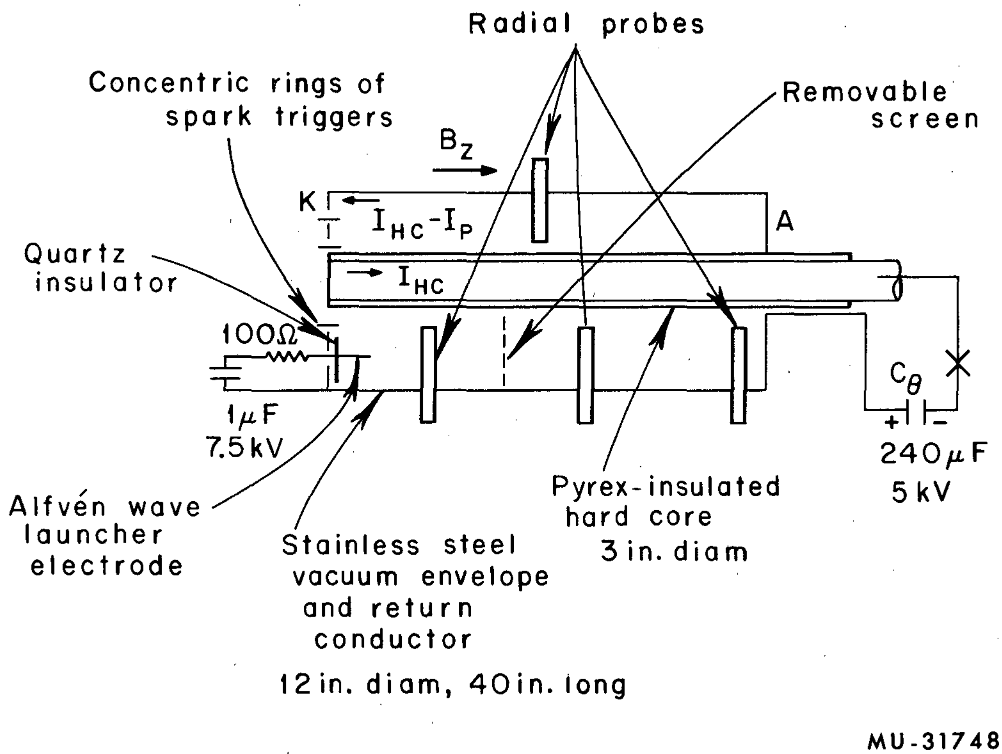

Fig. III-5. Experimental arrangement for Alfvén wave experiment.

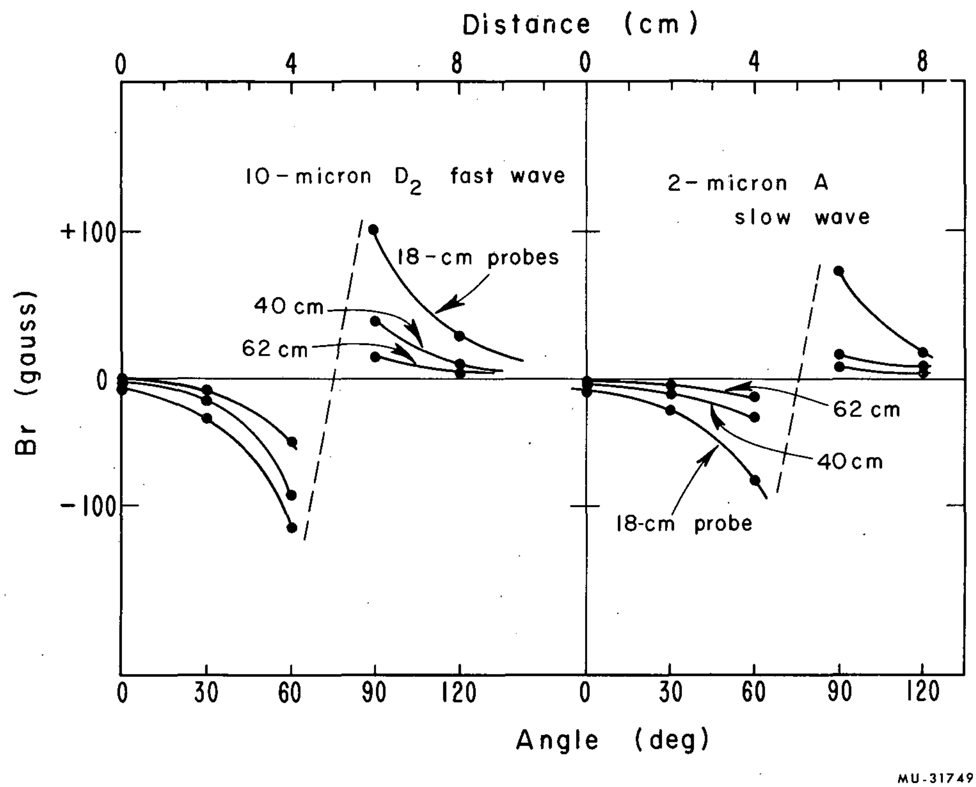

Fig. III-6. Radial magnetic field versus probe position.

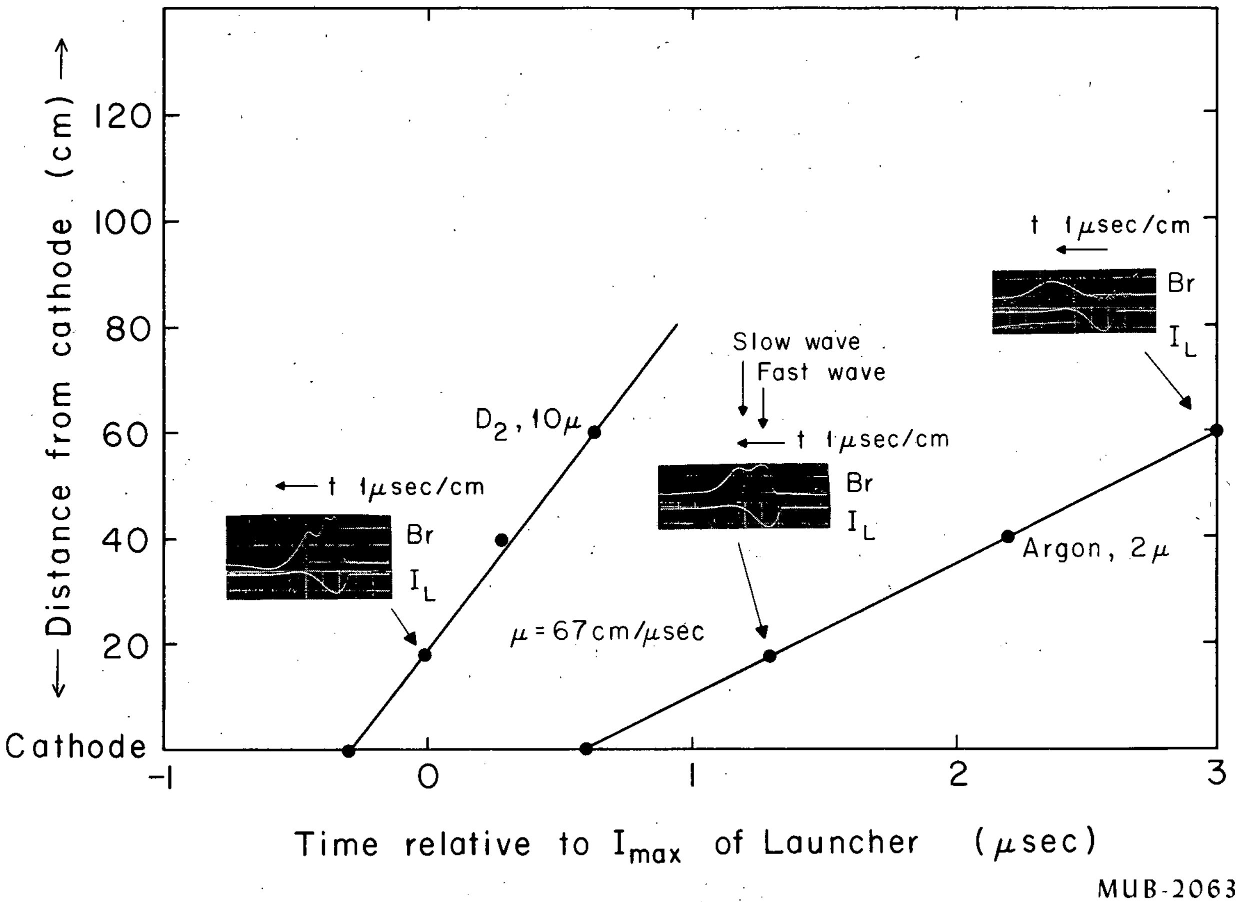

Fig. III-7. Propagation velocity of Alfvén wave.

3. COLLISIONLESS PLASMA SHOCK

Theoretical Studies

Shock calculations of mass ratio 100 have been extended to 15 ion periods. The long-wavelength mode reported in the preceding semiannual report, which appeared to have $\lambda/4 \approx$ length of the shocked plasma, has begun to establish a wavelength $\lambda \approx 20\ \lambda_{pi}$. Modifications of the computational accuracy of the code, the time step, and the number of sheets per Debye length have not altered the general potential distribution, indicating the long-wavelength effect is not computational.

Experimental Studies

More careful measurements have been made of the energy loss and collisional heating that occur when a moving plasma encounters a neutral D_2 background. For a combined density of about 1 to $2 \times 10^{15}\ D^+/cm^2$ and 1 keV kinetic energy, measurements of the stripping rates of 1% N_2 impurity, total photon flux, diamagnetic pressure, and loss of kinetic energy are found to be consistent with classical collisional heating of the electron background by the contrastreaming ions. For a predicted temperature rise (including ionization losses of about 30 eV/neutral) of about 40 eV the observed kinetic energy loss is consistent with the energy deposited by heating.

This experiment is now terminated.

4. INSTABILITY THEORY

Finite-Resistivity Instabilities

A kind of energy principle has been evolved for finite-resistivity hydromagnetic modes.[1] Starting with the equations of motion,[2] one finds a quadratic form

$$E = V + pM + p^2 K, \qquad (1)$$

which is identically zero when the field perturbation ψ and fluid displacement ξ entering V, M, K correspond to a true normal mode of growth rate p. For unstable finite-resistivity modes, p is real and positive. Here V is an integral that is quadratic in ψ and ξ, and that closely resembles the potential energy integral of the usual energy principle, going over into it in the limit of perfect conductivity. Similarly M is a positive definite quadratic measure of departure from the infinite-conductivity relation between ψ and ξ, and represents the (mainly dissipative) work of field-fluid decoupling. Finally, K corresponds to kinetic energy. Note that E varies monotonically with p.

---

1. H. P. Furth, Hydromagnetic Instabilities due to Finite Resistivity, UCRL-7107, March 1963.

2. H. P. Furth, J. Killeen, and M. N. Rosenbluth, Phys. Fluids 6, 459 (1963).

One can use the condition $E \leq 0$ to set an upper limit on possible growth rates p for various modes, and one thus confirms the expectation that the modes exhibited in reference 2 are the fastest-growing ones for the conditions treated. Furthermore, one finds somewhat surprisingly that if the zero-order configuration is in true static equilibrium then E gives a variational principle for ψ and ξ. That is to say, all choices of trial functions ψ and ξ for which E is stationary about the value $E = 0$ are true normal modes. In particular, if we select trial functions ψ and ξ so as to maximize p consistent with $E = 0$ (and possible auxiliary conditions, if desired), then we know that such a mode actually exists.

The tearing mode has been investigated at length in cylindrical geometry. By use of the extended energy-principle formulation, a number of useful theorems have been proved, among them the following.

1. If $F = \overline{K} \cdot \overline{B}_o$ has its null at the same radius for two distributions F_1, F_2, and if $F'_1 = F'_2$ there, then for $|F_1| \geq |F_2|$, other parameters being the same, it follows that configuration 2 is less stable. This theorem permits convenient comparison of given configurations with simpler ones for which the stability properties are known.

2. In a hard-core pinch with a strong vacuum-field component, a finite plasma current is needed to effect instability. (This contrasts with the plane case, in which enlargement of the vacuum field component has no stabilizing effect, and an infinitesimal plasma current can produce instability.) If the shear due to the plasma current augments the vacuum shear, the configuration is more stable than in the absence of vacuum shear. If the plasma-current shear everywhere reverses the vacuum shear, the configuration is more unstable than in the absence of vacuum shear. If the plasma-current shear everywhere opposes but nowhere reverses the vacuum shear, there is <u>absolute stability.</u> If the plasma-current shear reverses the vacuum shear <u>somewhere, but not</u> everywhere, then there are choices of $\overline{k}$ such that $\overline{k} \cdot \overline{B}_o$ has <u>two</u> nulls, in which case a "double tearing mode" takes place. Since the two nulls can be made to lie arbitrarily closely together, near the point where the shear changes sign, this mode can be of arbitrarily short wavelength and is thus always unstable, though its growth rate becomes small with wavelength.

Velocity-Space Instabilities in the E Layer

The relevance of the Harris instability to the E layer build-up problem has been investigated. As in reference 3, the infinite-homogeneous-medium approximation is effectively made, and $\overline{k}$ is assumed nearly transverse to the directed motion of the particles $(k \approx k_\perp)$. Under these conditions, the dispersion relation for the relativistic electrons[4] is very similar to the relation

3. E. G. Harris (University of Tennessee, Department of Physics, Knoxville, Tenn.), The Crossed Stream Instability (to be published).

4. S. A. Bludman, K. M. Watson, and M. N. Rosenbluth, Phys. Fluids 3, 747 (1960).

obtained by Harris for the DCX type machine. Essentially, the one case can be obtained from the other simply by a change in coordinate system: in the DCX the important interaction is between electrons at rest and ions in motion; in Astron, the electrons are moving relativistically and the ions are at rest. In both cases the electrostatic ion oscillation is the basic phenomenon: in Astron the ion electrostatic frequency is seen directly; in DCX, it is Doppler-shifted by the ion cyclotron frequency. There are two basic forms of the Harris instability: (a) the (better-known) wave-wave interaction between ions and cold electrons, which can occur only for $\omega_{pe} > \omega_c$; and (b) the wave-particle interaction, which depends on Landau antidamping of ion waves by warm electrons moving at nearly the wave velocity, and which is unstable over a much wider range of parameters.

The latter mode is of interest during early E layer build-up, since then one has for the beam plasma frequency $\omega_b < \omega_c$ (which corresponds to $\omega_{pe} < \omega_c$ for DCX). In the infinite-medium approximation, one concludes that there will be an instability oscillating at the ion plasma frequency (1 to 10 megacycles) and exponentiating at a slightly lower rate. The finiteness of the actual E layer geometry, however, mansifests itself in variation of the ion plasma frequency along the electron orbits (in the axial direction) and makes the real significance of the infinite-medium results somewhat problematical. An effort is currently under way to study electrostatic instabilities in finite geometry, and a new electrostatic instability dependent on beam-particle oscillation in a potential well (e. g., betatron oscillation) has been found.

The problem of magnetically coupled instabilities excited by a relativistic electron beam is also being studied. In the absence of cold stationary electrons, there are only the familiar cavity modes; but with a small density of cold electrons, the phase velocity of the extraordinary electromagnetic wave near the cold-electron gyrofrequency becomes sufficiently small so that excitation of short transverse waves within the plasma by Landau antidamping is possible. This line of investigation again follows the infinite-medium approximation, and is patterned after the work of Sudan.[5]

---

5. R. N. Sudan, Phys. Fluids 6, 57 (1963).

IV. BERKELEY PLASMA RESEARCH

1. ROTATING-PLASMA RESEARCH

A. Homopolar V

Klaus Halbach, Robert W. Layman, and G. Donald Paxson

Since it is of great importance to obtain reliable information about the presence of high-energy deuterons in Homopolar V a long time after the device has been crowbarred, we devoted considerable effort to developing a pulse-shape discriminator. A stilbene scintillation counter in conjunction with this circuit allows us to distinguish clearly between scintillations produced by γ rays and scintillations resulting from energetic neutrons, which will be produced in a hot deuterium plasma. Because of the high γ flux resulting from neutron capture, the scintillation counter is gated off during the first 50 μsec after the breakdown. The number of neutrons detected after this time is at present too small to allow a quantitative measurement of the decay time of the plasma. However, the fact that we observed energetic neutrons as late as 150 μsec after the device was crowbarred indicates that the plasma must still have a fairly high density and temperature at that time. To improve both the neutron production and the detection sensitivity, we intend to replace the present coil structure by a pair of mirror coils. With these coils we hope to achieve higher magnetic fields, which should enable us to increase the neutron production; the absence of epoxy between the plasma and the detector should decrease the scattering of neutrons, thus leading to an increased detection sensitivity.

B. Homopolar Gun I

Kenneth W. Ehlers and Klaus Halbach

The Homopolar Gun I has been operational since March 1963. Compared with Homopolar V, this device is basically different in three respects: (a) The center electrode does not extend over the whole length of the machine. (b) The electrical energy for the discharge is fed into the device from only one side. (c) If operated as a gun, this device has only one mirror coil. To establish how the first two of these deviations from the symmetrical Homopolar V design affect its operation, we introduced a second mirror coil so that we could operate this device in the Homopolar V mode. All experiments so far have been done with this magnetic field configuration. A schematic drawing of the Homopolar Gun I as we operate it now is given in Fig. IV-1.

When we started the experiments, we operated the device in the following way: The center electrode did not extend beyond the ports of the puff valve and was directly connected to the fast capacitor bank charged to - 30 to - 40 kV. About 10 msec after the charged electrolytic capacitor bank was connected to the coils, the magnetic field reached its maximum value of approximately 30 kG. At that time the fast-acting valve released about 30 μliter D_2 into the machine. About 100 μsec later a discharge took place which,

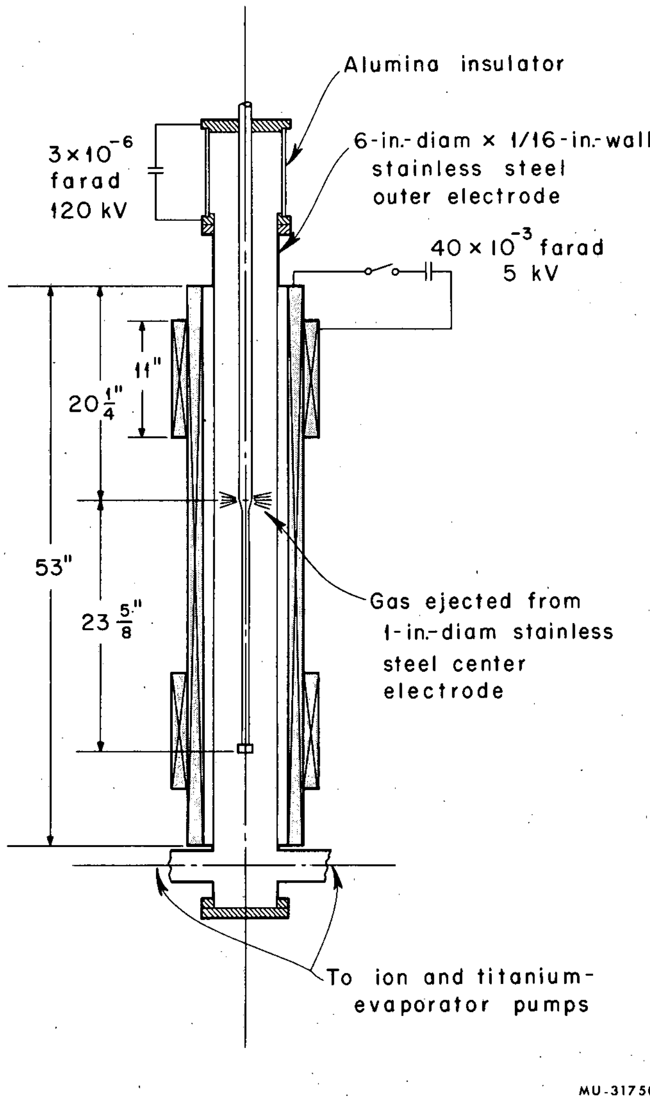

Fig. IV-1. Schematic drawing of Homopolar Gun I as it is presently operated.

however, did not result in a backvoltage; the fast capacitor bank simply discharged completely through the machine. Applying the fast capacitor bank through a switch up to 250 μsec after the opening of the fast valve resulted in somewhat better performance: The current showed an early maximum as in the operation of Homopolar V; before the current went down to very small values, as it does in Homopolar V, it increased again and the fast bank again discharged completely through the machine. This still very unsatisfactory behavior was not altered when the center electrode was extended by 30 cm beyond the valve ports. We interpret these experiments in the following way: In the region at the end of the electrode the electric field must have a component parallel to the magnetic field. If the plasma reaches to or beyond the end of the electrode, this field accelerates electrons axially so that they can easily penetrate the mirror and reach the grounded plate at the bottom of the machine. Although this current is space-charge-limited, it nevertheless is a very effective way to short out the capacitor bank. Since the thermalization time for ions is very long (of the order of 50 μsec) compared with that for the electrons (a fraction of a μsec), and it is essentially thermalization that allows particles to reach the end of the extended center electrode, we then operated the machine with a positive center electrode. With this polarity we obtained a backvoltage for about 5 μsec, which again was followed by an internal crowbar. To avoid this internal crowbar, we applied an external crowbar immediately after the rotation of the plasma was established. Because of inductances in the circuit, the voltage across the machine was ringing, and as soon as the voltage across the machine reversed we observed again a violent internal crowbar. We therefore introduced a resistor in series with the external crowbar in order to avoid the ringing of the voltage. This proved very successful, allowing us to crowbar the device externally without triggering the internal crowbar.

To detect directly the axial acceleration of charged particles, we used a collector electrode which was located on axis close to the bottom of the machine. When we were using a high resistance (4 ohms) in series with the external crowbar, resulting in a slow decay of the voltage across the machine, we observed an ion current of the order of 10 A/cm^2 shortly after the external crowbar was turned on. The maximum energy of the detected ions was 10 keV, which is in agreement with the axial acceleration mechanism described above. This experiment indicates that this device, if operated in this manner, can be utilized as a source of ions with large axial energy. Since we are at present more interested in producing a plasma with small axial energies and large transverse energies, we reduced the crowbar resistance so that the external crowbar was as fast as possible without triggering the internal crowbar. In this case, the voltage across the machine was practically zero at the time when the plasma reached the end of the electrode; consequently the axial ion current disappeared.

These experiments suggest the following procedure for the use of this device as a gun that delivers a hot plasma with low axial energy: The fast valve should be located at a mirror slope so that the plasma slides off this mirror at the desired axial velocity; the device should be externally crowbarred immediately after the plasma is created, and this crowbar should be as fast as possible without initiating an internal crowbar. The center electrode should be extended beyond the fast valve far enough so that the external crowbar is completed at the time when the plasma reaches the end of the center electrode.

At present we are working with a still longer electrode extension that reaches--as shown in Fig. IV-1--beyond the peak of the second mirror. We plan to repeat some of the experiments that we have done with Homopolar V and will then remove the second mirror to operate this device as a plasma gun.

2. HYDROMAGNETIC WAVES AND ION CYCLOTRON HEATING

A. Ion Cyclotron Resonance Experiment

Gordon W. Hamilton, John M. Wilcox, and Forrest I. Boley

Because of the indication[1] that impurities account for a major portion of the energy loss from this experiment, a series of modifications has been made to reduce the impurity content of the plasma and to improve the instrumentation. The result of these improvements is a doubling of plasma energy content and the discovery of some interesting relationships of the energy content as a function of time, position, and various plasma parameters.

Vacuum System

In order to eliminate contamination by diffusion pump oil and to improve the base pressure by two orders of magnitude, an oil-free vacuum system has been installed consisting of an ion pump, an evaporated titanium pump, and two molecular-sieve roughing pumps. A base pressure of 2×10^{-8} torr is now attainable.

The main vacuum shell has been changed from copper to stainless steel to reduce surface contamination and to eliminate soldered joints.

Heated Liner

A cylindrical 10-mil stainless steel liner has been inserted into the main vacuum shell, which can be heated electrically to bake the vacuum surfaces. This was inspired by the heated liner installed in the Levitron,[2] although there are many differences in the installation. A dc power supply is used rather than the inductive coupling required by the Levitron. A 400-ampere current produces sufficient heat to outgas the surfaces effectively without producing visible glowing. The heating current is turned off when the magnet is pulsed in order to avoid any interaction between the heated liner and the magnetic field.

---

1. G. W. Hamilton, F. I. Boley, and J. M. Wilcox , in Controlled Thermonuclear Research Semiannual Report, UCRL-10607, Jan. 1963, pp. 61-62.

2. C. K. Birdsall et al., in Controlled Thermonuclear Research Semiannual Report, UCRL-9969, Jan. 1962, p. 46.

The immediate result of heating the liner was a pressure rise to about 50 microns for several minutes, which corresponds to the outgassing of several monolayers of gas from the chamber surfaces. The base pressure then stabilized at 10^{-6} torr as outgassing continued at a slower rate. After the heating current was turned off, the pressure returned to its normal value of 2×10^{-8} torr in about 18 hours. These results indicate that the hot liner is performing its principal function in eliminating the monolayers and volatiles from the system.

Diamagnetic Signal

Four diamagnetic loops have been installed around the outside of the heated stainless steel liner as shown in Fig. IV-2, in order to measure the energy content of the plasma at four axial positions without the necessity for a probe tube inside the plasma chamber. The signals obtained with these new loops are consistent with (but not identical to) the signal measured by the diamagnetic probe previously reported.[1] As the plasma warms up, lines of flux are forced out of the hot regions into the cool probe tube and into the cool annulus between the heated liner and the main vacuum shell. This results in an increasing flux through the small coil inside the probe tube and a decreasing flux through the large loop around the heated liner. A simplified theoretical comparison of the two signals is given by the following equations, which assume perfect confinement of the flux by the outer shell and neglect the effect of the heated liner:

Old probe:

$$\text{Integrated diamagnetic signal} = \Delta H_1 = +\frac{a^2}{b^2}\frac{U}{B_0},$$

New loop:

$$\text{Integrated diamagnetic signal} = \Delta H_2 = -\frac{b^2 - a^2}{b^2}\frac{U}{B_0},$$

where $U = \langle nkT_{i_\perp} + nkT_{e_\perp} \rangle$ is the kinetic energy density averaged over the cross section, a and b are the radii of the loops and the outer shell, as illustrated by Fig. IV-2, and B_0 is the external applied magnetic field.

Two improvements are now being made to these loops:

(a) Ceramic insulated wire was found lacking in abrasion resistance. Since no other wire can be found with the required vacuum and thermal properties, the loops are being replaced with ceramic bead insulation.

(b) The flux lines diffuse through the steel vacuum shell with a time constant of several hundred microseconds. Since this complicates the interpretation of the diamagnetic signal, the outside of the shell is now wrapped with copper wire to confine the flux during the oscillator pulse. This will also have the effect of eliminating the 360-cps ripple in the magnetic field, which causes the curved base lines on the oscillograms displayed in Fig. IV-3.

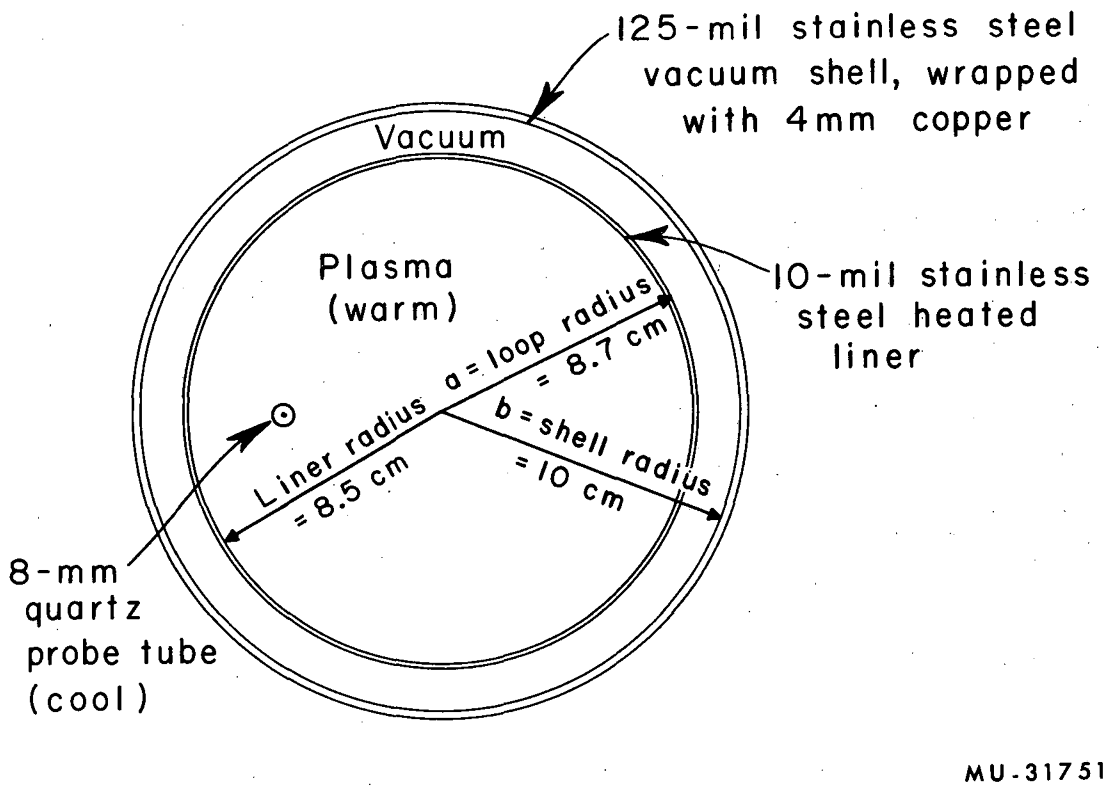

Fig. IV-2. Cross section of plasma chamber, showing heated liner, main shell, and location of probe tube and new diamagnetic loops.

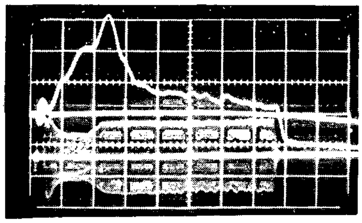

(a)

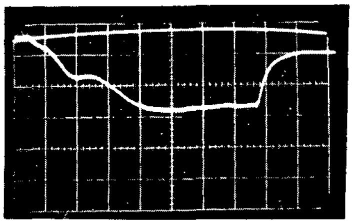

(b)

ZN-3934

Fig. IV-3. Oscillograms showing typical diamagnetic signals at 1.8 μ deuterium pressure. Horizontal scale = 100 μsec/cm. a. Upper beam: Signal from old diamagnetic probe, vertical scale = 1.5 G/cm. Lower beam: Electrode rf voltage, vertical scale = 2.3 kV/cm. b. Signal from new diamagnetic loop, vertical scale = 1.1 G/cm.

Figure IV-3 shows some typical diamagnetic signals as measured by the older probe in the 8-mm quartz probe tube and by the new diamagnetic loops. The difference in polarity of these signals and the curved base lines have been explained above. The fact that the signal does not immediately return to its baseline after oscillator crowbar is due to the imperfect confinement of the flux lines by the steel shell, which is also mentioned above. The lack of rapid fluctuations in the signal obtained from the new loops is because of the shielding effect of the 10-mil steel liner, which confines fluctuations with period of less than 30μsec. Most of the tests previously reported[1] have been repeated to make sure that these are real signals.

The relationships between the diamagnetic signal and the plasma parameters are rather involved, and have been only partially explored. Some of the salient features are as follows.

(a) The diamagnetic signal is twice as large, as a result of the vacuum system modification. The product of particle density and temperature is about 3×10^{15} eV/cm^3.

(b) When the probe tube is retracted from the plasma, the signal observed by the new loop increases by about 40%, thus indicating that the probe tube acts like a heat sink.

(c) When the initial D_2 pressure is reduced from 5μ to 1.8μ, the diamagnetic signal rises rapidly to a much higher peak (up to 5 gauss), and then decays rapidly. This behavior (shown by Fig. IV-3) is correlated with a change of oscillator loading. For about 150 μsec the oscillator is well loaded, as indicated by the relatively low rf electrode voltage seen on the first portion of the oscillogram. At the end of this time the oscillator loses most of its plasma load and the diamagnetic signal begins its rapid decline. This change in loading is most extreme for D_2 pressures below 2 μ.

Density Measurements

Two techniques of density measurements are under development, as follows.

(a) Density measurement by the velocity of a 2.5-Mc Alfvén wave propagating under nonresonant conditions. This technique has been developed and confirmed by other density measurements at higher pressures in the Hothouse I experiment.[3]

(b) Langmuir probe. This technique (with simplifications) will be modeled after recent Langmuir probe work reported by the Plasma Physics Laboratory in Princeton, N. J.[4]

---

3. A. W. DeSilva, Experimental Study of Hydromagnetic Waves in Plasma (Ph. D. Thesis), UCRL-9601, March 17, 1961.

4. J. M. Chapuk et al., A Probe System for Stellarator Plasma Research, MATT-139, June 1962.

Probably neither of these measurements will be possible in the presence of the 8.3-Mc rf field, but it is planned to crowbar the oscillator and make the density measurements a few microseconds thereafter.

B. Spectroscopic Observation of a Decaying Hydrogen Plasma

William S. Cooper, III, John M. Wilcox, and Forrest I. Boley

The average longitudinal variation of the ion density in the Hothouse I plasma as a function of time was determined by side-on observations at five longitudinal positions of the relative intensity of the continuum radiation at 5305 Å. The detector was an RCA 1P21 photomultiplier used with a narrow band-pass interference filter. The region of the plasma spectrum transmitted by the filter was scanned with a monochromator to guarantee that no impurity lines were also observed. At temperatures around 10,000 °K (typical of this plasma) the intensity of radiation from a hydrogen plasma at this wavelength is almost independent of the temperature, but is proportional to the product of the ion and electron densities. Relative ion density measurements made in this manner indicate a variation behind the ionizing wave of about 25%. A sharp jump occurs in the ion density at the end of the tube at 40 μsec, when the ionizing wave strikes the screen. This density perturbation disappears in about 40 μsec, approximately the time required for an acoustic wave to travel the length of the tube. After 80 μsec, the density seems to be uniform along the magnetic field lines to within about 15%.

The longitudinal variation of the temperature of the plasma was estimated from the continuum intensity measurements just described and from similar measurements of the relative intensity of the H_β line. These measurements indicated that after 80 μsec the temperature along a magnetic field line is probably uniform to within about 20%.

End-on measurements at five values of the radius (similar to but more accurate than those described in the preceding semiannual report), looking parallel to the axis of the tube, yielded radial profiles of the ion density and temperature, averaged over several shots. The measurements near the wall of the tube and late in time indicated an additional contribution to the continuum radiation, probably due to the H^- ion. These measurements, and also evidence obtained from end-on framing-camera pictures, indicate conclusively that there is no loss of the plasma during the observed decay period by diffusion of the plasma across the magnetic field. The fact that the longitudinal ion density profiles are essentially flat after 80 μsec indicates that the plasma is not lost to the ends of the tube either by diffusion through neutrals or by free streaming.

Very careful measurements of the ion density and temperature were made by end-on observations at one radius, about midway between the center of the tube and the outer wall. These measurements were similar to those described in the preceding semiannual report, but were more accurate. Absolute-intensity measurements were made of the intensity of the H_β line as a function of time, and also of the intensity of the continuum radiation at 5305 Å and 3225 Å. The ratio of any two of these intensities is a function only of the temperature. The time dependence of the temperature (a weighted average of the three temperature determinations) on a single shot, with estimated experimental errors, is shown in Fig. IV-4. By use of the temperature at a given

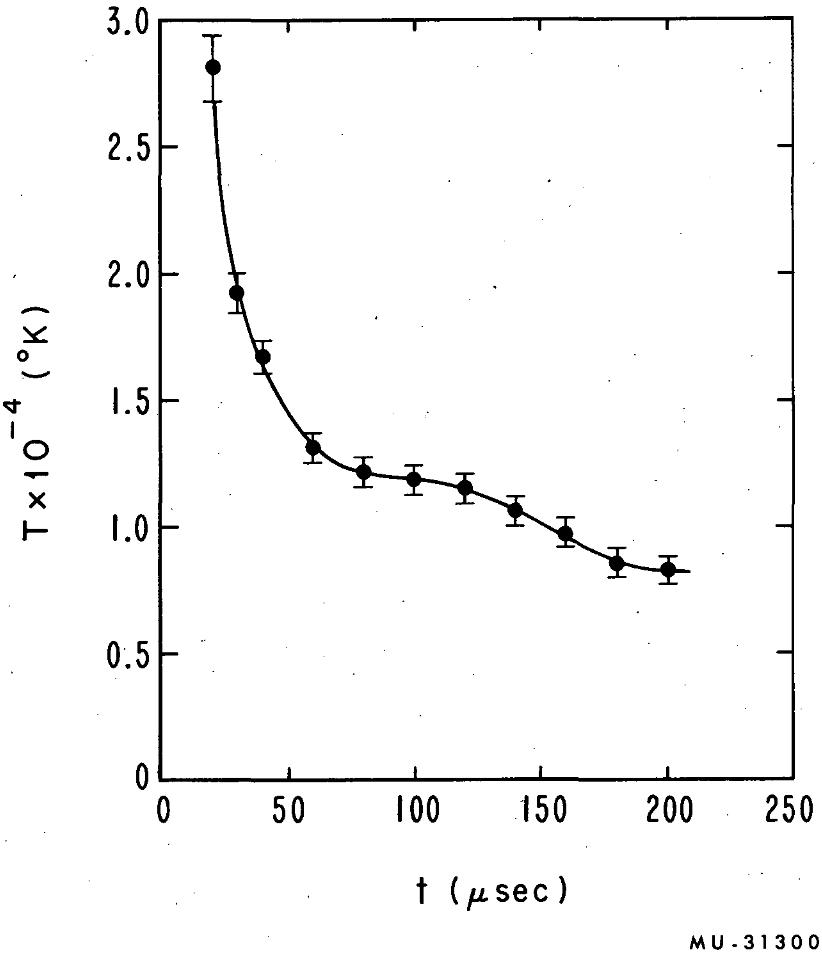

Fig. IV-4. Temperature as a function of time for a typical shot.

time as determined in this manner, three values of the ion density may be calculated. The time dependence of the ion density (a weighted average of the three density determinations) is shown in Fig. IV-5.

Departures of the state of the decaying plasma from LTE (local thermodynamic equilibrium) may be observed by plotting the ion density as a function of temperature for this particular shot. Figure IV-6 shows this "decay curve." Also shown is a theoretical curve calculated from Saha's equation (labeled "LTE"), assuming the plasma is always in LTE and fitted to the early portion of the decay curve, when the plasma apparently is completely ionized. The total particle density for this fit is 4.6×10^{15} cm^{-3}. Only experimental errors are shown; the points before 80 μsec are more uncertain than indicated because of the longitudinal nonuniformities. The plasma apparently is fully ionized initially but with an ion density less than the initial hydrogen atom density (which was 5.8×10^{15} cm^{-3}), cools for the first 120 μsec essentially in LTE, and then departs from the equilibrium curve. The departure from the LTE curve occurs at the temperature at which detailed balance in the collision rates affecting the population of atoms in the ground state fails. This fact has been verified by use of rate coefficients calculated by Bates, Kingston, and McWhirter.[5]

The recombination coefficient calculated from Fig. IV-5 varies from about 1.5×10^{12} cm^3/sec at 80 μsec to 7.2×10^{-12} cm^3/sec at 200 μsec. Comparison of the observed recombination coefficient with values of the recombination coefficient calculated from the theoretical work of Bates, Kingston, and McWhirter[5,6] shows that the observed values are approximately double the theoretical values obtained by assuming the plasma to be opaque to the lines of the Lyman series, and one-third to one-fifth the theoretical values obtained by assuming the plasma to be transparent to all radiation. This situation would be explained if the plasma were almost, but not completely, opaque to the Lyman lines, as is probably the case.

Our present understanding of the decay of the Hothouse I plasma may be summarized as follows: The plasma in most of the volume is initially fully ionized. The ion density never exceeds about 80% of the initial hydrogen atom density. The atoms are apparently redistributed during the ionization process; the "lost" atoms are probably located near the outer wall of the tube, where the plasma is never completely ionized. The plasma decays by volume recombination; losses by diffusion appear to be negligible. The plasma cools essentially in LTE until the temperature drops below about 1.2×10^4 °K; after this time the temperature is too low for detailed balancing of the collisional processes governing the population of the ground state to hold, and the plasma departs from the LTE cooling curve. The recombination rates agree well with those calculated from the theoretical work of Bates, Kingston, and McWhirter,[5,6]

---

5. D. R. Bates, A. E. Kingston, and R. W. P. McWhirter, Recombination Between Electrons and Atomic Ions. II. Optically Thick Plasmas, Proc. Roy. Soc. (London) 270A, 155 (1962).

6. D. R. Bates, A. E. Kingston, and R. W. P. McWhirter, ibid. 267A, 297 (1962).

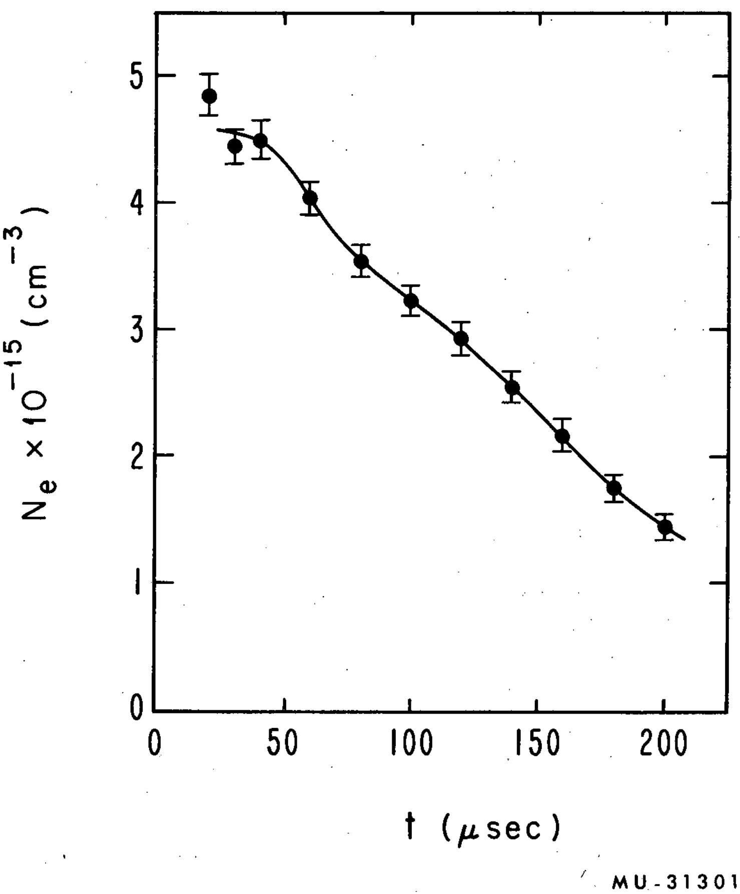

Fig. IV-5. Ion density as a function of time for the same shot as shown in Fig. IV-4.

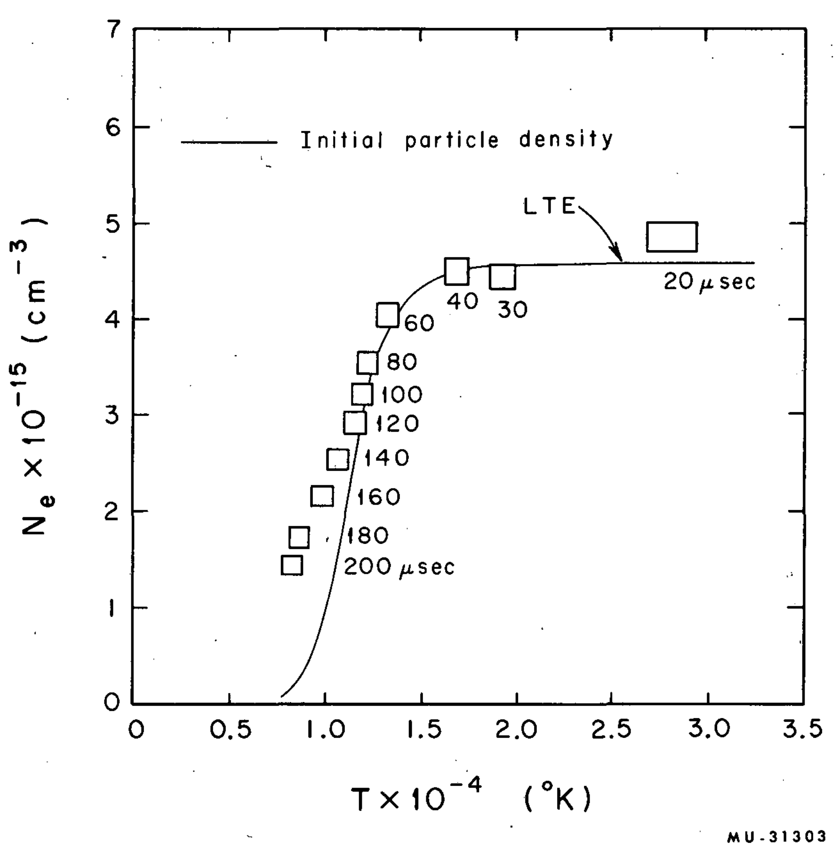

Fig. IV-6. Decay curve for the shot shown in Figs. IV-4 and IV-5. The curve labeled "LTE" was calculated from Saha's equation, fitted to the early portion of the decay curve.

assuming the plasma to be almost opaque to the Lyman lines. More accurate measurements of the rate of decay of the plasma and the departure of the state of the plasma from LTE would require a knowledge of the density of neutral atoms in the ground state.

C. Excitation of Two Hydromagnetic Modes in Hothouse

George R. Spillman, John M. Wilcox, and Forrest I. Boley

Theory

Solving the hydromagnetic wave equation in cylindrical geometry (see A. W. DeSilva, Ref. 3) gives two solutions. One solution (T wave) is a purely torsional wave at low frequency, and exhibits a resonance at the ion cyclotron frequency. The other solution is the TLA wave, which is a compressional wave at low frequency. In general a solution of the wave equation may be written,

$$b_\theta = \sum_n \left(C_{n1} e^{ip_{n1}z} + C_{n2} e^{ip_{n2}z}\right) J_1(k_{cn} r) e^{-i\omega t}, \tag{1}$$

$$b_r = \sum_n \left(A_{n1} e^{ip_{n1}z} + A_{n2} e^{ip_{n2}z}\right) J_1(k_{cn} r) e^{-i\omega t}, \tag{2}$$

and from assumed azimuthal symmetry ($\partial/\partial\theta = 0$) and $\nabla \cdot b = 0$ we have

$$b_z = \sum_n \left(\frac{i}{\chi_{n1}} A_{n1} e^{ip_{n1}z} + \frac{i}{\chi_{n2}} A_{n2} e^{ip_{n2}z}\right) J_0(k_{cn} r) e^{-i\omega t}, \tag{3}$$

where

$$\chi_{n\frac{1}{2}} \equiv \frac{P_{n\frac{1}{2}}}{k_{cn}},$$

and the notation is otherwise the same as DeSilva's:

b ≡ wave magnetic field,

z ≡ axial position,

r ≡ radius.

From DeSilva's field expressions we may obtain

$$\frac{A_{n\frac{1}{2}}}{C_{n\frac{1}{2}}} = \frac{-i\chi_{n\frac{1}{2}}^{2}\Omega}{\beta_n^2 - (1 - i\alpha)(1 + \chi_{n\frac{1}{2}}^{2})} , \tag{4}$$

where

$$\beta^2 \equiv \frac{\omega^2 V_A{}^2}{k_{cn}{}^2}, \quad \text{(MKS units)}$$

$$\alpha \equiv \frac{\omega\eta}{\mu_0 V_A{}^2},$$

$$\Omega \equiv \omega/\omega_{ci} ,$$

$V_A \equiv$ complex Alfvén velocity (see DeSilva) $\equiv$ Alfvén velocity for 100% ionization,

$\frac{\omega_{ci}}{2\pi} \equiv$ ion cyclotron frequency,

$\frac{\omega}{2\pi} \equiv$ wave frequency,

$\eta \equiv$ resistivity.

Equations (1) through (4), together with equations for the wave-exciter fields, determine the relative amplitudes of the field components of the two modes at the exciter end of the plasma tube.

The wave exciter is as shown in Fig. IV-7. We assume the distance between "wastebasket" and outer tube is infinitesimal, and we also assume the wastebasket to be a perfect conductor. From the condition $E_\theta = 0$ at the wastebasket we may obtain

$$\left.\begin{aligned} b_z &= 0 \\ \frac{\partial b_r}{\partial z} &= 0 \end{aligned}\right\} \text{at wastebasket,}$$

and the solution of the wave equation in the region between the wastebasket and the plasma is of the form

$$b_r = DZ_1 (\sqrt{k^2 - k_v{}^2}\, r) \cos k_v z\, e^{-i\omega t},$$

$$b_z = CZ_0 (\sqrt{k^2 - k_v{}^2}\, r) \sin k_v z\, e^{-\omega t} ,$$

with a similar equation for b_θ, where Z_i is a linear combination of Bessel and Neumann functions.

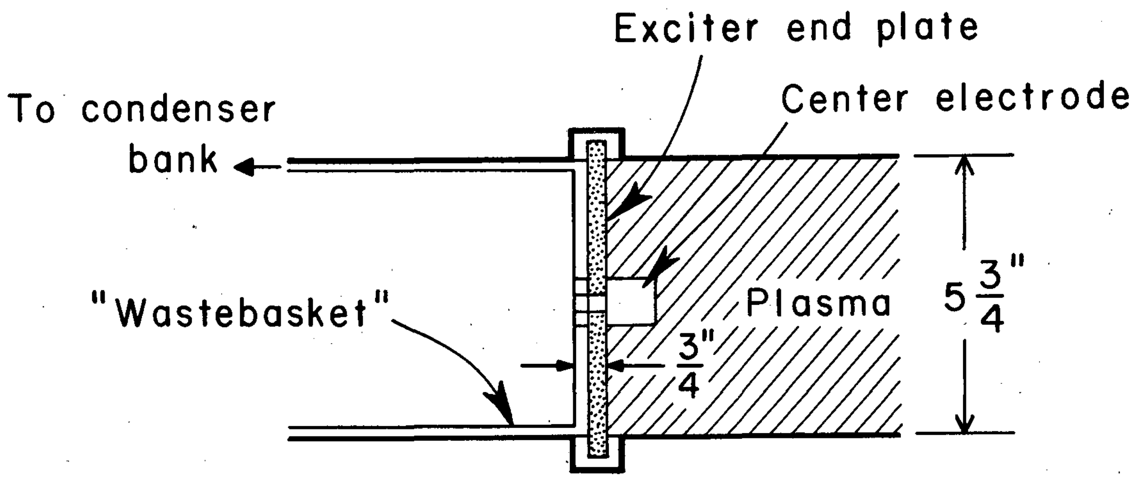

MU-31752

Fig. IV-7. The "wastebasket" is the center conductor of a transmission line from the condenser bank which excites the wave to the center electrode. The distance between "wastebasket" and outer conductor (≈ 0.08 in.) is considered infinitesimal and the wave solution in the cavity region between "wastebasket" and plasma is matched to the plasma wave solution to calculate partition between wave types.

For a frequency of 10 Mc/sec, $k_v \approx 2 \times 10^{-3}\ cm^{-1}$, so we assume $k_v z << 1$, and from $\nabla \cdot b = 0$ and $\partial/\partial\theta = 0$ we have

$$\frac{C \sin k_v z}{D \cos k_v z} = i\sqrt{k^2 - k_v^2}\, z \ .$$

Letting a = distance from wastebasket to plasma, we have, at the plasma boundary

$$\frac{b_z}{b_r} = \frac{Z_0(\sqrt{k^2 - k_v^2}\, r)}{Z_1(\sqrt{k^2 - k_v^2}\, r)}\ i\sqrt{k^2 - k_v^2}\, a. \qquad (5)$$

We assume that there are no sheet currents present in the plasma and that Neuman functions do not exist in the plasma (to avoid infinite fields in the tube center), and from Eqs. (1) through (3) and Eq. (5) we obtain

$$\frac{A_{n2}}{A_{n1}} = - \frac{(1/\chi_1 - k_{cn} a)}{(1/\chi_2 - k_{cn} a)} . \qquad (6)$$

From Eqs. (4) and (6) the excitation ratios of field component in T mode to field component in TLA mode have been calculated for several values of a under the following conditions:

(a) the lowest Bessel mode is assumed for a plasma radius of 7 cm;

(b) axial magnetic field is 16 kG;

(c) deuteron density is $5.3 \times 10^{15}/cm^3$ (80 μ of D_2);

(d) the electron temperature is 10^4 °K .

The results are given in Table I.

The Hothouse III experiment is run at a standard pressure of 80 μ of D_2. However, wave velocity measurements on Hothouse III and spectroscopic measurements on Hothouse I (see IV. 2.B of this report) indicate that a substantial amount of the gas does not become plasma. Calculations in this table assume no loss of gas. Frequencies in parentheses (ν') are multiplied by the ratio of theoretical Alfvén velocity (assuming no loss of gas) to experimental Alfvén velocity. Such scaling is strictly correct only for frequencies far below ion cyclotron frequency (12.2 Mc/sec).

The value $k_{c1} a = 1.04$ is appropriate for all past wave experiments on Hothouse I and III, assuming the plasma does not pull away from the exciter end plate.

Table I. Ratios of field component of T mode (subscript 12) to field component of TLA mode (subscript 11) at exciter for the lowest Bessel mode.

$$b_\theta = \sum (C_{n1} e^{ip_{n1}z} + C_{n2} e^{ip_{n2}z}) J_1(k_{cn} r) e^{-i\omega t}$$

$$b_r = \sum (A_{n1} e^{ip_{n1}z} + A_{n2} e^{ip_{n2}z}) J_1(k_{cn} r) e^{-i\omega t}$$

$k_{c1}a$	a (inches)	(ν')(Mc/sec) / ν (Mc/sec)	(3.93) 2.97	(5.56) 4.20	(6.81) 5.15	(7.86) 5.94
large	large	A_{12}/A_{11}	1	1	1	1
		C_{12}/C_{11}	0.99	3.16	1.59	1.44
1.04	3/4	A_{12}/A_{11}	38	0.23	0.39	0.55
		C_{12}/C_{11}	38	0.73	0.62	0.78
0.52	3/8	A_{12}/A_{11}	11	4.4	3.0	0.81
		C_{12}/C_{11}	11	14	4.8	1.2
0.35	1/4	A_{12}/A_{11}	7.8	2.7	3.2	2.8
		C_{12}/C_{11}	7.7	8.5	5.1	4.0
0.17	1/8	A_{12}/A_{11}	6.1	2.0	2.2	2.0
		C_{12}/C_{11}	6.0	6.3	3.5	2.9
0.085	1/16	A_{12}/A_{11}	5.8	1.9	1.9	1.9
		C_{12}/C_{11}	5.7	6.0	3.0	2.7
0	0	A_{12}/A_{11}	5.1	1.8	1.8	1.8
		C_{12}/C_{11}	5.0	5.7	2.9	2.6

Experimental Results

The wave field $\vec{b}$ for the T wave rotates about the axial magnetic field lines in the same sense as the ions, and $\vec{b}$ of the TLA wave rotates in the same sense as the electrons; hence the two waves may be distinguished by measuring the relative phase of b_r and b_θ. For this purpose a probe capable of measuring the three magnetic field components simultaneously was constructed and used for a series of relative phase measurements. A series of measurements taken at a distance of 32 cm from the exciter end plate are shown in Fig. IV-8. For these data the probe was oriented in such a way that the b_r signal at 0.6 Mc was minimum[7] ($b_r << b_\theta$ for T wave and $\omega << \omega_{ci}$). Fifteen shots were then taken at each frequency. The averages of these shots are plotted in Fig. IV-8 as circles. Occasional wild shots had considerable effect on some of the averages, and where deviations greater than 90° from the average occurred such shots were thrown out and the set of data reaveraged. These recalculated points are plotted as Δ's in Fig. IV-8.

To allow a correction for the finite spacing between the b_r and b_θ coils (6.6 mm) the probe was rotated 90° and selected points were taken. These sets are plotted as squares in Fig. IV-8. We see that the phase reverses sign somewhere between 5.1 and 5.4 Mc.

The relative amplitudes of the two wave types depend upon their attenuation as well as on the relative amplitudes excited at the exciter. To attempt to minimize attenuation effects the probe was moved to about 8 cm from the exciter end plate and further measurements were made. These results are shown in Fig. IV-9. In addition to data at the standard pressure (80 μ) data were also taken at 40 μ pressure. It may be noted that the frequency of transition from positive to negative phase increases from the higher to the lower pressure.

The theoretical predictions of Table I indicate that the presence of a conducting plate close to the plasma may have an important effect on partition of energy between the two wave types. To test this prediction an end plate has been constructed with concentric copper rings imbedded within the exciter end plate. Rings were chosen rather than a solid plate or a screen because the theory requires only the condition $E_\theta = 0$, and it was felt that holding $E_r = 0$ so close to the plasma might have a decoupling effect for the wave exciter. The rings are 0.040 in. wide and 0.030 in. thick with 0.030 in. spacing between, and extend from the o. d. of the center electrode to the i. d. of the copper tube. An upward shift of the transition frequency with insertion of this plate will be sought.

---

7. This turned out to be an 8° correction on the geometrically aligned probe. It is believed that this 8° can be accounted for by drooping of the probe tube, which was not taken into account in the geometrical alignment. (This does not rule out the possibility of other important effects.)

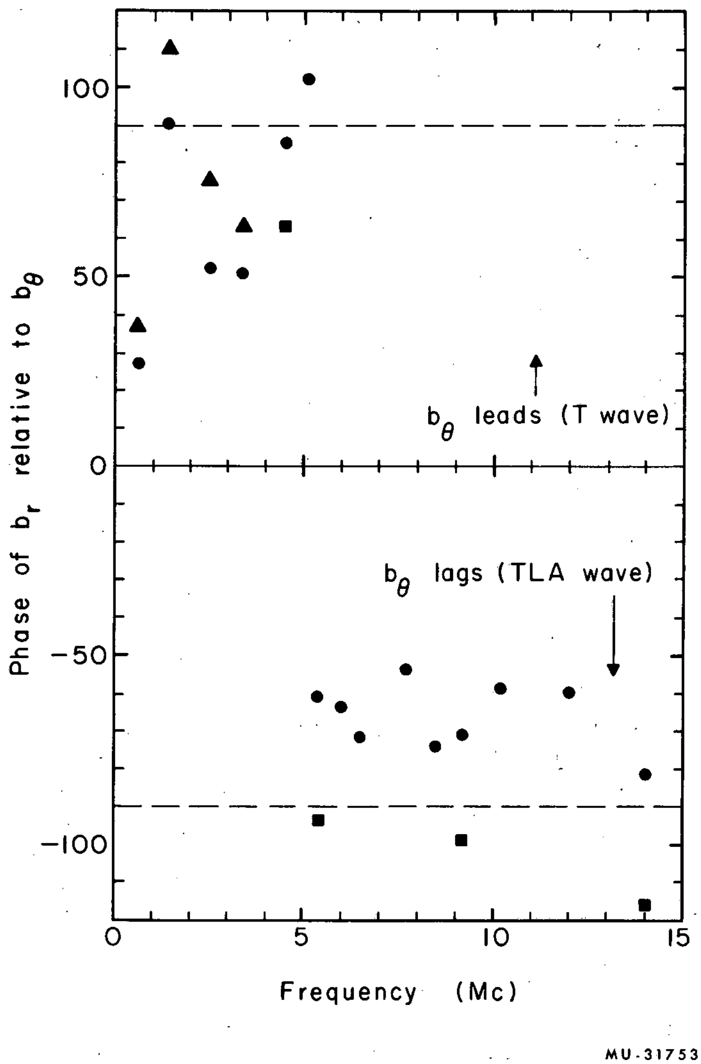

Fig. IV-8. Relative phase of b_r and b_θ at an axial position 32 cm from exciter end plate. O: averages, usually more than 15 shots. Δ recalculation of average after throwing out shots varying more than 90° from average. For both O and Δ the b_θ coil is in front of the b_r coil. □: data obtained by rotating the probe 90° so that b_r coil precedes b_θ coil.

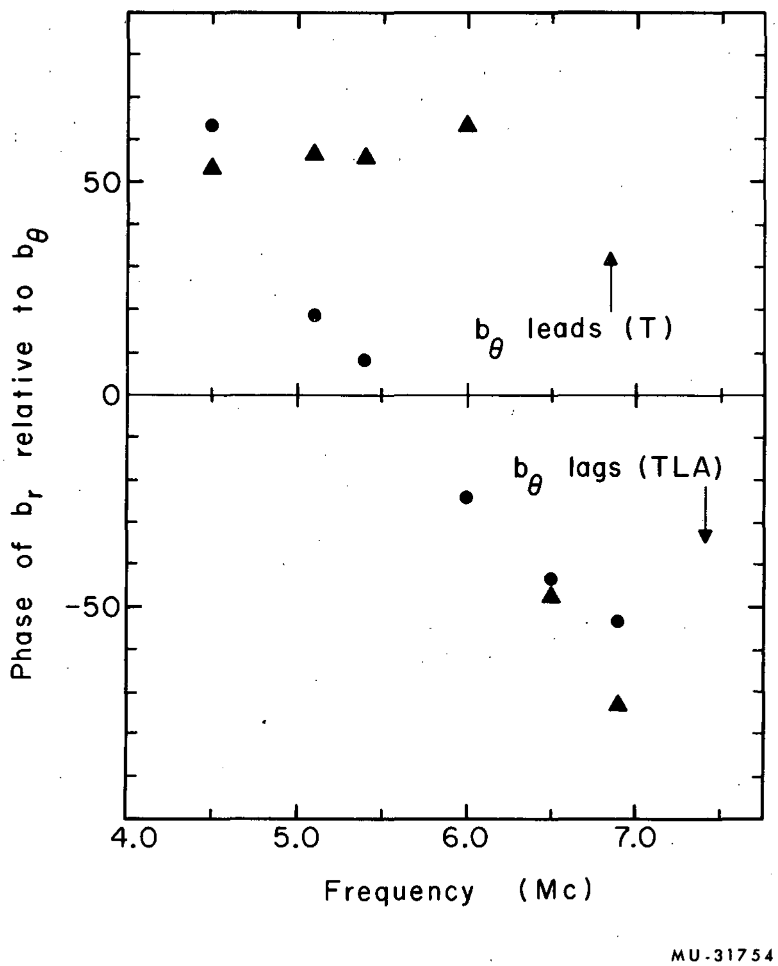

Fig. IV-9. Relative phase of b_r and b_θ for two gas pressures at an axial position of 8 cm from the exciter end plate. Data are not corrected for finite spacing between coils. Each point is an average of about 15 shots. O: 80 μ D_2; Δ: 40 μ D_2.

D. A Plasma Surface Wave

George R. Spillman, John M. Wilcox, and Forrest I. Boley

The cylindrical plasma in which the propagation of hydromagnetic waves is to be studied established by a hydromagnetic ionizing current sheet.[8] When the tube is filled with plasma this current is crowbarred, and the plasma then begins to decay. The behavior of Alfvén waves induced at various times in the decaying plasma has been investigated. A sudden increase in the apparent Alfvén velocity was observed for a wave that was induced after the plasma had decayed for 200 μsec. Closer examination of the wave form at a fixed radial and axial position and various wave times revealed a small peak appearing before the Alfvén wave (Fig. IV-10a) which grew in amplitude relative to the Alfvén wave for later and later wave times (Figs. IV-10b through 10d). An investigation of the time of arrival and amplitude of this "precursor" peak and of the Alfvén wave was initiated. Some results are shown in Figs. IV-11 through IV-13.

From such data it has been concluded that a fast wave propagates in a low ion density region near the tube wall (surface wave) and diffuses radially into the plasma. For diffusion into a uniform plasma with a plane boundary the radial velocity should be given by

$$v_r = \sqrt{\frac{2\omega\eta}{\mu_0}} \qquad \text{(in MKS units)},$$

where η is the local plasma resistivity and ω is the radian frequency of the wave. The amplitude of the wave as a function of radius should be given by

$$b_\theta \approx \exp[-\gamma(r_0 - r)],$$

where r_0 is the outer plasma radius and

$$\gamma \equiv \sqrt{\omega\mu_0/2\eta} .$$

Experiments were performed at a frequency of 3.1 Mc/sec. Measured radial velocities for wave times of 150 to 240 μsec are about 30 cm per μsec, which indicate a temperature of 0.24×10^4 °K in the region.

The wave amplitudes are not exponential. This is likely due to cylindrical geometry and nonuniformity of temperature with radius. Rough estimates for γ were obtained by assuming γ to be the reciprocal of the distance in which the amplitude falls by 1/e as measured near the point of the half-maximum amplitude. The average value of γ thus obtained for wave times of 100 μsec to 240 μsec is

$$\gamma_{exptl} = 0.56/\text{cm} .$$

8. For a description of method of plasma production and of properties of a plasma in an essentially identical device, see Wilcox et al., J. Nucl. Energy-Part C, 4, 337 (1962), and Cooper, this report.

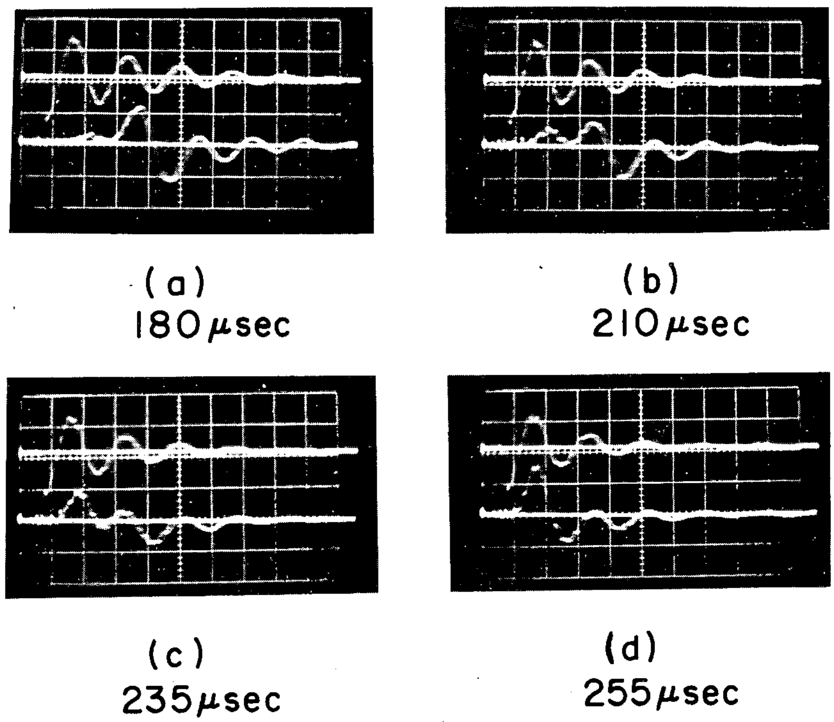

ZN-3933

Fig. IV-10. Appearance of surface wave on probe signals. Wave times are given beside pictures. Top trace is dI/dt of wave exciter, bottom trace is db/dt at probe. On shot a the surface wave is barely visible. By 255 μsec (shot d) the surface wave dominates. Gains are the same for all four shots. The probe is at midplane and 4 cm radius.

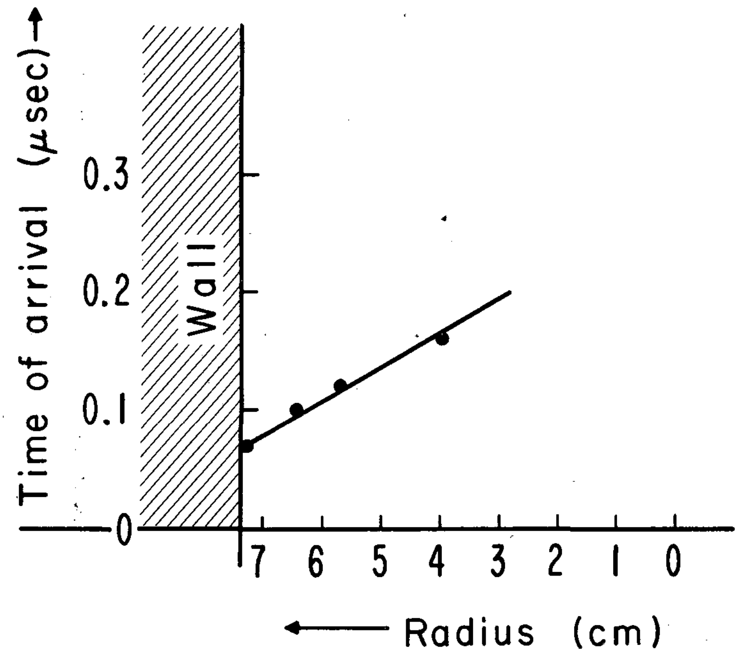

MU-31747

Fig. IV-11. Time of arrival of surface wave vs radius at midplane. Wave time is 210 μsec.

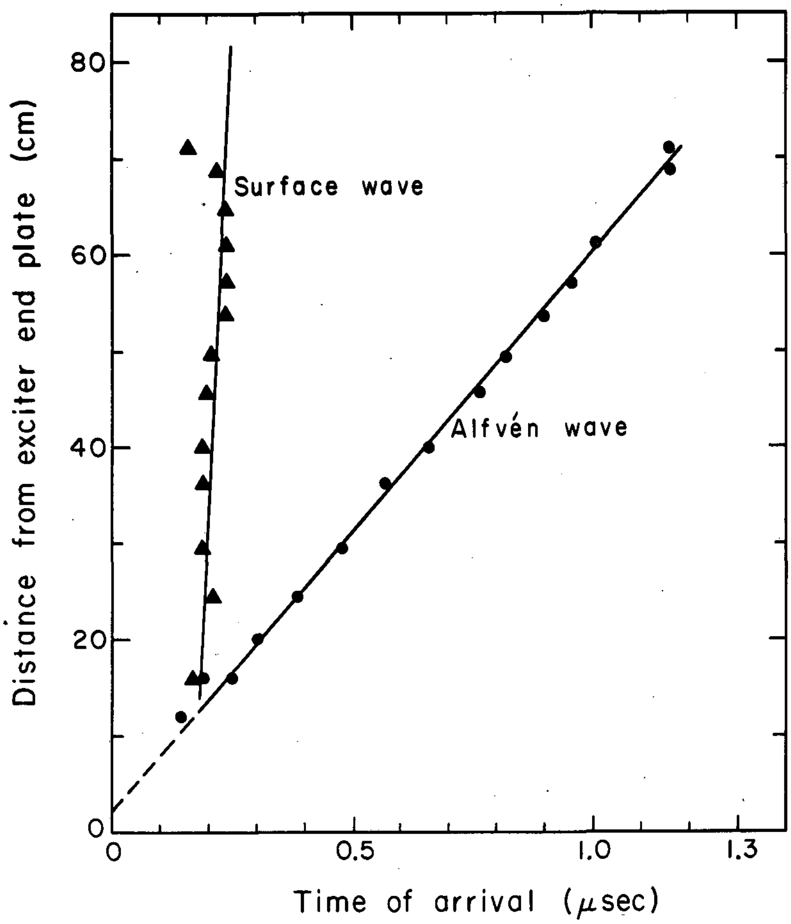

Fig. IV-12. Times of arrival of surface wave (Δ) and Alfvén wave (O) as a function of axial position. The radius is 4.8 cm and the wave time is 132 μsec. Each point is an average over three shots. Below the intersection of the two lines the Alfvén and surface waves are not readily distinguishable.

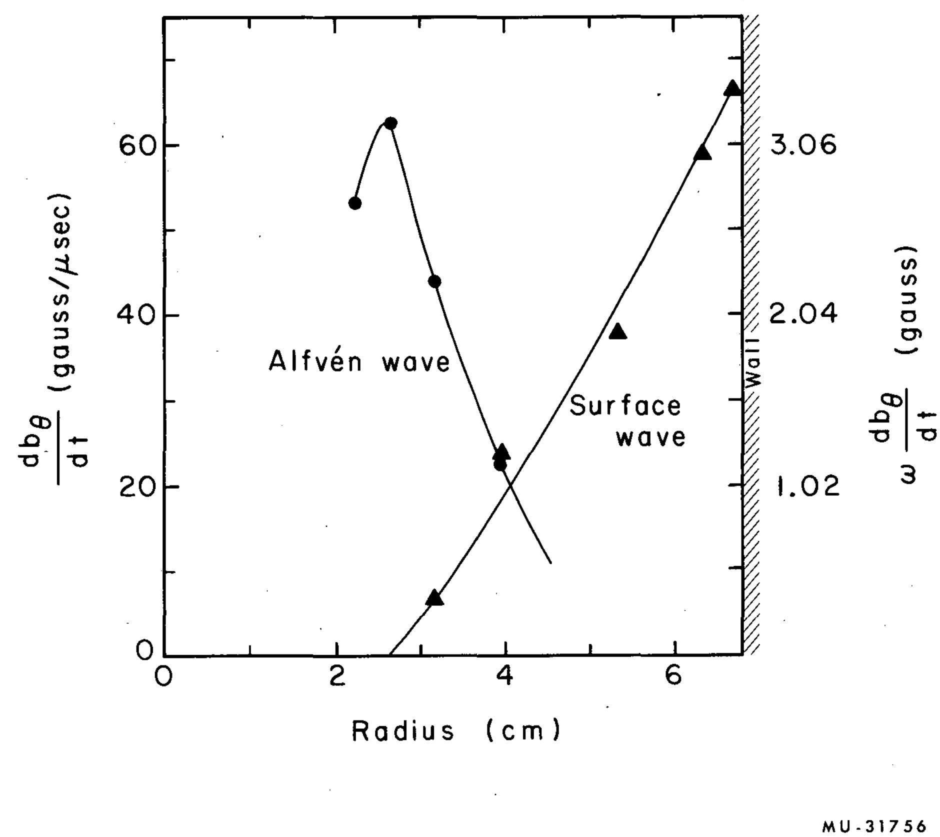

Fig. IV-13. Alfvén wave (O) and surface wave (Δ) amplitudes as a function of radius at midplane. The wave time is 180 μsec. Each point is averaged over three shots.

(Over the wave times mentioned here the fluctuations in both v_r and γ do not appear to be systematic with wave time.)

The calculated value for γ, assuming $T = 0.24 \times 10^4$ °K, is 0.67/cm.

3. HYDROMAGNETIC IONIZING FRONTS

Arthur R. Sherwood and Wulf B. Kunkel

It has been found that our apparatus[1] is not yet properly producing the hydromagnetic ionizing front that we wish to study. Typical conditions are a gas pressure of 200 μ H_2, an axial magnetic field of 14 kG, and a driving current of 10,000 A. A front is produced, and it travels down the apparatus parallel to the axial magnetic field as it should. It has been determined, however, that the initial breakdown occurs as a single spoke in the annular experimental region rather than as an azimuthally uniform ring. Thus the front now being produced is a rotating spoke which "cork-screws" down the apparatus. At present we are still attempting to eliminate this azimuthal asymmetry and to produce a uniform front.

The principal means of diagnosis used to arrive at the above conclusions were the signals from current buttons located in the outer wall and photographs of the luminosity pattern of the discharge. The current buttons are similar to those used in Hothouse I.[2] The photography was done using first a Kerr cell and later an image-converter camera. In both cases the camera looked up axially through the annular pyrex end plate at the "receiving" end of the apparatus. In order to eliminate confusing wall reflections, the lenses of a large surplus aerial camera were used to obtain a parallax-free optical system.[3]

---

1. Arthur R. Sherwood and Wulf B. Kunkel, in Controlled Thermonuclear Research Semiannual Report, UCRL-9969, Jan. 19, 1962, p. 66.

2. John M. Wilcox et al., Experiments on Alfvén-Wave Propagation, UCRL-9482, Nov. 1960, p. 17.

3. Klaus Halbach, Matrix Representation of Gaussian Optics, UCRL-10709, Section 5f, May 24, 1963.

4. ON THE HEATING OF ELECTRONS IN WEAKLY IONIZED GASES BY APPLIED ELECTRIC AND MAGNETIC FIELDS

Wulf B. Kunkel and Gary A. Pearson

The analytic work on the behavior of electrons in very weakly ionized gases in the presence of crossed electric and magnetic fields has been brought to a conclusion. The study had begun as an attempt to shed light on the initial phase of the Homopolar discharges described elsewhere in these reports. Later it appeared that the considerations may be of a more general significance. The major contribution of our efforts consisted of a detailed analysis of the electron velocity distribution by describing the latter in the frame of reference that moves along with the E x B drift velocity.[1,2] This description is useful in discussing strong magnetic fields, such that the electron gyrofrequency is much larger than the electron collision frequency. Our analysis was applied to the case of hydrogen, including inelastic and ionizing collisions, and some numerical computations were carried out that could be compared with experimental observations.[2,3]

In principle, these calculations should be more accurate than those based on the conventional method of solution.

In the conventional approach the electron velocity distribution is expanded in spherical harmonics and the first term is assumed centered in the gas frame of reference rather than in the drift frame.[4] Moreover, it should be noted that the conventional analysis is usually applied to steady-state or nearly steady-state problems. In the final phase of our study we investigated the conditions under which the usual method by expansion in spherical harmonics can be applied to nonstationary conditions. In particular we were interested in the evolution of the distribution of electron speeds and the rate of change of the mean energy when a steady electric field is applied abruptly--i.e. fast compared with a mean collision time.

---

1. Gary A. Pearson and Wulf B. Kunkel, Phys. Rev. <u>130</u>, 864 (1963).

2. Gary A. Pearson and Wulf B. Kunkel, Electron Energy Distributions and Ionization Rates in Hydrogen with Crossed Electric and Strong Magnetic Fields, UCRL-10366, Sept. 5, 1962.

3. Gary A. Pearson, in Controlled Thermonuclear Research Semiannual Report, UCRL-10294, July 20, 1962, p. 59.

4. W. P. Allis, Handbuch der Physik (Springer-Verlag, Berlin, 1956), Vol. 21, p. 404.

It was found that the primary condition can be written in the form[5]

$$\left| u_c \frac{\partial f_0(v,t)}{\partial v} \right| << f_0(v,t), \tag{1}$$

where $f_0(v,t)$ denotes the isotropic part of the velocity distribution of the electrons (assumed uniform in space, for simplicity). Here $u_c(v) = eE/m(\omega^2 + \nu^2)^{1/2}$ is the drift speed of electrons with random speed v, $\omega = eB/cm$ is their gyrofrequency, and $\nu(v)$ is their collision frequency. Condition (1), in turn, is usually satisfied after several mean momentum-transfer collision times, provided inelastic collisions are relatively unimportant so that $2\bar{\epsilon}/m \equiv \langle v^2 \rangle >> u_c^2$. The analysis breaks down, of course, when electron "runaway" occurs.[6] This phenomenon is precluded for $E << B$, however, because then $u_c(v) \leqslant cE/B << c$ for all values of v.

When condition (1) is satisfied the evolution of $f_0(v,t)$, which is spherically symmetric in v, obeys the equation

$$\frac{\partial f_0}{\partial t} = \nabla_v \cdot (D \nabla_v f_0 + \frac{m}{M} \vec{v} \nu f_0) + \left(\frac{\partial f}{\partial t}\right)_{inel}, \tag{2}$$

where ∇_v denotes differentiation in velocity space, $(\partial f/\partial t)_{inel}$ describes the effect of inelastic collisions, m/M is the mass ratio of electrons and gas molecules, and the diffusion coefficient in velocity space is defined by

$$D(v) = \frac{\nu}{3}\left(u_c^2 + \frac{3kT_g}{M}\right). \tag{3}$$

The right-hand side of Eq. (2) is identical with the form obtained for the steady state.[4] The effect of a finite gas temperature T_g has been taken into account. We note that for $\omega \gg \nu$ we have $u_c \approx cE/B$, and the quantity in parentheses in Eq. (3) is the mean square velocity of the gas molecules in the E x B drift frame, i.e., in the frame of reference in which the electric field is zero. Hence, when viewed in this frame the electrons gain energy only from gas collisions and not from the electric field.

Equation (2) may now be multiplied by $mv^2/2$ and integrated to give the rate of change of mean energy $d\bar{\epsilon}(t)/dt$. If the inelastic collisions are primarily exciting rotational and vibrational energy levels of the molecules so that only small amounts of energy are removed, they may be formally combined with the elastic recoil losses by means of a dimensionless multiplier $\lambda(v)$. The result of the integration then takes the form

$$\frac{d\bar{\epsilon}}{dt} = \frac{m}{M}\left\langle (Mu_c^2 + 3kT_g)(\nu + \frac{v}{3}\frac{d\nu}{dv}) - \frac{3}{2} m\lambda \nu v^2 \right\rangle, \tag{4}$$

5. Wulf B. Kunkel and Gary A. Pearson, On the Heating of Electrons in Crossed Electric and Magnetic Fields, UCRL-10800, June 19, 1963.

6. G. Ecker and K. G. Müller, Z. Naturforsch. 16A, 246 (1961).

where the angular brackets, as usual, indicate the average over the distribution function. The term $(\nu + v d\nu/3dv)$ is, of course, always positive for electron-atom collisions, just as for screened Coulomb collisions, except sometimes in narrow velocity regions caused by the so-called Ramsauer effect. The latter may cause a distortion of the shape of the distribution function, but the average over-all speeds make the heating term in Eq. (4) always greater than zero.

5. SHEET PINCH STUDIES

Oscar A. Anderson

Furth's theory of resistive instability[1] has been responsible for a recent shift in emphasis in the sheet pinch program. Formerly the behavior of the Triax pinch at high power levels was studied with the main techniques of spectroscopy and stereoscopic streak photography. These yielded useful information about the early part of the discharge, up to approximately half of peak current. However, at higher currents the light from the main discharge region is so weak compared with light from the cooler electrode regions that these methods are unsuitable.

The one firmly established fact about the high-current part of the discharge was that shortly before peak current, neutrons start to appear simultaneously with a spike in the tube voltage. This was reminiscent of the behavior of simple unstabilized pinches, except that in the Triax the neutrons show no measurable energy shift. Correspondingly, the amplitude of the voltage spike is of the order of 1 kV instead of hundreds of kilovolts.

It was impossible to understand the production of neutrons on the basis of such incomplete experimental information. Plasma-stability theory gave no assistance because it was also in a primitive state. According to conventional infinite-conductivity theory, unstable modes were not expected on the observed time scale. Lately the situation has been changed by Furth's finite-conductivity theory, which predicts completely new unstable modes. One of these, called the tearing mode, is important in sheet pinches such as the Triax or the reversed-field θ pinch. Rough estimates show that this mode may develop in the Triax under the high-power, low-density conditions associated with a neutron burst. If this were verified, it would lead toward an understanding of the neutron production mechanism. Moreover, an experimental study of the tearing mode at finite amplitude would encourage further development of the theory, which presently treats only infinitesimal perturbations.

The linearized theory is rather complete, and it is possible to make fairly accurate calculations of initial growth rates and to predict the wavelength of the fastest-growing small-amplitude mode in the Triax. But in order

---

1. Harold P. Furth, John Killeen, and Marshall N. Rosenbluth, Phys. Fluids 6, 459 (1963).

to make such calculations, one must know the zero-order conditions. For example, the magnetic field distribution across the current layer must be measured experimentally. Also, in order to confirm that the instability occurs and to study its large-amplitude form, new methods of observation are needed. For these reasons an experimental program has been undertaken which aims to correlate with the finite-conductivity theory as completely as possible.

As the first step in this program, a magnetic probe was used to obtain the field profile in the Triax under high-level operation. Somewhat surprisingly, there was no difficulty with probe breakage or excessive contamination of the tube. The probe signals showed reasonable reproducibility up to the beginning of neutron emission. Violent fluctuations were observed at all probe positions subsequently. These fluctuations, which are related to the tube voltage spike mentioned above, show that the neutron production is certainly associated with some kind of instability. To determine the wavelength and direction of the instability, multiple probes are necessary. Both internal and external types will be provided. Meanwhile, the single-probe data are being analyzed for use in the growth-rate calculations.

The second step in the program, which is still in progress, was to photograph the entire volume of the Triax at various times and conditions of interest. A new screen-anode which permits this has been designed and installed. Photographs have been made with a six-channel Kerr-cell framing camera. Since, the light from the main discharge region is weak with deuterium at high power levels, the best results have been obtained at reduced power, particularly with helium or argon. An unforeseen result, most pronounced with argon, was that current bunching can occur without necessarily leading to gross hydrodynamic instability. However, the expected helical distortion of the bunches did appear with helium at low pressures. (See Fig. IV-14.) Since there are many pitfalls in optical diagnostics, some obvious checks will be made. Another present objective is to find optimum conditions of bank energy and tube pressure for photographing the instability associated with the voltage spike. Then, later, these same conditions will be used for multiple-probe correlation studies.

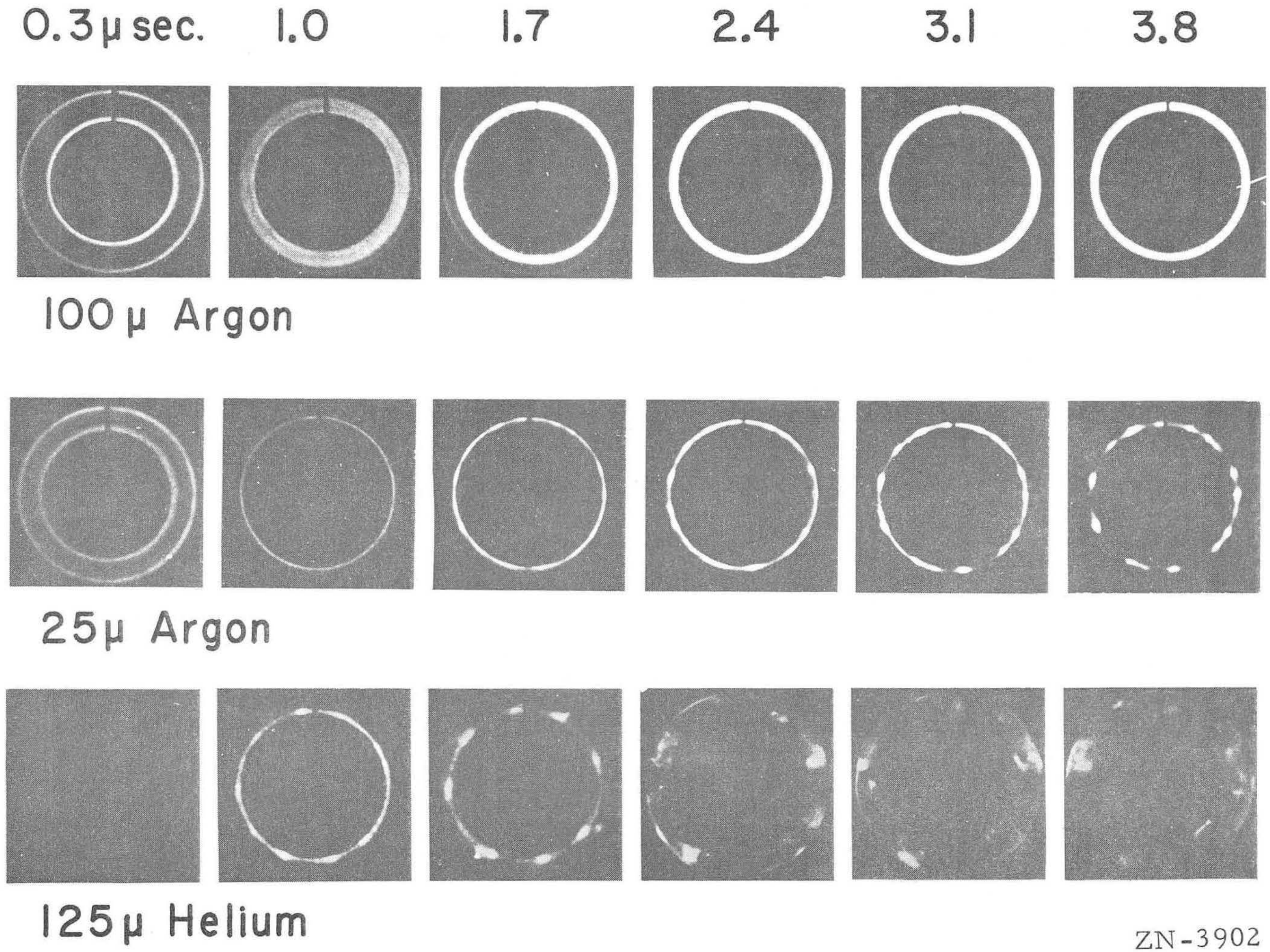

Fig. IV-14. Kerr-cell photographs of 6×10 Triax. Condenser bank: 85 μF at 18 kV. Rise time: 2.3 μsec.

6. EXPERIMENTS ON LORENTZ IONIZATION, GAS COLLISIONAL EXCITATION AND ELECTRON DETACHMENT, AND DIFFUSION OF PARTIALLY IONIZED PLASMAS

Reported by Robert V. Pyle

(Klaus H. Berkner, Vincent J. Honey, Robert V. Pyle, Henry F. Rugge, and J. Warren Stearns have contributed to most of the following experiments. In addition, John R. Hiskes, Selig N. Kaplan, and George A. Paulikas have been associated with the Lorentz ionization and the gas collision experiments, and Joseph Winocur with the diffusion from a line source experiment.)

A. Excitation of H^0 by Nonionizing Collisions and Lorentz Ionization

Hiskes has shown that changes in the excitation level of a neutral hydrogen atom, brought about by nonionizing collisions with trapped particles in a thermonuclear machine, may contribute greatly to the growth of the trapped plasma.[1] This is because Lorentz ionization appears to be the main trapping mechanism in present high-energy neutral injection experiments, and only one or two of the quantum levels can be trapped in a useful region of the magnetic field. However, if the charged-particle density within the confining geometry exceeds some reasonably low level then many of the otherwise wasted atoms in the beam, which have lower excitation levels, can be raised into the Lorentz region and contribute to the trapped density. We are carrying out experiments to investigate the excitation cross sections for such processes. To date the experiments have been performed with neutral rather than ionized targets, at high energies, with dc magnetic fields, and for the quantum levels $n = 5$ through 10. The experiment and the results have been described.[2] A typical excitation cross section is from the $n = 6$ to the $n = 7$ level: $\sigma_{6,7} \approx 1 \times 10^{-18}\, cm^2$ per atom with H^0 atoms incident at 10 MeV on H_2 gas. We believe from theory and from analogy with other high-energy collision experiments (although we have not yet demonstrated this experimentally) that the cross section can be extrapolated as $1/E$ down to approx 100 kV.

We have also demonstrated that the probability for production into quantum level n by the breakup of H_2^+ ions in hydrogen gas goes approximately as $(2 \text{ to } 3)/n^3$, that the electron detachment probabilities in electric or magnetic fields are in good agreement with the calculations of Rice and Good, and that the collisional ionization cross sections are approximately 1/5 of the collisional excitation cross sections in this region.

---

1. John R. Hiskes, Cascade Processes in Energetic Neutral Hydrogen Beams, UCRL-7356, June 1963; presented at the Sixth International Conference on Ionization Phenomena in Gases, Paris, July 8-13, 1963.

2. Klaus H. Berkner, John R. Hiskes, Selig N. Kaplan, George A. Paulikas, and Robert V. Pyle, The Excitation and Lorentz Ionization of 10-MeV Hydrogen Atoms (UCRL-10802, June 1963)(paper for presentation at Third International Conference on the Physics of Electronic and Atomic Collisions, London, July 22-26, 1963).

Hiskes' cascade calculations are based on an analysis by Milford and co-workers for neutral collisions with charged particles. These excitation cross sections vary as n^4. The theoretical opinion based on neutral-neutral collisions for very low quantum levels was that the neutral-neutral collision cross sections might be expected to be similar to those for neutral-charged collisions, but smaller by perhaps a factor of 10. Our measured cross section for the $n = 6$ to $n = 7$ transition is lower by a factor of 600 than the extrapolated neutral-charged cross section. In a yet unpublished paper Bouthilette, Healey, and Milford have calculated excitation cross sections for inelastic collisions of hydrogen atoms with hydrogen atoms for processes of the type

$$H(n, \ell) + H(1, s) \rightarrow H(n', \ell') + H(2s, 2p)$$

for $n = 2, 3,$ and 4, and for those excitations in which $n' = n + 1$. It would appear that these excitation cross sections vary approximately as n rather than as n^4, and assuming that this dependence can be extrapolated to the $n = 6$ level, we obtain for the sum of all the partial cross sections a figure which is slightly lower than our experimental value. If excitations into the continuum, of the form

$$H(n, \ell) + H(1, s) \rightarrow H(n', \ell') + H^+ + e^-,$$

are estimated and added to the nonionizing estimate we can obtain a value in good agreement with the experiment. It is of course too early to tell if this is the correct procedure. Milford has shown that in neutral-charged collisions the excitation cross sections with $|\Delta n| \geq 2$ are smaller by at least an order of magnitude than that for $|\Delta n| = 1$. We have some evidence to show that this may not be true for neutral-neutral collisions.

Two types of IBM 7090 programs have been set up and debugged for calculations of the populations at various levels after the beam has traversed an arbitrary thickness of gas. Sets of input parameters that give fair agreement with experiment have been deduced.

We are currently developing two kinds of ionized gas targets to replace the neutral gas target. If measurements with plasma targets are successful we will reduce the beam energy by a factor of 10 or more to check the energy-extrapolation formula.

B. The Instability of an Alternating-Current Positive Column in a Magnetic Field

The work on the instability of an alternating-current positive column in a magnetic field has been completed and described.[3] The instability, which was discovered by Lehnert and identified at this Laboratory in dc discharges, was explained by a theory of Kadomtsev and Nedospasov.[4] The driving term

3. Henry F. Rugge, Instability of an Alternating Current Positive Column in a Magnetic Field (Thesis), UCRL-10698, April 1963.

4. B. B. Kadomtsev and A. V. Nedospasov, J. Nucl. Energy, Part C 1, 230 (1960).

in their model is such that we would expect that the instability could not grow if the axial electric field were reversed periodically in a time comparable to or shorter than the e-folding time for the instability. We have examined this hypothesis experimentally in dc half-wave rectified (unidirectional) current and in square and sinusoidal alternating current glow discharges in H_2, D_2, He, Ne, and Ar at frequencies up to 70 kc; we find that with the alternating current the onset of the macroscopic instability is indeed pushed to higher magnetic fields as the frequency is increased.

The Kadomtsev and Nedospasov calculation has been criticized because of the assumed perturbations and unrealistic boundary conditions, and it has frequently been observed that the K-N dc calculation predicts instability at perhaps half of the experimental magnetic field. Johnson and Jerde have attempted to apply the K-N model in a quantitatively and physically more acceptable manner.[5] The IBM 7090 has been programmed to yield both the real part of ω (rotation frequency) and the imaginary part of ω (growth rate) for any m value, and for both dispersion relations obtained from the two analyses. (Assumed perturbations are of the form $f(r) \exp[i(m\theta + kz - \omega t)]$. The solid lines in Fig. IV-15 are an example of the calculations for argon with n = 1, 2, and 3, where the growth rate [Im(ω)] are plotted as a function of magnetic field. This figure gives an example of the greatest differences observed between the K-N and J-J calculations. The difference is less pronounced when neon is used, and with helium the two analyses give almost identical results; helium is also the gas that is most extensively investigated by various experimenters. To compare these calculations with the experiment we take as the ordinate the field-reversal frequency, with the same scale as Im(ω), and plot the critical magnetic field at which an instability develops for a given field-reversal frequency as the abscissa. According to the calculations with dc electric fields the m=1 instability is the first to grow, but at some higher frequency a higher-order mode may grow faster. We might thus expect that the experimentally determined instability fields as a function of frequency should fall along an envelope of the various mode-value curves, as indeed they do in the example shown and in the many other cases that have been experimentally investigated, which cover a variation in growth rates of nearly three orders of magnitude. Unfortunately, the discharge is not bright enough that we can identify the modes from streak photography except in the simple case of m = 1, and indeed it is not clear how the large-amplitude disturbance should be related to the small-amplitude rapidly growing instability.

We conclude that the Kadomtsev and Nedospasov model, as we have applied it to alternating current discharges, can describe the observed phenomena. The K-N and J-J analyses give almost identical results for helium, but for other gases the Johnson and Jerde expressions give results that agree better with experiment in both the dc and ac cases.

---

5. R. R. Johnson and D. A. Jerde, Phys. Fluids 5, 988 (1962).

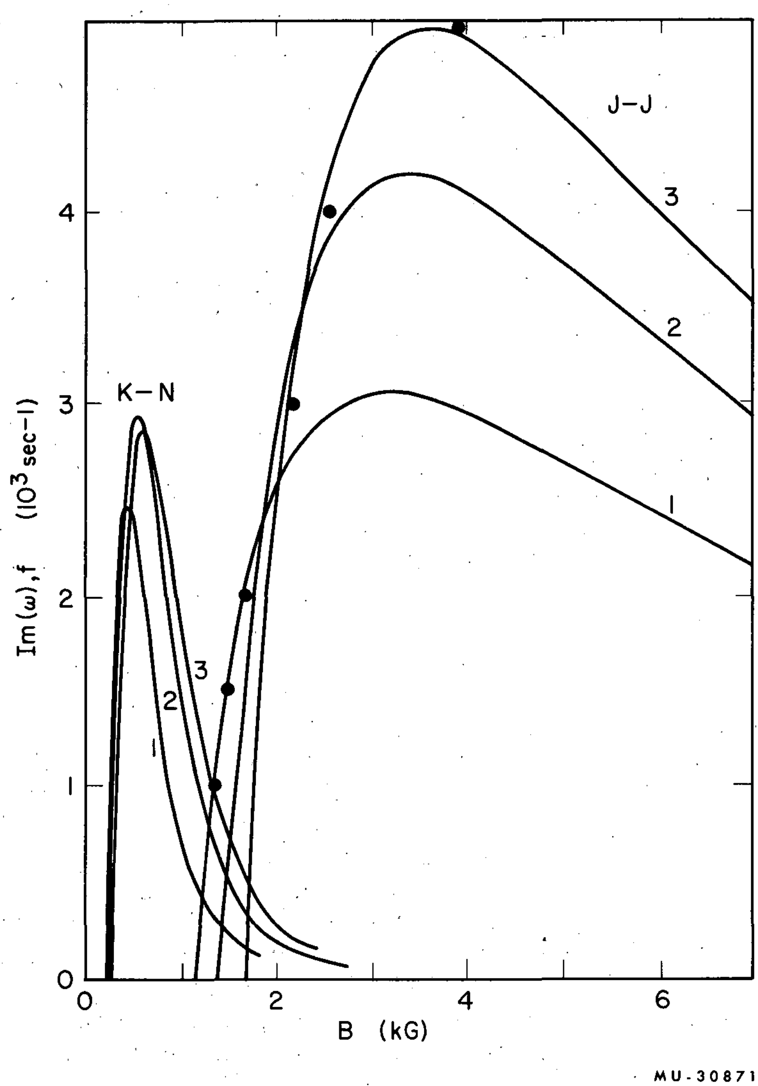

Fig. IV-15. Im(ω), f vs B, with Ar^+, R = 2.75 cm, p = 0.20 mm Hg, I = 500 mA, square wave.

C. Diffusion from a Line Source in a Magnetic Field

The diffusion of plasma in a weekly ionized gas from a line source at the axis of a conducting cylinder with conducting end plates has been remeasured, with emphasis on the ion temperature and the density distribution in the axial direction. The density distributions have been compared with the expression

$$n(r, z) = n_0[AI_0(r/q) + BK_0(r/q)] \cos\frac{\pi z}{L} \qquad (1)$$

$$\approx n_0 r^{-1/2} e^{-r/q} \cos\frac{\pi z}{L}, \qquad \text{for } q \leqslant r < R,$$

where I_0 and K_0 are modified Bessel functions, L is the length of the cylinder, and[6]

$$q = \frac{L}{\pi\omega_i \tau_i}\left(\frac{T_i}{T_i + T_e}\right)^{1/2},$$

or[7, 8]

$$q = \frac{L}{\pi\omega_i \tau_i}.$$

To compare radial density distributions with expression (1) we use values of T_e obtained from Langmuir probe measurements, and λ_i from the work of Chanin and Biondi, and measure T_i, which has been variously estimated to lie between 0.1 eV and 2 eV for experimental situations similar to ours, by an optical absorption technique. Light from a rubidium source at 4215Å wavelength is coincident with a principal line of singly ionized strontium. An argon discharge at 2μ or less is seeded with strontium, the rubidium light is transmitted along various chords, and the absorption measured with a phase-sensitive detection device which records the output of a scanning Fabry-Perot interferometer. From this information a strontium-ion line width is determined, and after correction for instrumental and Zeeman broadening, ion temperature are inferred which we believe are close to the ion temperatures of the predominant argon component in the plasma. These temperatures increase with increasing discharge current and with decreasing pressure and are, for example, close to 0.1 eV at $p = 2\times10^{-3}$ torr argon and $I = 10$ A. The values obtained in this way yield results for the radial density fall-off that seem to be well described by the theories of Zharinov or Tonks ($f = 0$).

We know of only one other attempt to measure the axial density dependence under similar experimental conditions,[9] in which case the density

6. Albert Simon, in Proceedings of the Second United Nations International Conference on the Peaceful Uses of Atomic Energy(United Nations, Geneva, 1958), Vol. 32, p. 343.

7. A. V. Zharinov, J. Nucl. Energy Part C 1, 267, 271 (1960).

8. Lewi Tonks, Phys. Fluids 3, 758 (1960).

9. Stephen D. Rothleder, Charged Particle Diffusion and Energy Transport in a Highly Ionized, Magnetically Confined Plasma (Ph. D. Thesis), Massachusetts Institute of Technology, 1962 (unpublished).

appeared to be independent of the axial position. In our case the measurements agree with a cosine distribution (Fig. IV-16), but--as one might expect--the value of L to be inserted is greater than the actual length of the discharge chamber. We can assume by analogy with the customary diffusion approximation to transport theory that an extrapolation length of about 3/4 of the axial transport mean free path should be added to each end of the chamber. If we assume that there are no axial electric fields the value of L to be inserted in expression (1) is approximately 32 cm. On the other hand, Simon's analysis corresponds to ambipolar diffusion in the axial direction; in this case the effective transport mean free path is increased by the factor $(1 + T_e/T_i)$, and the effective length for our example would be about 38 cm. The experimental values agree well with the latter value of L, although we have no other experimental evidence to suggest that the Simon model is preferable. This work is described elsewhere.[10]

---

10. Klaus H. Berkner, Robert V. Pyle, Henry F. Rugge, J. Warren Stearns, and Joseph Winocur, Diffusion from a Line Source in a Magnetic Field (UCRL-10801, June 1963), submitted to Proceedings VI International Conference on Ionization Phenomena in Gases, Paris, July 8-13, 1963.

7. THERMAL INSTABILITY OF THE GLOW COLUMN*

Günter Ecker†

Kadomtsev and Nedospasov were the first to tackle the problem of the instability of a collision-dominated plasma column with a superimposed external longitudinal magnetic field. In subsequent papers Johnson and Jerde, Holter, and others treated the problem in more detail and with more mathematical rigor. Simon and Krall considered the Kadomtsev-type instability of a low-pressure discharge.

The result of these calculations shows that with increasing magnetic field the m = 1 mode becomes unstable if the magnetic field surpasses a certain critical value B_c.

One of the basic assumptions of all the calculations quoted above is that no temperature disturbance occurs together with the density disturbance. Under these circumstances the m = 0 mode is stable, independent of the magnetic field. The onset of the instability is determined by the m = 1 mode. However, there are experiments that show an instability of the m=0 mode with increasing pressure. Because they neglect the temperature disturbance the calculations of the Kadomtsev type cannot be applied to these observations.

---

*This material is the introduction of a mathematical description of the analysis (unpublished) that is unfortunately too long to include here. --RVP, editor.

†Institute of Theoretical Physics, University of Bonn, consultant to the Lawrence Radiation Laboratory.

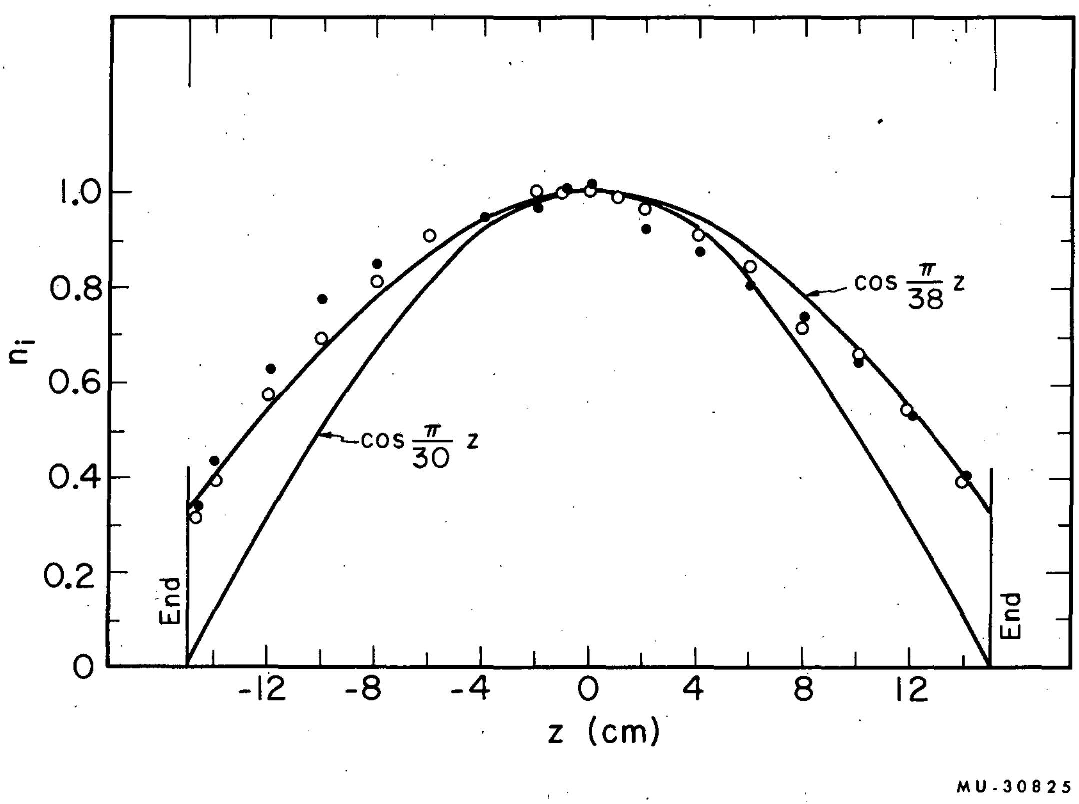

Fig. IV-16. Axial probe measurements. $p = 2 \times 10^{-3}$ torr, B = 700 gauss, I = 10 amperes. •, 2 cm; o, 5 cm.

A temperature disturbance may cause instability even in the absence of a magnetic field. It is the aim of this chapter to investigate this "thermal instability" of a cylindrical collision-dominated plasma column, with and without a longitudinal magnetic field.

System

The subject of this investigation is again an infinite cylindrical plasma column of radius R. The column is homogeneous in the z direction. It contains a gas of one kind. The theory of a column with several neutral-particle components follows exactly the same lines and requires only additional summation. The gas is partially ionized and we have electrons and one kind of singly charged ions. The concept of quasineutrality holds. A longitudinal external magnetic field of strength B can be superimposed.

Concept

Within the range of the normal glow column (Schottky column) we expect no temperature instability. As we will see, the temperature instability depends decisively on the coupling between the density and temperature disturbance. Since the Schottky concept assumes the temperature to be independent of the density distribution, thermal instability cannot be expected.

The situation is different in the case of the thermal glow column. Here, per definition, the energy balance is of importance and couples the temperature distribution with the density distribution. Therefore a density disturbance of necessity produces a temperature disturbance. The temperature disturbance results in a change of the production coefficient. In this way an increase in the particle production via the electron temperature beyond the Kadomtsev mechanism can be expected and may cause instability even if there is no instability of the Kadomtsev type.

More precisely, a spontaneous increase in the electron density near the axis of the discharge results in a decrease of the neutral-particle density, which in turn produces an increase in the electron temperature and, with that, in the particle production. This mechanism can cause instability.

The problem has been treated by the method of normal modes and the existence of an instability has been demonstrated. Investigations of the approximation methods and numerical evaluations are in progress.

V. THEORETICAL AND BASIC EXPERIMENTAL PLASMA PHYSICS

1. A SELF-CONSISTENT DISTRIBUTION OF ELECTRONS IN THE ASTRON E LAYER

Warren Heckrotte and V. Kelvin Neil

A modification has been made in the previously reported calculations of the distribution of electrons in the Astron E layer.[1,2] In reference 2 a distribution was found that produced a surface current density in the azimuthal direction given by

$$j(z) = j_o \cos(\pi z/\ell), \tag{1}$$

in which ℓ is the length of the layer. Boundary conditions required that the axial component of the self-field be zero at the ends of the layer. As a consequence, the radial component of the self-field was a maximum at the ends. This created problems in providing the proper external field to maintain such a distribution in the actual machine.

To alleviate this difficulty, a new distribution was sought that would provide a surface current distribution given by

$$j(z) = \frac{j_o}{2}\left[1 + \cos(2\pi z/\ell)\right]. \tag{2}$$

Provided $\ell \gg R$, where R is the radius of the layer, both the axial and radial components of the self-field are (to a good approximation) zero at the ends of the layer.

In reference 2 the externally applied field was taken in the axial direction and uniform in space. A coil arrangement that gives rise to a variation in the external field over the length of the layer has since been designed by Christofilos.[3] By using the field configuration in reference 3, it was possible to find a self-consistent distribution that provides a current density given by Eq. (2). It is also possible, just as with the previous model,[4] to insert a central section in which the current density of the layer is uniform in z. Again, the distribution is a steady-state solution to the Vlasov equation. The time-dependent buildup of the layer is not yet fully understood.

---

1. Warren Heckrotte and V. Kelvin Neil, in Controlled Thermonuclear Research Semiannual Report, UCRL-10294, July 20, 1962, p. 72.

2. Warren Heckrotte and V. Kelvin Neil, A Self-Consistent Distribution of Electrons in the Astron E Layer, UCRL-6942, June, 1962.

3. N. Christofilos, Proposed Current Distribution of the Astron E Layer, UCID-4577, June 4, 1963.

4. Warren Heckrotte and V. Kelvin Neil, in Controlled Thermonuclear Research Semiannual Report, UCRL-10607, January 16, 1963, p. 72.

2. COMPUTATIONAL STUDY OF ELECTRON INJECTION IN THE ASTRON DEVICE

V. Kelvin Neil and Warren Heckrotte

A theoretical investigation of the electron injection mechanism of the Astron machine is in progress. This scheme for trapping electrons in a magnetic mirror field has been described by Christofilos.[1] The calculation undertaken here involves some analytic work and a computation on the LARC. The following model is used: Perfectly conducting surfaces, infinite in extent, are located at $y = 0$ and $y = 3h$ in rectangular coordinates, with $h = 10$ cm. Located at $y = 2h$ is a thin layer of material with finite conductivity in the x direction and zero conductivity in the z direction. This layer replaces the thin wire resistors in the actual machine. A thin layer of electrons with finite extent in z is located at $y = h$. These electrons have velocity components $v_x \sim c$ and $v_z << c$, where c is the speed of light. The entire system is uniform in the x direction.

The purpose of the resistive layer is twofold. First, it creates a net focusing force in the z direction by acting as a shield for the electric self-forces while allowing some magnetic self-field to penetrate into the region $2h < z < 3h$. Second, the resistive layer dissipates energy as the electrons move in the z direction. In the actual machine, this reduction in kinetic energy will allow the particles to be trapped in an externally applied magnetic mirror field.

It was possible to obtain an analytic expression for the electric and magnetic fields generated by a single beam of electrons. With this Green's function known, the mutual interaction forces can be calculated for a distribution of electrons in $z - v_z$ phase space. All electrons have the same v_x, and are confined to the plane $y = h$. This is equivalent to neglecting radial motion in the actual machine. A computational program was undertaken that numerically integrates the Vlasov equation in two-dimensional $(z - v_z)$ phase space. The initial distribution was taken as uniform in z for 180 cm, and providing a total current of 3000 A in the x direction. Initially all particles have $v_z = 0.03$ c, and the calculation is done in a frame moving with this velocity. The conductivity of the resistive layer was taken to correspond to that of the "focusing" resistors in reference 1.

The half-width (full width at one-half maximum) of the distribution shrinks to a minimum of about 60 cm at the time the moving frame has traveled 33 cm. The average v_z has decreased to 0.017 c. A contour plot of the density in phase space at this time is shown in Fig. V-1. The half-width rapidly increases again, reaching a maximum of about 80 cm when the frame has moved 42 cm. By the time the frame has gone 50 cm the half-width again shrinks to about 70 cm. Contour plots of density in phase space at this time are shown in Fig. V-2. The average v_z has decreased to 0.014c. Thereafter the half-width remains fairly constant at about 65 to 70 cm, and the average v_z slowly increases to a value of 0.01 c when the frame has traveled 80 cm. This is as far as the present calculation has been run.

---

1. N. Christofilos, Astron Electron Injection, UCRL-5617-T, June 22, 1959.

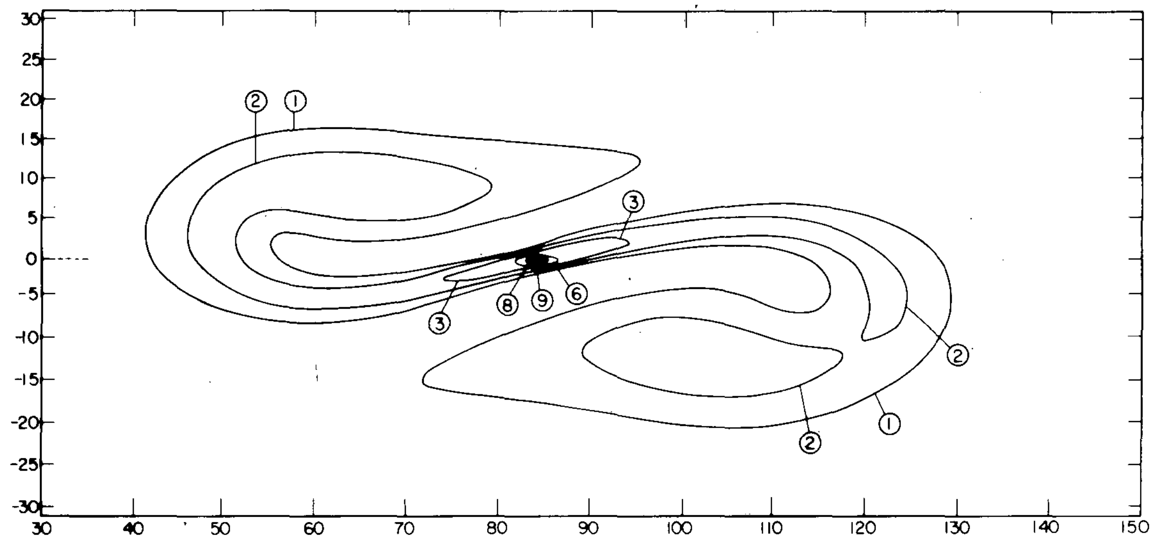

MU-31554

Fig. V-1. Contours of constant density in phase space after particles have traveled 33 cm. The curves are labeled in units of 0.1 times the maximum density. The abscissa is in cm from the initial end of the bunch, and the ordinate is in units of 0.01 c.

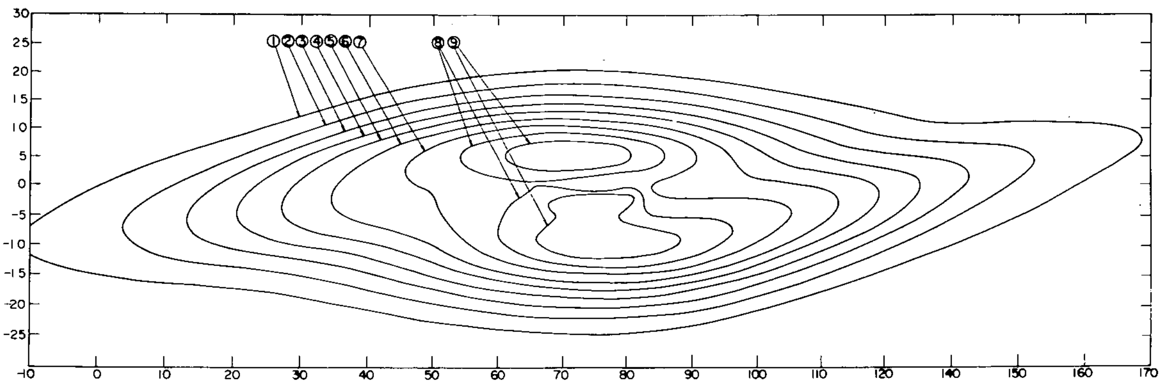

MU-31555

Fig. V-2. Contours of constant density in phase space after the particles have traveled 50 cm. The curves are labeled in units of 0.1 times the maximum density. The abscissa is in cm from the initial end of the bunch, and the ordinate is in units of 0.01 c.

These results indicate that the bunch will not shrink to 20 cm as expected according to reference 1. The implication of this is not clear. The behavior of the bunch certainly depends upon the initial distribution, and other distributions will be examined. The magnetic mirror field has not been included, since it is not present in this region in Astron. It will be represented by a net force in the positive z direction which acts after the particles have traveled a given distance. The conductivity of the resistive layer may also be varied. A continuation of the program into a region of mirror field and higher conductivity will give a better understanding of this unique scheme, thus aiding in the design of the mirror field and the choice of resistors in the Astron machine.

We wish to acknowledge the enthusiastic help of Robert Dickinson, who wrote the program for LARC and has made many useful suggestions.

3. STATISTICAL DERIVATION OF HYDRODYNAMICS FOR A COULOMB SYSTEM*

Allan N. Kaufman

The basic equations of hydrodynamics are the three conservation laws (of mass, momentum, and energy) expressed in differential form:

$$\frac{\partial \rho}{\partial t} = - \nabla \cdot \underline{g}, \tag{1}$$

$$\frac{\partial \underline{g}}{\partial t} = - \nabla \cdot \underset{\sim}{\pi}, \tag{2}$$

$$\frac{\partial U}{\partial t} = - \nabla \cdot \underline{S} . \tag{3}$$

The quantities ρ, $\underline{g}$, $\underset{\sim}{\pi}$, U, and $\underline{S}$ are local functions of position and time, and represent the densities respectively of mass, momentum (or mass flux), momentum flux, energy, and energy flux.

The aim of statistical mechanics is to derive macroscopic relations from known microscopic laws. Accordingly, the set (1) (3) has previously been derived for the following models:

(a) low-density gas, short-range interaction, from the Boltzmann equation (cf. Chapman and Cowling,[1] for example);

(b) arbitrary-density fluid, short-range central forces, from the Liouville equation (Irving and Kirkwood[2]),

---

* Paper to be published in Physics of Fluids.

1. S. Chapman and T. G. Cowling, The Mathematical Theory of Nonuniform Gases (Cambridge University Press, New York, 1953).

2. J. H. Irving and J. G. Kirkwood, J. Chem. Phys. 18, 817 (1950).

(c) low-density quiescent plasma, from the Fokker-Planck equation.

This work considers a system of charged particles interacting by Coulomb forces, at arbitrary density and for arbitrary time scale. Equations (1)–(3) are derived from the exact equations of motion, under the assumption that the two-particle correlations have a range short relative to the macroscopic scale. The quantities U, $\underline{S}$, and $\underset{\approx}{\pi}$ each consist of three parts:

(a) a kinetic part, well-known;

(b) a self-consistent field part, partly well-known [see Eq. (9)];

(c) a correlation part, usually neglected.

The neglect of the correlation parts is justifiable for a low-density plasma where the Debye condition is satisfied. However, at high density (where the correlation energy becomes comparable to the kinetic energy), the correlation parts are of importance.

The correlation parts are

$$U^c(\underline{r}, t) = \frac{1}{2} \sum_{i \neq j} q_i q_j \int \frac{d^3 s}{s} g_{ij}(\underline{r}, \underline{s}, t), \tag{4}$$

$$\underline{S}^c(\underline{r}, t) = \frac{1}{2} \sum_{i \neq j} q_i q_j \int d^3 v_1 \int d^3 v_2 \int d^3 s \, \frac{\underset{\approx}{I} + \hat{\underline{s}}\hat{\underline{s}}}{s} \cdot \frac{\underline{v}_1 + \underline{v}_2}{2} \times$$

$$g_{ij}(\underline{r}, \underline{s}, \underline{v}_1, \underline{v}_2, t), \tag{5}$$

$$\underset{\approx}{\pi}^c(\underline{r}, t) = \frac{1}{2} \sum_{i \neq j} q_i q_j \int d^3 s \, \frac{\hat{\underline{s}}\hat{\underline{s}}}{s} g_{ij}(\underline{r}, \underline{s}, t). \tag{6}$$

The sums are over all particles, q_i is the charge of the ith particle, and g_{ij} is the correlation function for particles i and j:

$$g_{ij}(\underline{r}, \underline{s}, \underline{v}_1, \underline{v}_2, t) \equiv f_{ij}(\underline{r} + \tfrac{1}{2}\underline{s}, \underline{r} - \tfrac{1}{2}\underline{s}, \underline{v}_1, \underline{v}_2, t) - f_i(\underline{r} + \tfrac{1}{2}\underline{s}, \underline{v}_1, t) f_j(\underline{r} - \tfrac{1}{2}\underline{s}, \underline{v}_2, t), \tag{7}$$

$$g_{ij}(\underline{r}, \underline{s}, t) \equiv \int d^3 v_1 \int d^3 v_2 \, g_{ij}(\underline{r}, \underline{s}, \underline{v}_1, \underline{v}_2, t). \tag{8}$$

In Eq. (7), $f_{ij}(\underline{r}_1, \underline{r}_2, \underline{v}_1, \underline{v}_2, t)$ is the joint probability density for particles i at $(\underline{r}_1, \underline{v}_1)$ and j at $(\underline{r}_2, \underline{v}_2)$, at time t, and is normalized to unity. Correspondingly f_i and f_j are one-particle probability densities.

In the low-density limit, under conditions of local thermal equilibrium, U^c and $\underset{\approx}{\pi}^c$ reduce to the Debye-Hückel corrections to the perfect gas laws, while $\underline{S}^c$ vanishes to lowest order.

The self-consistent field parts are found to contain a correction to the conventional formulas. For example, the self-consistent field part of the energy density is

$$U^F = \frac{1}{8\pi}\left[\left\langle \underline{E} \right\rangle^2 - \sum_i \left\langle \underline{E}_i \right\rangle^2\right], \tag{9}$$

where $\left\langle \underline{E}_i \right\rangle (\underline{r}, t)$ is the mean field of particle i, that is,

$$\nabla \cdot \left\langle \underline{E}_i \right\rangle = 4\pi\, q_i \int d^3v\, f_i\,(\underline{r}, \underline{v}, t); \tag{10}$$

and

$$\left\langle \underline{E} \right\rangle \equiv \sum_i \left\langle \underline{E}_i \right\rangle . \tag{11}$$

For a many-body system ($N \gg 1$), the second term of (9) is negligible, while the first term is the conventional one.

4. THE INTERCHANGE INSTABILITY

William A. Newcomb

The hydromagnetic energy principle has been so modified as to include the stabilizing effects of finite Larmor radius on the interchange modes of a mirror machine. These effects give rise to velocity-dependent macroscopic forces which do no work and consequently do not appear directly in the energy integral itself (actually the CGL energy integral, the appropriate one for the present case). But, in the same way as the velocity-dependent magnetic force on a charged particle, they bring in a new constant of the motion similar to the canonical angular momentum. This new constant results in the requirement of a certain minimum kinetic energy for any given displacement away from equilibrium which, under the appropriate conditions, may be greater than the potential energy released by the displacement. In that case the system is stable even though the potential energy is not a minimum, and the stability condition is readily deduced from the energy principle in conjunction with the new constant.

5. LORENTZ IONIZATION STUDIES

David S. Bailey, John R. Hiskes†, and C. Bruce Tarter‡

The calculations of the electric ionization thresholds, cascade processes, and radiative lifetimes for the excited states of the hydrogen atom are essentially complete. The limiting values for the electric ionization thresholds have been calculated through $n = 25$. The radiative lifetimes have been calculated through $n = 25$ in spherical coordinates (field-free case) and in parabolic coordinates (Stark). This work will be reported in Laboratory reports currently in preparation.

---

†Presently on assignment with United Kingdom Atomic Energy Authority, Culham Laboratory, Culham, Abingdon, Berkshire, England.

‡Physics Department, Cornell University, Ithaca, New York.

6. MAGNETIC SHOCKS

Stanley A. Zwick and Douglas E. Gonzales

Solutions to the equal-mass magnetic pulse problem have been obtained for adjacent loop trajectories that touch (in the pulse frame) over a range of Alfvén-Mach numbers from 6 to 12. A typical pair of touching solutions (for Mach 7) is presented in Fig. V-3 in terms of the reduced equal-mass displacements $\bar{x}/R$ and $\bar{y}/R$, and the reduced magnetic field $b = B/B_0$. The plasma length unit R, Alfvén-Mach number α, and stress parameter σ used here are defined by

$$R = (Mc^2/2\pi Nq^2)^{1/2}, \quad \alpha = (8\pi NMV^2/B_0{}^2)^{1/2},$$

$$\text{total plasma stress} = 2nMV^2(1+\sigma) + (B_0{}^2/8\pi),$$

where q and M are the ion charge and mass, N is the number density of plus ions in the undisturbed plasma, B_0 denotes the applied (uniform) magnetic field, and V is the pulse speed relative to the undisturbed plasma. Convergence on a single member of the four-parameter family of simple overlap solutions for Mach 10 has also been attained at a least four significant figures of accuracy. However, since the overlap is only a few percent of the loop spacing (center to center), a plot of this solution is not distinguishable from that of touching loops.

For looping trajectory solutions thus far obtained at the higher Mach numbers, convergence on the IBM 650 has required extremely long times (the simple overlap solution mentioned above required more than 20 hours for convergence). In order to investigate further the parametric relations between Alfvén-Mach number and plasma stress giving rise to the various overlap orders, we have therefore decided to continue the calculations on the LARC computer. A program for numerical integration of the general multiple overlap equations is now being prepared, and should be put into operation shortly.

The relation between the Alfvén-Mach number α and stress parameter σ corresponding to the pulse solutions considered thus far is summarized in Fig. V-4. Regions I and II characterize the respective nonlooping and separated loop solutions, and the solutions generated by the parameters in region III constitute a system of overlapping trajectories which we are starting to calculate. The solitary pulse solutions are represented by points on the α axis (σ=0), for $\alpha \geq 1$.

Apart from the numerical results discussed above, a uniqueness theorem has been constructed for the loop trajectories. Since it is possible in principle to generate symmetric loop solutions by an iterative procedure, the uniqueness theorem establishes the general symmetry of the trajectories. This means, for example, that compression-rarefaction waves, which might be produced by a train of asymmetric loop trajectories, are not allowed by the (steady state) model. A system of symmetric overlapping loops may be considered the analog of a uniform plasma at a finite temperature.

1. S. A. Zwick and D. E. Gonzales, in Controlled Thermonuclear Research Semiannual Report, UCRL-10294, June 1962, p. 77.

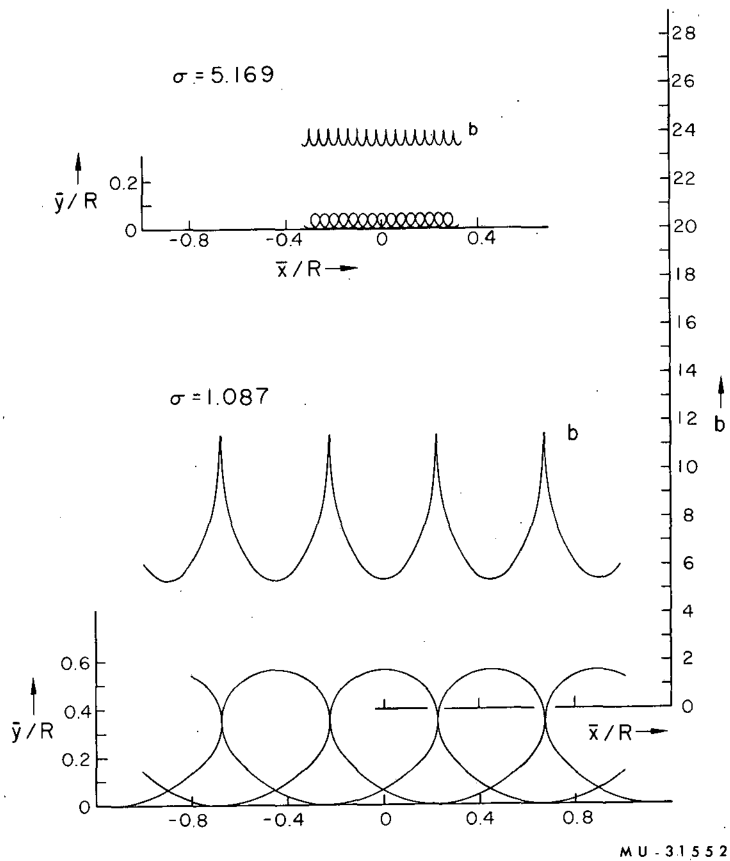

Fig. V-3. Mach 7 touching loop trajectories and corresponding field ratios $b = B/B_0$. Overlap solutions occur for $1.087 < \sigma < 5.169$, for $\alpha = 7$.

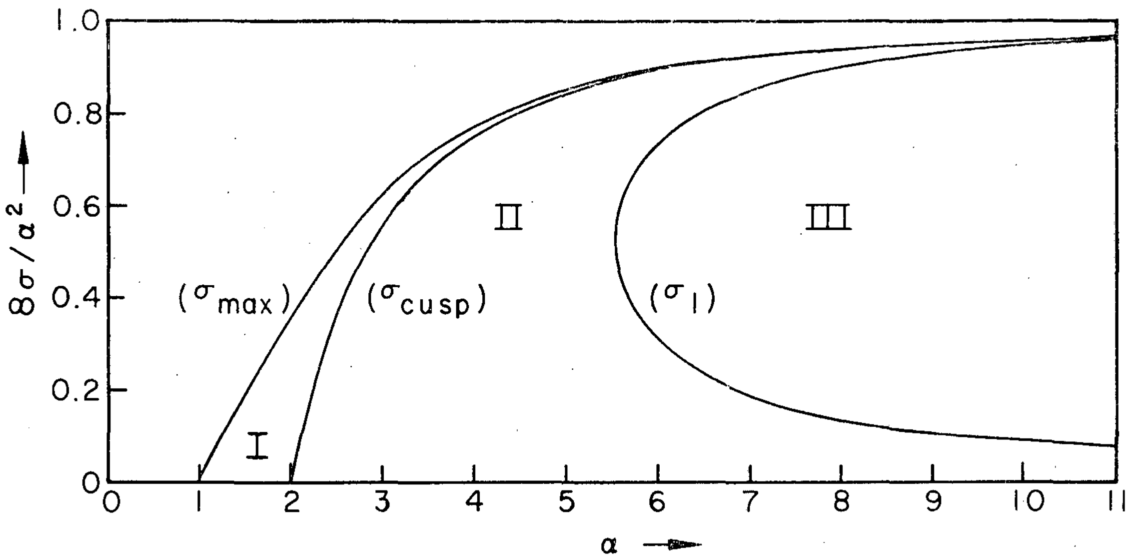

MU-31553

Fig. V-4. Values of $8\sigma/a^2$ vs a, for $\sigma = \sigma_{max}$, $\sigma_{cusp} = (a^2-4)/8$, and σ_1(lowest-order touching solutions). Nonlooping trajectories correspond to points in region I, separated loops to points in region II, and overlap solutions to points in region III.

Our conclusions concerning the problem of looping trajectories involving ions of unequal mass given in a previous Controlled Thermonuclear Research report[1] were incorrect. The particle trajectory and magnetic field curves indicated there apply only for equal-mass plasmas, and relations stated for the longitudinal electric field should be disregarded. Nonlooping trajectories for the unequal-mass case are, however, related to the corresponding equal-mass solutions by the described change of scale.[2] The situation for plasmas of unequal-mass ions will be investigated at the conclusion of the present studies.

A report covering the analytic and numerical work on the equal-mass problem is now being prepared.[3]

---

2. J. H. Adlam and J. E. Allen, Phil. Mag. 3, 448 (1958).

3. S. A. Zwick and D. E. Gonzales, The Magnetic Pulse in a Cold Collision-Free Plasma (UCRL-7170), to be submitted to Phys. Fluids.

7. THE BOLTZMANN EQUATION FOR A PLASMA

Donald P. Geeseman

A plasma is being examined within the Green's function formalism of quantum statistical mechanics. The purpose is to obtain a Boltzmann-type equation which consistently includes both large- and small-angle scatterings without introduction of arbitrary cutoff parameters. By appropriate approximation of the two-particle Green's function the problem essentially potential. If the resulting Boltzmann equation can be put in a manageable form it will be used to develop the associated transport theory.

8. STATISTICAL THEORY OF TRANSPORT PHENOMENA

Laurence S. Hall

The preliminary work[1] on a statistical theory of transport has been extended to show the effects of keeping the time-dependence parameter $\bar{\omega}$ through second order in the expansion of the kinetic correlation in powers of the characteristic time in first-level truncation. The results justify the approximation $\bar{\omega} = 0$, which is part of the adiabatic approximation adopted earlier.[2] In addition, the transitive conservation of normalization condition, which was inconsistently dropped in the previous work, has been used. Work is continuing in order to evaluate Λ when the transitive conservation of normalization condition is retained.

---

1. L. S. Hall, Ann. Physics 20, 383 (1962).

2. Ibid, p. 408.

9. THEORETICAL EXAMINATION OF THE OAK RIDGE PTF EXPERIMENTS

Laurence S. Hall

In the PTF (plasma test facility) experiments at Oak Ridge,[1-6] a source of plasma has been developed in which it is claimed that a plasma of 10^{12} - 10^{13} particles/cm^3 filling approximately 10 liters and having an electron temperature of 50 keV or more, such that $nT = 8 \times 10^{16}$ eV/cm^3, is produced when operating in the "glow" mode.[7] Many of the electrons are relativistic, a density of 10^9 electrons/cm^3 with energies above about 3 MeV, having been reported,[5,6] and the ions are pictured as of relatively low energy, 20 eV.[4] The magnetic field in the mirror regions has a pressure $B_0^2/8\pi \sim 3 \times 10^{17}$ eV/cm^3, so that $\beta \geqslant 25$ percent.

Due to the great interest of the controlled thermonuclear fusion program in such a plasma source, it was decided to look for a theoretical understanding of the experiment. Unfortunately, it was found that a consistent interpretation of the data on the basis of the above characteristics did not seem possible. On the other hand, it has been possible to find at least one model which provides a consistent explanation of the available data. In this model, the plasma has the following characteristics: an electron density of roughly 10^{11} - 10^{12} particles/cm^3 over most of the volume, an electron temperature somewhere in the range 1-100 eV, and an ion temperature of 1 eV or less. The high power microwaves which provide ionization and heating are confined to the region outside the plasma, and at the surface of the plasma is a shell of relativistic electrons, heated by electron-cyclotron resonance in the ring-like zones in which the plasma surface intersects the resonance surfaces defined by the external magnetic field. However, most of the ionization is provided at the surface of the plasma by relatively cold electrons (~ 100 eV) which are alternately accelerated and decelerated by the oscillating microwave field, as in normal rf discharges.

---

1. M. C. Becker, R. A. Dandl, H. O. Eason, Jr., A. C. England, R. J. Kerr, and W. B. Ard, Nuclear Fusion, 1962 Supplement, Part 1, p. 345.

2. R. A. Dandl, R. J. Kerr, H. O. Eason, M. C. Becker, and F. T. May, in Thermonuclear Division Semiannual Progress Report, ORNL-3104, January 31, 1961, p. 29.

3. R. A. Dandl, A. C. England, H. O. Eason, M. C. Becker, R. J. Kerr, and W. B. Ard, in Thermonuclear Division Progress Report, ORNL-3239, October 31, 1961, p. 16.

4. M. C. Becker, A. C. England, R. A. Dandl, R. J. Kerr, H. O. Eason, and W. B. Ard, in Thermonuclear Division Semiannual Progress Report, ORNL-3315, April 30, 1962, p. 21.

5. W. B. Ard, H. O. Eason, M. C. Becker, A. C. England, R. A. Dandl, and R. J. Kerr, in Thermonuclear Division Seminannual Progress Report, ORNL-3392, October 31, 1962, p. 28.

6. W. B. Ard, M. C. Becker, R. A. Dandl, H. O. Eason, A. C. England, and R. J. Kerr, Phys. Rev. Letters 10, 87 (1963).

7. R. A. Dandl, Bull. Am. Phys. Soc. II-8, 168 (1963) (invited paper).

The present model can be used to explain:

(a) both the long decay times observed in the "afterglow" and the analytical form of the decay of microwave noise after shutdown;

(b) the diamagnetic signal far from the center plane and as well the apparent paramagnetism observed in the center of the machine;[8]

(c) the microwave phase-shift measurements of density;

(d) the mode transition;[3] and

(e) the x-ray and neutron-emission observations.

In addition, since β is small in our model, there is no longer a conflict between the interpreted characteristics of the plasma and current hydromagnetic stability theory.

8. Reference 4, Fig. 3.8.

10. STABILITY OF LONGITUDINAL OSCILLATIONS IN ANISOTROPIC PLASMA

Terry Kammash[†] and Warren Heckrotte

The stability of longitudinal oscillations in an infinite collisionless anisotropic plasma in a uniform magnetic field has been investigated. Although the investigation has not yet been carried to completion, a number of significant results has emerged. Most significant is the fact that longitudinal oscillations propagating at an angle to the magnetic field in a plasma in which the electrons are isotropic and the ions are anisotropic with a temperature ratio $T_{\perp}/T_{\parallel} = 10$ were found to be stable. This case is quite comparable to that studied by Drummond, Rosenbluth, and Johnson,[1] in which instability was predicted. In addition, we have shown that longitudinal modes propagating along the magnetic field are stable and that purely growing modes (as in the gravitationally driven Rayleigh-Taylor instability[2]) cannot be driven by anisotropy.

[†]Department of Nuclear Engineering, University of Michigan, Ann Arbor, Michigan.

1. W. E. Drummond, M. N. Rosenbluth, and M. L. Johnson, Bull. Am. Phys. Soc. II, 6, 185 (1961).

2. S. Chandrasekhar, Plasma Physics (University of Chicago Press, Chicago, 1960.

The dispersion equation for longitudinal oscillations in a plasma whose particles have a two-temperature Maxwellian velocity distribution is[3]

$$F(\omega) = \frac{v_A^2}{c^2} + \int_0^\infty \left\{ \frac{M_e}{M_i} \exp\left[-i\omega_e x - \frac{\gamma_e^2 t_e^2 n_z^2}{4} x^2 - \gamma_e^2 n_\perp^2 \sin^2\left(\frac{x}{2}\right)\right]\right.$$

$$\left. + \exp\left[-i\omega_i x - \frac{\gamma_i^2 t_i^2 n_z^2}{4} x^2 - \gamma_i^2 n_\perp^2 \sin^2\left(\frac{x}{2}\right)\right]\right\}\left\{n_z^2 x + n_\perp^2 \sin x\right\} dx = 0,$$

where the subscripts e and i denote electrons and ions respectively. The remaining terms are defined as follows: v_A/c is the ratio of the Alfvén speed to the speed of light, $\omega_e = \omega/\omega_{ce}$, $\omega_i = \omega/\omega_{ci}$, $t^2 = T_\parallel/T_\perp$ is the ratio of temperature along the field to that perpendicular to the field, $n_z = k_\parallel/k$ is the cosine of the angle of propagation, and $\gamma = k\rho$ is the ratio of the radius of gyration to the wavelength. We have shown[3] that $F(\omega)$ is positive definite [and hence no solutions for $F(\omega) = 0$] when $i\omega$ is positive and real and thus no purely growing modes. This fact has been utilized in plotting the Nyquist diagram shown in Fig. V-5. According to the Nyquist criterion, the number of zeroes of $F(\omega)$ inside a closed contour in the complex ω plane is equal to the number of times the corresponding contour in the F plane enclosed the origin. The closed curve shown in the figure is, in effect, the mapping of the lower half of the complex ω plane (the unstable region) for the case in which the electrons are isotropic, i.e., $T_\perp = T_\parallel$, and the ions are anisotropic with $T_\perp = 10T_\parallel$. We note in this case that the curve does not enclose the origin and therefore there are no unstable roots. Similarly, we have shown that all modes propagating along the magnetic field--i.e., $n_\perp = 0$--are also stable.

We are indebeted to L. S. Hall for coding the problem on the IBM 7094 and for many valuable suggestions.

3. Terry Kammash, Stability of Anisotropic Plasma against Oscillations of the Rayleigh-Taylor Type, UCRL-7330, April 15, 1963.

11. VERTICAL INSTABILITY OF THE BEAM IN A PARTICLE ACCELERATION

V. Kelvin Neil and Andrew M. Sessler*

Recent experiments with the MURA electron accelerator have discovered instability in the stacked beam when the circulating current reaches a value of about 7 A.[1] Before onset of the instability, the beam is very nearly uniform in azimuth. The mean particle energy is 35 MeV with a deviation of about 5 MeV. The instability is manifest as a coherent vertical oscillation of the entire beam, accompanied by rf electromagnetic fields in the vacuum tank.

*Theoretical Division, Lawrence Radiation Laboratory, Berkeley, California.

1. F. Mills and F. Cole (Midwestern Research Association, Madison, Wisconsin), private communication, April 1963.

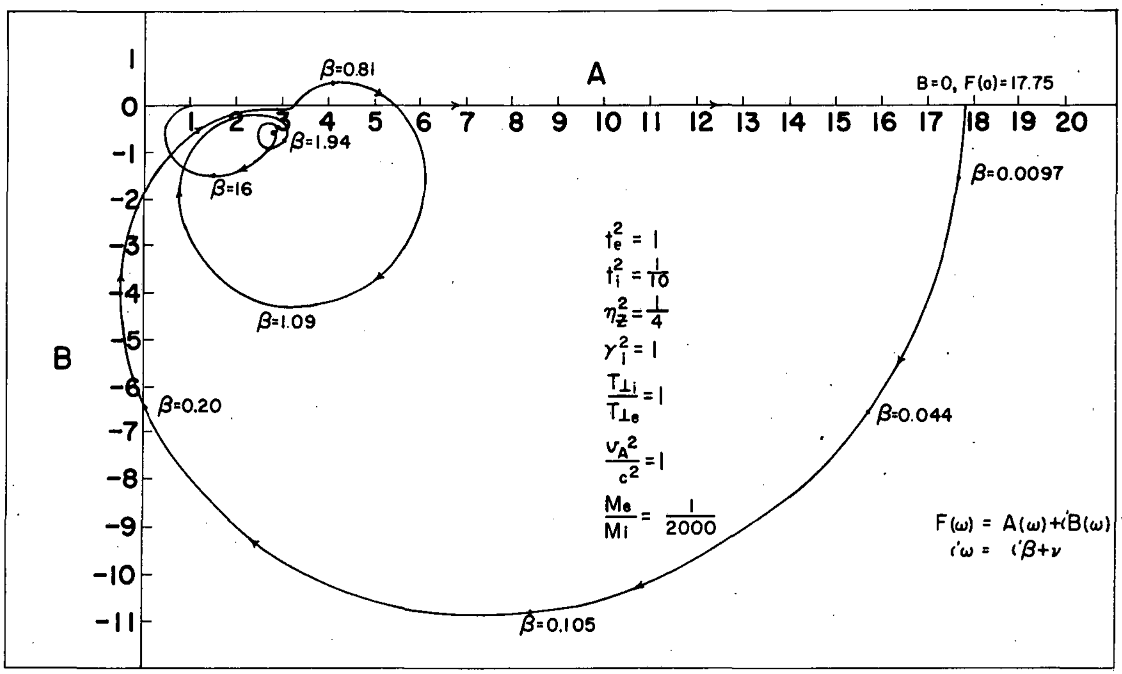

Fig. V-5. Nyquist diagram.

There is no azimuthal bunching of the beam associated with the instability.

It is believed that this instability arises because of the finite conductivity in the walls of the vacuum tank. A theoretical treatment of the problem is in progress. The purpose of this calculation is not only to explain the phenomenon observed by the MURA group, but also to determine whether or not this effect will be an inherent limitation on the beam intensity in future accelerators. It is also possible that such an instability could occur in the resistor region of the Astron device. This possibility must be investigated.

12. STABILITY OF AN INHOMOGENEOUS PLASMA

Cornelius H. Woods and Terry Kammash†

We have investigated the stability of an inhomogeneous plasma using the guiding center concept and the adiabatic equations for drift velocity. A linear, filamentary current producing the magnetic induction $B_\theta = 2\mu I/r$ is assumed to be clad with guiding centers of density n(r) belonging to monoenergetic positrons having the momentum p, and with an equal distribution of guiding centers belonging to electrons of the same momentum. The unperturbed electric field is therefore zero. It is further assumed that $p_\theta = 0$, so that the guiding centers all drift with the same velocity $v_o = cp^2/4\, em\mu I$ parallel to the filament, the direction depending on the sign of charge e.

The densities of positron guiding centers and electron guiding centers satisfy two separate equations of continuity in the perturbed plasma. To carry out the analysis, we have linearized these equations of continuity, and have taken the charge density equal to e times the guiding center density. The perturbed magnetic field is neglected (low β), and we consider perturbations in the electric potential of the form $\phi = \psi(r) e^{i(\omega t + kz)}$ where the z axis coincides with the filament; the potential satisfies the Poissan equation $\nabla^2\phi = -4\pi\rho$, ρ being the net charge.

With one further approximation--that the perturbed electric field does not change the momentum of the particles (although it causes them to drift)--we find that the unknown radial dependence of the perturbed potential satisfies the equation

$$\frac{d^2\psi}{dr^2} + \frac{1}{r}\frac{d\psi}{dr} - k^2[1 - f(r)]\,\psi = 0,$$

where

$$f(r) = \frac{8\pi c e V_o\left[2\, n(r) + r\frac{dn(r)}{dr}\right]}{2\mu I\,(\omega^2 - k^2 V_o^{\,2})}.$$

†Department of Nuclear Engineering, University of Michigan, Ann Arbor, Michigan.

This equation has been solved for an unperturbed distribution of guiding centers of the form

$$n(r) = N \qquad \text{for } 0 < r < R,$$

$$n(r) = NR^2/r^2 \qquad \text{for } R < r < \infty,$$

where N and R are constants. Also, ψ and $d\psi/dr$ are required to be continuous, with $\psi(\infty) = 0$. The solution involves modified Bessel functions, and the dispersion relation is

$$kI_o(\alpha R)\, K_1(kR) + \alpha I_1(\alpha R)\, K_o(kR) = 0,$$

where α may be complex, and is given by

$$\alpha^2 = k^2 \left[1 - \frac{8\pi ceV_o(2N)}{2\mu I(\omega^2 - k^2 V_o^2)}\right].$$

The frequency ω is therefore given by

$$\omega^2 = k^2 V_o^2 + \frac{8\pi ceV_oN}{\mu I}\left(\frac{1}{1 - \frac{\alpha^2}{k^2}}\right)$$

The series for $I_o(\alpha R)$ and $I_1(\alpha R)$ converge rapidly, and by retaining terms through $(\alpha R)^4$, the quantity α is found to have the values

$$\alpha^2 = \begin{cases} -\dfrac{8}{R^2} \\ -\dfrac{8}{R^2} \left[\dfrac{1}{1 + \dfrac{4K_o(kR)}{kRK_1(kR)}}\right] \end{cases};$$

clearly the four values of ω are real, and the perturbed modes are stable for all values of k. In the limit $N \to 0$, the frequency reduces to $\omega = \pm kV_o$.

13. BUMPY TORUS

Gordon Gibson,[†] Willard C. Jordan,[‡] and Eugene J. Lauer

Numerical Calculations

The results of three sets of numerical calculations on the Bumpy Torus configuration have been summarized in a report that is being submitted for publication.[1] The abstract of this report is as follows.

Drift surfaces of guiding centers in the static BumpyTorus magnetic field have been located and analyzed for various torus parameters by making use of the transverse adiabatic invariant $\mu = p_{\perp}^2/B$ and the longitudinal adiabatic invariant $J = \oint p_{\parallel}\, dl$. In addition, the drift equations (for which μ is an invariant) have been solved numerically to investigate limitations on the application of the invariance of J. In general, J is an invariant for the drift equations under adiabatic conditions; however, some special guiding-center trajectories are presented for which the drift per longitudinal period is sufficiently large that the assumption of the invariance of J is not valid. Closed surfaces of const $U = -\oint dl/B$ have been found. These are also surfaces of constant plasma pressure under static equilibrium conditions at low β for a hydromagnetic model. The stability of the equilibrium is discussed.

Injection Apparatus and Purpose of Tests

The injection apparatus shown schematically in Fig. V-6 is currently being tested. The purpose of the tests is to study the important parameters so that an appreciable fraction of the accelerated electrons is trapped in the gap between the iron poles, and to verify that their subsequent motion is as predicted.[2] The only essential part of the apparatus not shown in the figure is the accelerator which directs a focused beam of electrons through the hole in the tantalum mask. The accelerator is usable up to about 100 kV, but electric discharges in the vacuum region inside the pyrex insulator have thus far prevented operation at 150 kV, which is the maximum for the power supply. A new insulator with voltage-divider rings is being prepared. The accelerator is mounted at a 45° angle to the plane of Fig. V-6, and it is rigidly attached to the iron pole tip assembly, the position of which can be adjusted with respect to the remainder of the apparatus during operation. The spacing and angle between the two injection coils are also separately adjustable. The two torus coils are fixed in position. Power supplies for these two coils have just recently

---

[†] Westinghouse Electric Corporation, Atomic Power Division, Pittsburgh, Pa.

[‡] The Bendix Corporation, Research Laboratories Division, Southfield, Mich.

1. G. Gibson, W. C. Jordan, E. J. Lauer, and C. H. Woods, Guiding Center Motion and Plasma Behavior in the Bumpy Torus (to be issued as UCRL-7246).

2. Gordon Gibson, Willard C. Jordan, and Eugene J. Lauer, in Controlled Thermonuclear Research Semiannual Report, UCRL-9969, January 19, 1961, p. 166.

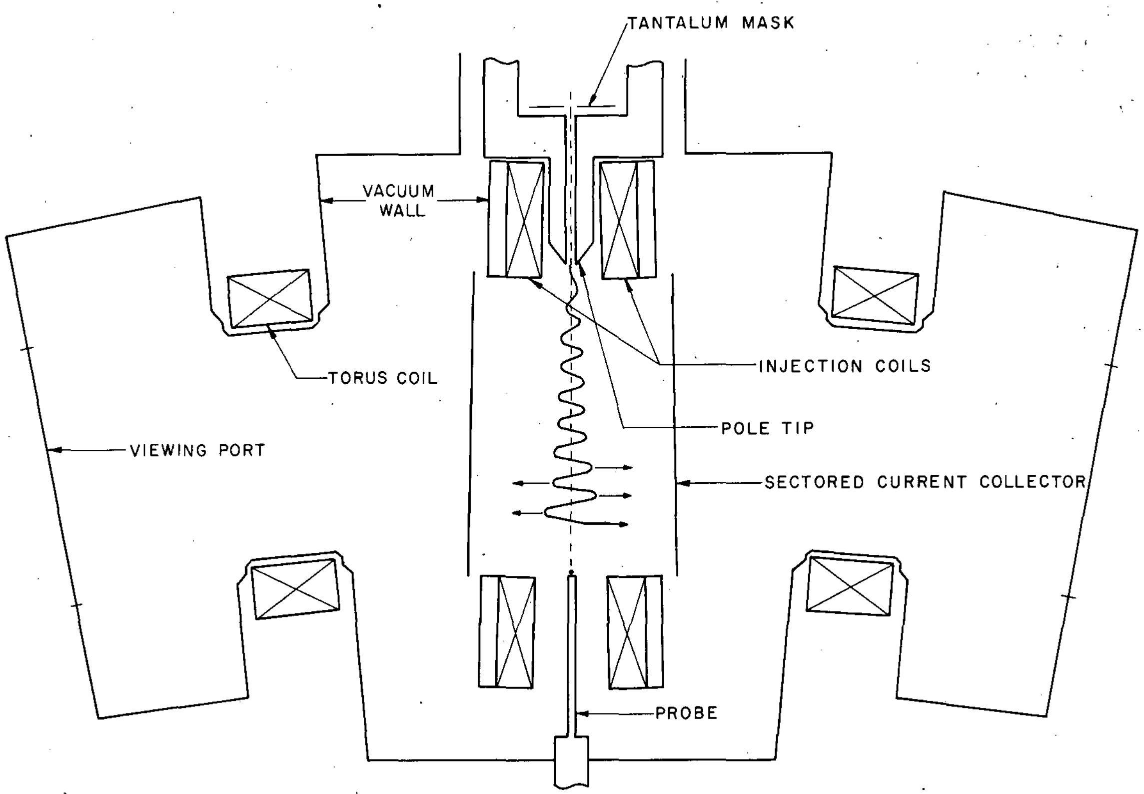

Fig. V-6. Injection test schematic. The projected paths of the guiding centers after leaving the poles are depicted qualitatively.

been connected. The results presented in this report were obtained with these coils not energized. However, it has been established that turning on the current in the torus coils does not grossly affect the injection. Figure V-7 is a photograph of the injection apparatus.

Figure V-8 shows two experimentally determined curves of constant magnetic induction, B, in the plane midway between the injection coils and perpendicular to the plane of Fig. V-6. The measured properties of the field for the parameters as given in the caption indicate that these curves meet the conditions for injection. It is planned to vary the angle and mean distance between the injection coils, but the configuration of Fig. V-8 was used for all the tests so far.

If the accelerated electrons have the proper starting conditions their motion is such that they are "injected" into the Bumpy Torus. This motion, which has previously been described,[2] can be broken down into the following steps:

(a) the particle becomes trapped near the iron pole corner,

(b) the guiding center (g. c.) drifts parallel to the step separating the narrow and wide pole gap,

(c) the g. c. follows the predicted drift path (B = const) in the transition region from the poles to the cresent-shaped path between the injection coils,

(d) the g. c. follows the cresent-shaped path in the region where it is "mirror stable" (that is, confined by the pair of injection coil mirrors),

(e) near the boundary of mirror stability the g. c. should leave the region between the injection coils and move approximately along a flux lines through one or the other of the injection coils.

Diagnostics

The following kinds of observations have been made.

(a) Current-collecting probes can be moved in the plane of Fig. V-8. One of these, which can explore the narrow gap between the pole tips, is shown in Fig. V-6.

(b) A sectored array of insulated metal plates is oriented approximately perpendicular to $\overline{B}$ just outside of each injection coil (see Fig. V-6). One can monitor the current of electrons that passes through a particular injection coil and strikes a collector plate.

(c) At times the collector plates of (b) have been replaced by a glass plate coated with phosphor.

(d) A few μ Hg pressure of neon gas has been put in the chamber and the red light emitted by excited neon atoms photographed.

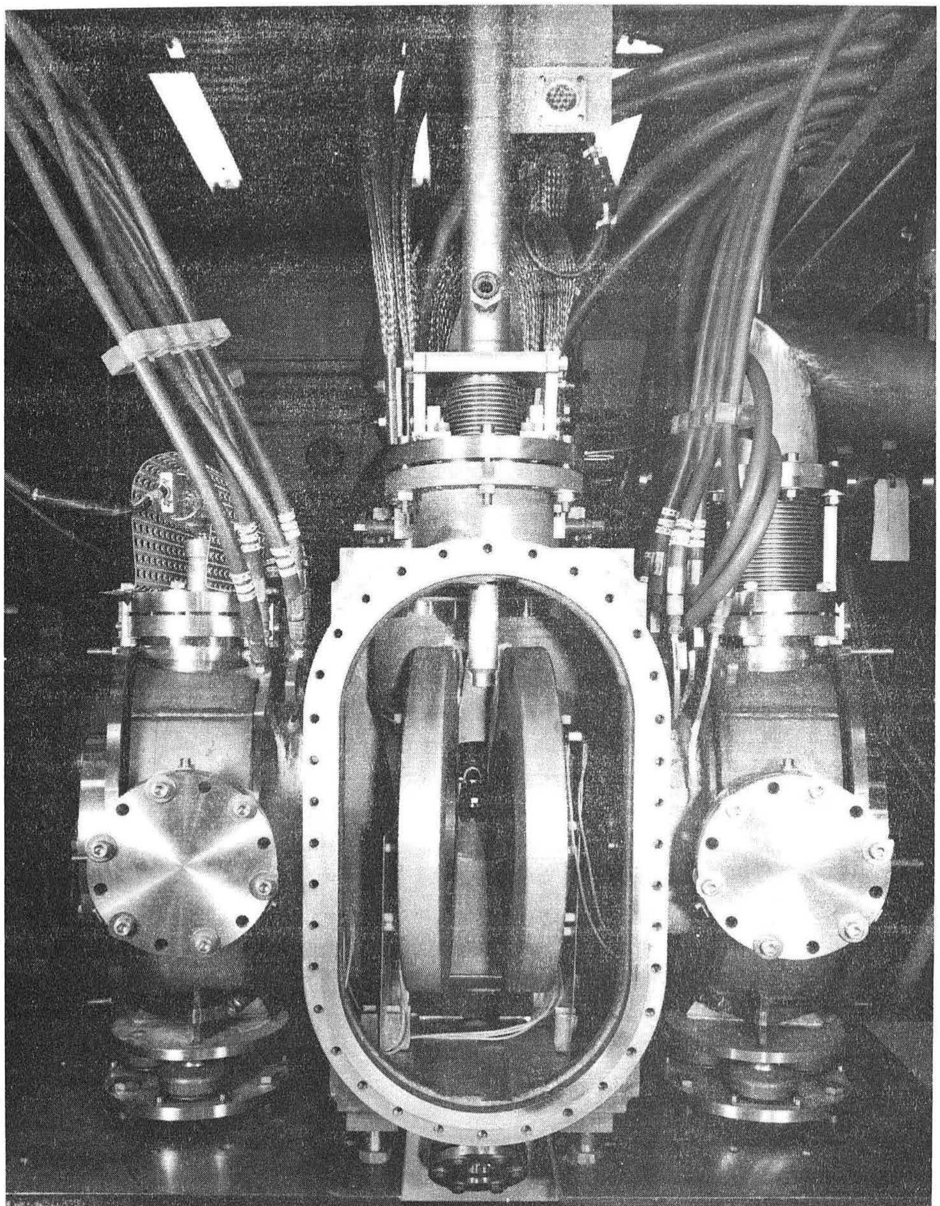

ZN-3930

Fig. V-7. Photograph of injection apparatus; cover plate which carries the horizontal probe removed. The two injection coils and the sectored collector plates can be seen. The iron pole tips are in the center background. Since this photograph was taken, water cooling has been installed on the poles. The electron gun has its axis in the vertical plane and is located behind the injection chamber and cannot be seen. The adjacent torus coils can be seen on each side of the injection chamber. The end of the vertical probe is at the top of the chamber between the coils.

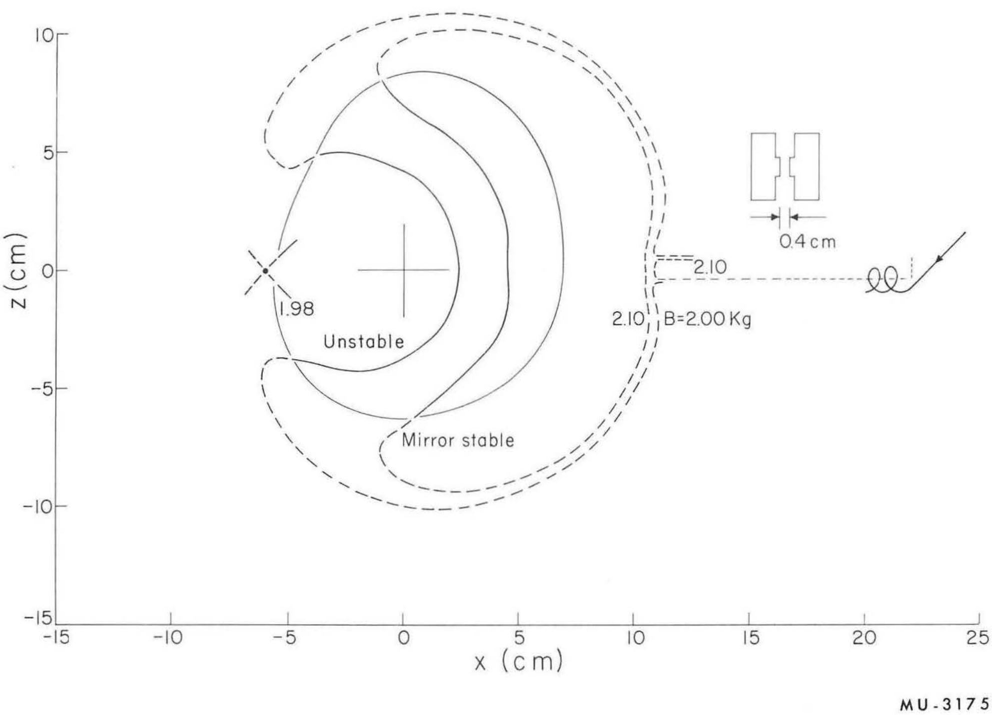

Fig. V-8. Experimentally determined curves of B = constant in the plane midway between the two injection coils and midway between the two iron poles. The injection coils have a mean radius 1.5 times the mean radius of the torus coils (1.5×9.53 = 14.3 cm). The inside radius is 10 cm. Each coil has 12 turns and the current in each turn was 2020 A. The mean distance between the coils was 0.69 times their mean radius and the angle between them was 0.11 radian. (x = 0, y = 0) is the point where the line connecting the centers of the two coils intersects the page. A cross section through the iron poles near the injection corner is shown. The particle trajectory is depicted qualitatively, with about the mean results of curvature used in the tests that are reported. The dashed portions of the curves on which the magnetic induction is constant are mirror-stable, the solid portions of the curves are mirror unstable. The solid closed curve is the mirror stability boundary.

Results

The observations indicate that an appreciable fraction of the accelerated electrons can be trapped and that their motion is as predicted. Most of the observations have been made with 60-keV electrons. (At this energy the x rays do not penetrate the vacuum chamber walls appreciably, so that there is no health hazard in making observations and adjustments near the apparatus). The coil currents have been set so as to make the injection orbit radius ≈ 1.3 times the narrow gap width ($1.3 \times 0.4 = 0.52$ cm). (With the radius less than the narrow gap width, the trapping at the iron pole corner was inefficient.)

As a small probe is moved between the pole tips parallel to the step in gap width, the current collected is a maximum at regular intervals of the probe position. The interval corresponds to the drift of the particles per gyration, and the particles gyrate about 10 times during their trip between the iron poles. Furthermore the current readings indicate that a negligible amount of current is lost during this motion along the gap between the poles. The current collected either at the mask (see Fig. V-6) or on the probe when it is inserted in the gap between the poles is equal to about one-half the current drain at the power supply. By moving the probe normal to the drifting motion of the particles it was found that the particles were confined to the region near the plane separating the narrow and wide gaps.

Electrons that spill out of the injection mirrors near the stability boundary and in the region defined by $x < 0$, $z < 0$ on Fig. V-8 will have their g.c.'s on flux lines which lie on drift surfaces that do not intercept the wall. (These were calculated for the Bumpy Torus without the injection apparatus.) When the current passing through the high-voltage supply was 5 mA, the current collected in this region was 2 mA (uncorrected for secondary electrons). This condition could be maintained steady in time. The currents to the collectors on the two sides are equal within ± 10%.

None of the electrons was observed to escape above the plane of Fig. V-6, i.e., for $z > 0$ in Fig. V-8. Those electrons, which are initially trapped between the iron poles, but do not spill out in the region $z < 0$, $x < 0$, either spill out in the region $z < 0$, $x > 0$, or drift on a circular-type path (which has mirror stability) back to the iron poles. Some of the electrons may strike the injection coil encasement as they oscillate about the plane of Fig. V-8.

Efficient injection is dependent upon accurate alignment of the tungsten filament tip on the axis of the bias and anode (grounded) electrode holes in the gun, and on having the temperature of the filament sufficiently high. Also, efficient transfer of the electrons from the pole region to the injection coil region depends upon centering the poles between the coils within approx 0.5 mm.

Figure V-9 is a photograph of the light emitted by the phosphor-coated plate placed just outside one injection coil (at the position of one of the sectored current collectors shown in Fig. V-6). This was obtained with very much lower injection current than the above. The distribution of electrons striking the fluorescent plate is consistent with the measured current distributions delivered to the sectored current collectors. The circles appear to have the Larmor diameter. The pattern of discrete circles can be explained in the following manner. If the beam entered the magnetic field with the particles symmetrically distributed in angle and position about the plane of symmetry, then half of those

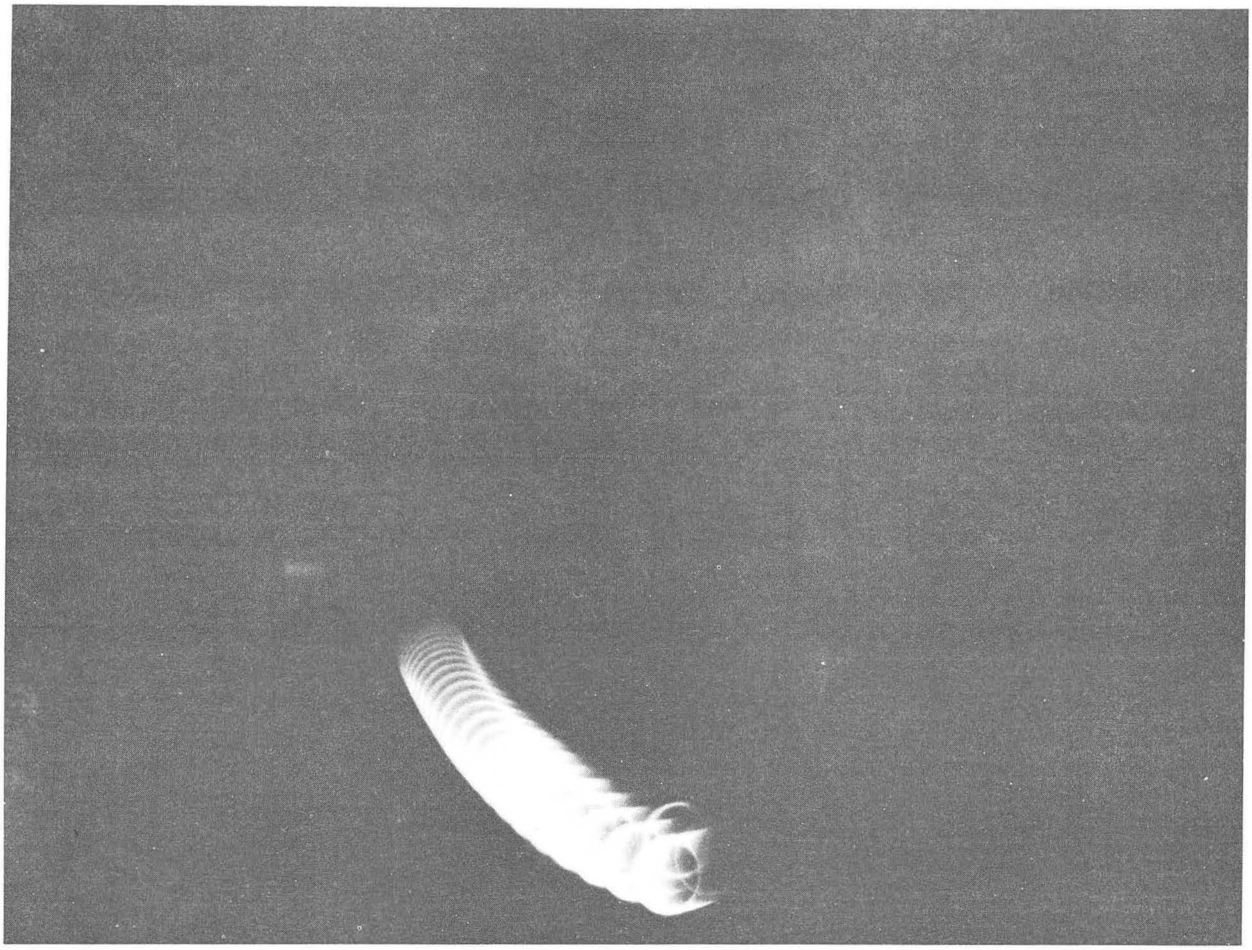

ZN-3931

Fig. V-9. Photograph of fluorescent plate pattern caused by electrons escaping through an injection coil. The light spot in the left center locates the horizontal symmetry plane. The iron poles are to the right.

particles whose g. c.'s were on a particular B ≈ constant curve would leave the injection region in a direction parallel to $\overline{B}$ and the other half in a direction antiparallel to $\overline{B}$. On the other hand, if the beam entered the gap between the poles at a small angle then all the particles whose g. c.'s were following a particular curve of B ≈ constant would oscillate coherently about the midplane between the injection coils, and all would leave the injection region either parallel or antiparallel to $\overline{B}$ depending on which direction they were moving as they passed the mirror stability boundary on the B ≈ constant curve. However, those particles whose g. c.'s are on nearby B≈ constant curves would have to drift a greater or shorter distance before reaching the mirror stability boundary, hence they may leave in the opposite direction. This would explain the discrete circles if we further assume that the phase of the particle in its gyrating motion about the field is unimportnat. If the beam enters perpendicular to the field, but the tips of the iron poles are not symmetric with respect to the plane midway between the injection coils, then a similar behavior is expected. This effect will be investigated further.

Status of Torus Construction

The modular parts of the torus are on order from outside shops with a delivery date of about July 15, 1963. The torus power supply installation is complete. The pumping system and water manifold parts are on hand.

14. ATOMIC SCATTERING AND CROSS-SECTION MEASUREMENTS

Gilbert O. Brink,* Edmund S. Chambers, and Robert H. McFarland

Research has been interrupted during this period because of the necessity of moving into new quarters. This operation is roughly 75% complete. The electron crossed-beam machine will be moved at a later date on a schedule to cause minimum down time.

Charge Transfer of Hydrogen Ions on Hydrogen Gas

Experimental work on this subject, involving fast neutral detection, has been completed. The final report is written.[1]

Charge-transfer cross sections of the hydrogen ions H^+, H_2^+, or H_3^+ on H_2 gas have been obtained by measuring the fast neutrals produced. For H^+ on H_2, the maximum σ_{10} is 8.3×10^{-16} cm^2 at an ion energy of 7.5 keV. The results agree with previous work at all energies. For H_2^+ on H_2, the largest σ_{10} is 7.3×10^{-16} cm^2, and is attained at the lowest energy observed. For H_3^+ on H_2, the maximum σ_{10} is 5.5×10^{-16} cm^2, at an ion energy of about 34 keV. Estimated error is ± 4%. The data can be correlated by plotting in the impulse exerted on an orbital electron of H_2 vs collision time. Previous data for H^+ on H are also treated for comparison.

*On leave of absence until May 15, 1963 at the University of Pittsburgh.

1. E. S. Chambers, Charge-Transfer Cross Sections for H^+, H_2^+, or H_3^+ on H_2, 2keV to 55 keV (UCRL-6987, June 1963), to be submitted to Phys. Rev.

The principal experimental results are shown in Fig. V-10. Figure V-11 shows the correlation obtainable when the impulse transferred to the orbital electron of the molecule is plotted against the collision time, τ. Here the impulse,

$$\int F\,dt = \bar{F}\,\tau, \text{ is approximated by } \tau/\sigma_{10}, \text{ since } \bar{F} \approx e^2/r^2 \text{ and } \sigma_{10} \approx \pi r^2,$$

where r is the effective interaction distance.

Secondary Electron Emission of Hydrogen Ions and Neutrals on Copper-Beryllium

Experimental work on this subject has been completed. A report is being written.[2] The secondary-electron coefficient, δ, has been obtained for H^+, H_2^+, or H_3^+ impinging on copper-beryllium at 60° and 72° angles of incidence. The energy range 2 keV to 55 keV was covered.

Figure V-12 shows the ratio of secondary electron current from a neutral beam divided by the secondary-electron current from the corresponding ion. These data were obtained by making a comparison calorimetrically.

An energy analysis of the secondaries was made. No significant difference was found between those from the ions and from the neutrals.

Electron Scattering

Recent interest in using lithium as a neutralizer has led to a need for absolute cross section for electron ionization of lithium. Work is under way at this time to provide that information. Since measurements have been made of relative cross section versus electron energy, only a single measurement, which can be made above the troublesome low-energy range, is needed.

A second series of measurements involving the cross sections for neutralizing of hydrogen ion beams with alkali vapors is planned for this same machine subsequent to its transfer into Building 180B.

Electron excitation experiments with helium have successfully demonstrated nonzero polarization at threshold for a number of helium lines. Also, it has been demonstrated that the threshold excitation for selected helium lines follows the square-root law, as predicted by theory. Previous conflict between experiment and theory was apparently of experimental origin. This work has been reported,[3] and additional details will be presented at the Third International Conference on Electronic and Atomic Collision Phenomena, University College, London, England.[4]

---

2. E. S. Chambers, Secondary-Electron Yield on Copper-Beryllium for H^+, H_2^+, H_3^+, H^0, H_2^0, and H_3^0 (UCRL-7421, July 1963), to be submitted to Phys. Rev.

3. Robert H. McFarland, Phys. Rev. Letters 10, 397 (1963).

4. Robert H. McFarland, The Cause of the Observed Polarization of Electron-Induced Radiation from Helium, UCRL-7254, May 1963.

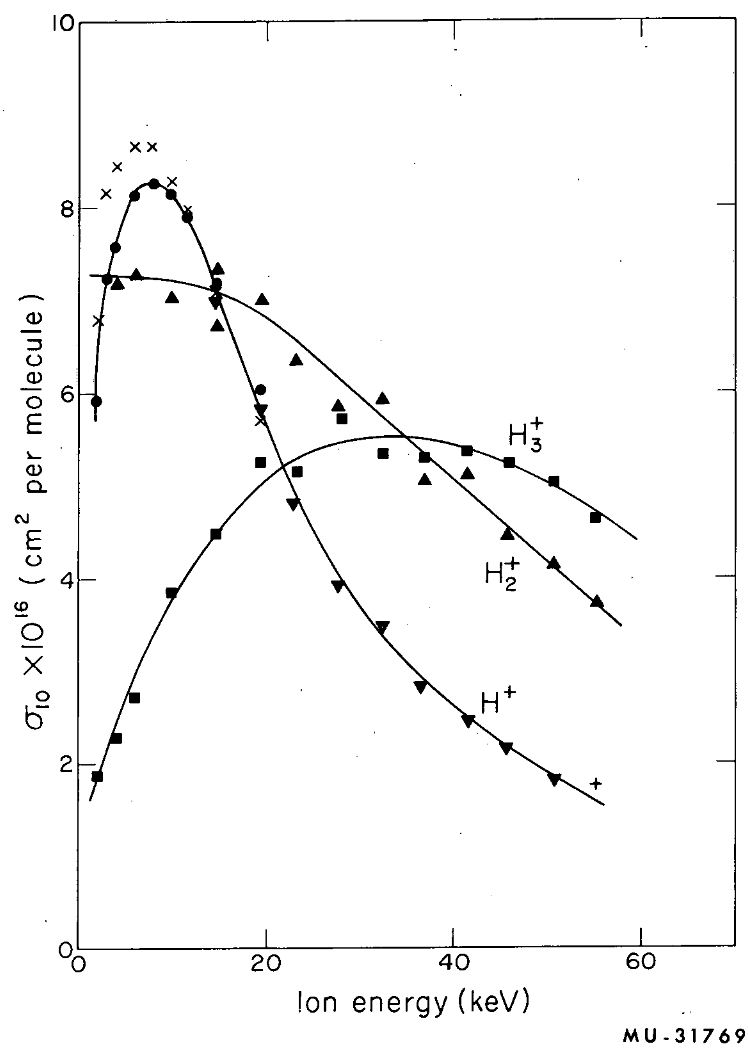

Fig. V-10. Fast neutral production (charge transfer) cross-sections, σ_{10}, for hydrogen ions on H_2 gas as a function of ion energy.

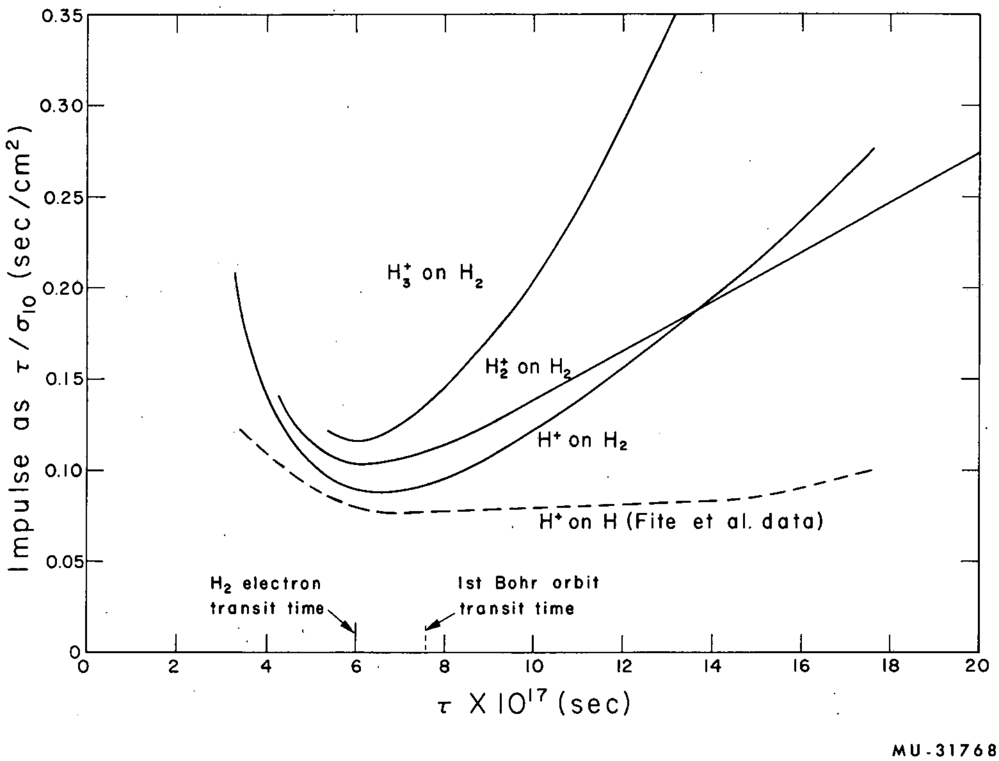

Fig. V-11. Impulse transferred to orbital electron in terms of τ/σ_{10} for hydrogen ions on H and H_2 gas as a function of collision time.

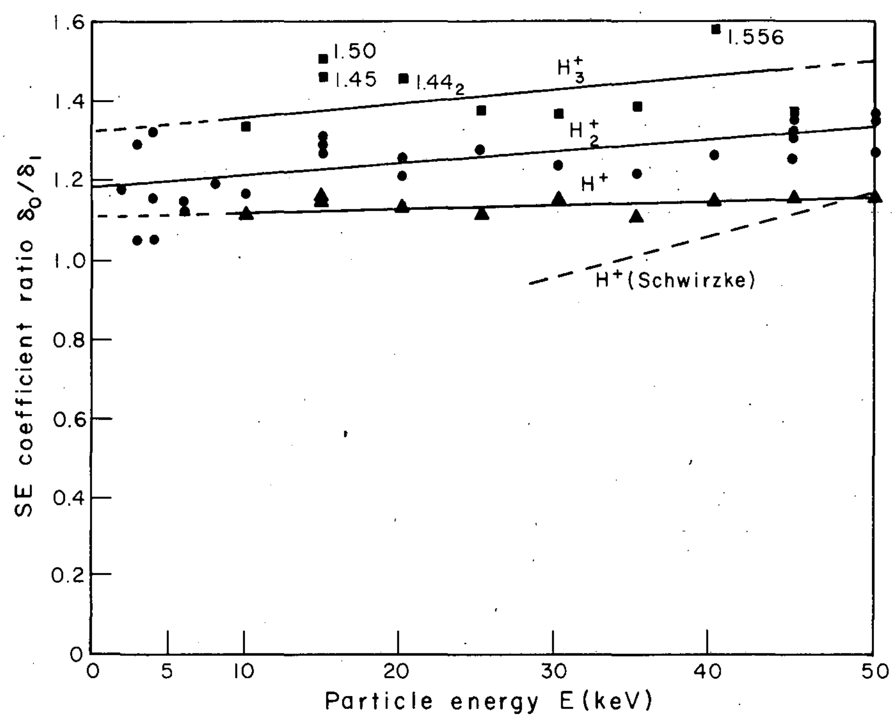

Fig. V-12. Ratio of secondary electrons produced by neutrals to secondary electrons from corresponding ion [by beam power calorimetry on copper-beryllium (Berylco 25 alloy)]. Angle of incidence = 60°.

VI. ENGINEERING AND TECHNOLOGICAL DEVELOPMENT

1. ULTRAHIGH-VACUUM DEVELOPMENT

Norman Milleron

Efforts to optimize oil diffusion pump design continue. Specifically, the oil boiler cracking problem was attacked. The temperature of the I^2R heated metal tape was reduced by making the ribbon twice as long as before. Cracking of OS-124 Monsanto oil at a boiling rate of 1/2 liquid cc/sec was reduced from > 1 part/10^6 to < 1 part/10^7. The metal ribbon was coated with teflon in an attempt to reduce cracking, but this was deemed a failure. Inquiries were made of the DuPont Company and the Minnesota Mining and Manufacturing Company looking toward possible use of fluorocarbon oils for ejector and diffusion pump service.

A two-stage 5-in. i.d. oil diffusion pump with a jet system directed inward (instead of outward) was built using OS-124 oil. Preliminary results pumping He gas indicate the entrainment probability for the top jet is greater than 0.4.

A 5-in. i.d. optimized valve-trap diffusion pump with pressure manometer calibrator was designed. The valve is a stainless-to-stainless blocking plate closure that can be baked at $> 400°$ C while closed against air (thus permitting the artificial zeolite surface trap to be activated). Also, provision is made for cooling the trap with liquid nitrogen. The calibrator is a plate with two orifices that can be positioned at the entrance to the valve trap. A metered gas flow Q into a given vacuum system is pumped at the speed set by the orifice plate. Thus the steady-state pressure established can be calculated, permitting mass spectrometers and ionization gauges to be calibrated in their position and environment of use.

A PIG discharge leak detector especially designed for locating large leaks was partially tested. Leaks large enough to stall systems at pressures 1 to $< 10^{-4}$ torr are the intended prey of this gadget. A PIG discharge with constant current between 10^{-3} and 5×10^{-1} torr is used as a light source. Band-pass interference filters in front of a photomultiplier tube analyze the light in terms of the leaking in of N_2, He, or Ar gas (or some combination of these).

2. MECHANICAL ENGINEERING DEVELOPMENT

Thomas H. Batzer

2X Multistage Compression Facility

John R. Benapfl, Edward G. Scarlett, and James N. Doggett

During this period work on the 2X machine has consisted of assembly and test of components on hand, installation of various utilities, and design and fabrication of incidental parts necessary for final assembly.

Two 5500-liter vacuum vessels were assembled. Four of the 10-inch mercury diffusion pump systems were installed on the east tank and two on the west tank. Base pressures in these systems range from 1×10^{-7} to 3×10^{-7} torr. Pumping speed measurements have yet to be made.

All 25 of the 6-ft i. d. dc coils have been installed and checked both electrically and hydraulically. One coil required reworking by the fabricator because of an inclusion of uncured potting resin.

Utility systems for low-conductivity water, air, and drainage were installed. Recirculating chilled-water cooling systems for electronic racks in both corridors in Buildings 180 and 156 were installed.

Various accessory parts, such as pulse-coil supports, dc coil blocking and tie rods, miscellaneous vacuum components, and diagnostics were designed and fabricated. A mezannine on the south side of the machine and a wall between the 2X and Alice areas were added to the structure.

Mechanical assembly for the first experiment will be complete this summer.

Low-Energy Neutral-Beam Experiment

William S. Neef, Jr.

Magnet failures occurred on two successive days in February. These failures occurred as shorts, and are atrributed to accumulation of moisture in cracks during thermal cycling between liquid nitrogen temperature and room temperature. One coil was repaired by replacing two pancakes; the other was scrapped and replaced with the one remaining coil section. A new coil design has evolved from this experience, and is reported elsewhere under Magnet Development.

The Alice machine is being reassembled in the "B" version with some new diagnostic equipment. Diagnostics now include a fast atom counting tube and the axial limiter and radial profile detector. A completely new trapping-chamber pressure probe with a mass spectrometer and magnetron gauge are included. Nearing completion is a new rf vector probe for the trapping chamber.

The experimental 40-kV ion source has been assembled and tested in the 100-kV injector facility. A number of changes are under way to speed this development test, including a remote steering control for the two focusing magnets. The chamber for this new 40-kV source has been installed on the "B" version of ALICE.

A Hiskes effect pre-ionizer chamber using electrostatic dissociation has been designed and is being fabricated. A similar chamber using magnetic dissociation is under study by the Magnion Company of Cambridge, Massachusetts.

A rotating-shaft seal test rig is being assembled. The vacuum seals for a 7000-rpm vaned drum will be evaluated prior to fabrication and testing of the drum. This drum, or "molecular bat," will serve to reduce streaming of cold gas down the Alice beam tube should the present water vapor curtain not perform as expected.

Astron

Charles F. Hurley, James F. Ryan, and Carl J. Anderson

720-kV Electron Gun

Leaks in the accelerating column, in the ceramic-to-copper braze joint, continues to be a problem. The new accelerating column ordered from Eitel-McCullough has small leaks in these joints which can be sealed; however, an integral column (no patches) is desired, and one more has been ordered.

The Freon blower oil-seal problem seems to have been solved. No leaks have been observed after many hours of operation using a superior grade of wiper-type oil seal.

The heat exchanger for the Freon gas has been modified. The method used is to wrap copper tubing around a length of pipe which has internal fins. This eliminates the possibility of a water leak in the Freon gas stream

New diagnostics include a tank with a remotely controlled Faraday cup for monitoring the gun beam and a new 87° turning magnet with a larger gap and modified pole faces.

Astron Main Chamber

Magnet-power supply connections consist of flexible straps run vertically from 128 magnet connections to copper bus bars overhead which extend 12 ft north, at which point they connect to 1.66-in. -diameter air-cooled copper pipe. The copper pipe goes vertically down through and under the floor to the concrete shielding wall. At this point the pipe, in bundles, passes through twelve 12-in. -diam holes and terminates at the other side with flags for attaching cables.

The installation of the magnet power supplies requires a raised deck to allow room for the many feet of cable that will connect them to the copper pipe. A commercially available deck with a removable floor has been selected for this purpose. This deck is now being installed.

The system for aligning the internal coils in the main chamber has worked as planned. The 29-ft cantilever is completed, and the coils on it were located well within the allowed tolerance of ±.040 in. from the machine axis. The 20-ft west cantilever is about 2/3 complete.

Auxiliary cantilever coils are now required to enclose the primary 6-in. -long internal coils on the two cantilevers. These coils are 16.25 in. in diameter, 20 ft long on the west cantilever, and 29 ft long on the east cantilever. They are wound from 0.807-in. -square hollow aluminum conductor. Loads simulating the weight of the auxiliary coils were imposed on the cantilevers, and the ability of the pull-back rods to compensate for the additional deflection was verified.

Beam Research Facility

The beam shutter has been assembled and operated at 10^{-6} torr. The required aperture for the beam was increased from 0.75×1.50 cm to a circle 2 cm in diameter, which renders the existing orifice system obsolete. Design studies show that a six-stage system, using three rotary shutters, should hold a pressure ratio of 2×10^8. This would allow operation without a foil in the beam path.

Bumpy Torus

Manuel Calderon and Eugene T. Bradley

All the mechanical design for Bumpy Torus as originally planned has been completed and the hardware ordered; most of it will be delivered in July.

Preliminary planning of a new injector box assembly has begun. This will include a change in the flux leader itself and the two injection coils.

Levitron

Dave C. Holten

A cryogenic pump has been developed for installation in the Levitron. The pump consists of a high-purity copper finger, 0.5 in. in diameter and 4 in. long, in thermal communication with a liquid helium Dewar. The finger is pneumatically inserted and withdrawn from the Levitron vacuum chamber. The latter operation, accomplished in a time less than 100 msec, occurs immediately before the machine is pulsed.

Tests of the unit indicate pumping speeds of 190 liters/sec, 340 liters/sec, and 350 liters/sec for carbon dioxide, air, and nitrogen respectively, all in the pressure range 10^{-5} torr. Total consumption of liquid helium is at the rate of approximately 1.6 liters/h.

The apparatus is now being modified for complete automatic operation prior to installation on the Levitron.

Cryogenic Project

Clyde E. Taylor and Robert L. Nelson

Test results for the 7-1/8-in. i.d. by 12-in. -long sodium cryogenic coil, along with a mechanical description of the coil, have been reported.[1]

1. Clyde E. Taylor and Robert L. Nelson, Test Results for A 7-1/8-Inch I. D. × 12-Inch Long Sodium Cryogenic Coil, Lawrence Radiation Laboratory, Livermore Report UCRL-7401, June 19, 1963, 12p.

The observed resistance was about 4×10^{-6} ohm at 21 kG, 11° K, with 10,000 A; this resistance is lower than what was expected on the basis of small sample measurements, by a factor of about 2.

In the past 6 months, two new 6-in. i.d. sodium coils were designed in order to develop a coil with sufficient mechanical integrity to withstand repeated temperature cycling and 100 kG or higher magnetic fields. One coil uses sodium encapsulated in long lengths of thin-wall tubing with high-purity copper electrical end connections. Each length is wrapped into a short spiral-wound coil and the complete solenoid is a stack of such coils with copper connections between each coil and the next. The second approach uses a series of concentric aluminum cylinders. A spiral groove is machined in alternate cylinders and end connections between layers form a continuous mold. Sodium is then cast in place, resulting in a multilayer coil with helical windings. Protective varnish provides the necessary insulation.

Investigations were made of the resistance of the ultrahigh-purity sodium to contamination from encapsulation boundaries, such as anodized and varnish-coated aluminum, bare copper, Mylar, and silver-solder joints in stainless steel tubing. Materials used to encapsulate the sodium conductor in the two 6-in. coils were found to have little or no effect on sodium purity. Contact resistance between copper surfaces in liquid helium temperature, as influenced by surface condition and contact pressure, was investigated. Temperature instrumentation was developed for the next coil tests.

A test Dewar was designed and built for preliminary low-power testing of sodium coils. The existing pulse refrigeration system or the Collins cryostat can be used for a source of liquid helium.

Magnet Development and Fabrication

Arthur H. Harvey

Previous failures of the Alice magnet coils were mechanical in nature and resulted in open circuits. Two recent failures were definitely short circuits. There were thermocycle cracks in the coil sections. A Hipot test across a thermal crack in a sectioned coil gave current leakages as high as 100 A with voltages as low as 20 V when this crack was saturated with water. On the basis of these tests a search was made for a more suitable material than cotton tape. Test results for dacron and dacron-glass combinations indicate this to be a superior material from the standpoint of abrasion resistance, dielectric strength, ability to withstand severe bending at cryogenic temperatures, and moisture resistance.

A one-pancake section of the new bifilar wound design for Alice "C" was successfully thermocycled to liquid nitrogen temperatures eight times. There was no evidence of any thermal cracking.

Sodium Coil Development

Sample bends have been made on sodium-filled stainless steel tubes 3/8-in.-square and with 0.010-in. walls. It became apparent from the first bend attempts that the conductor must be confined on the sides and inside surface of the bend. Attempts to bend the conductor without this confinement collapses the tube regardless of tensions used. A successful 6-in.-diameter helical coil section was wound in a grooved mandrel. The minimum tension has been set at 550 lb for this diameter.

Miscellaneous Winding and Impregnating Techniques

The fabrication and sealing of impregnation fixtures has in the past been one of the most costly and difficult operations. Oddly shaped voids had to be filled with hand-tailored blocks, and the enclosure in the coil terminal region often is an extremely complex sealing problem. With the aid of a very thixotropic epoxy (Scotchcast 10), voids can be filled and a peripheral enclosure can be made in one operation. This material does not run or sag, even in relatively thick sections. Enclosure fabrication and sealing time in some cases have been reduced from 1-1/2 weeks to 2 days with the use of this material.

Analysis of heat dissipation by radiation and natural convection of wire-wound coils operating at fairly high power levels indicate that more than 50% is by radiation. We have therefore added a black pigment to the binding resin of our coils in hope of increasing the emissivity. Since Formvar is depended upon for electrical insulation in the wire-wound coils, the epoxy acts mainly as a binder. To improve the thermal conductivity of the coil, we are adding 175 parts of fine copper powder per 100 parts of resin used. (With loadings of silicone rubber we have been able to improve its thermal conductivity by a factor of 3.)

Component Development

Thomas H. Batzer, James F. Ryan

6-Inch Mercury System

The 6-inch mercury-pumped ultrahigh-vacuum system has twice been subjected to simulated up-to-air accidents. The first such accident consisted of breaking an Advac seal in a nude ion gauge on the high-vacuum side. Baking readily restored the low pressure of 2×10^{-10} torr. A second up-to-air accident consisted of opening the leak-checking valve in the foreline and letting the system up to air in 3 to 4 seconds. The pressure recovered without baking was 1×10^{-9} and the pressure recovered with baking was back to 4×10^{-10} torr. This system uses a trap of zeolite plus copper wool in liquid nitrogen as a forepump so that the mercury pump and vacuum chamber are free of oil vapor. The system ran for 69 days at 2 to 3×10^{-10} torr. No pressure bursts were seen at any time during this period. We conclude that little mercury gets to the liquid nitrogen baffle, as the pump continued to operate steadily. At bake-out temperatures of 300° C, the nude gauge pressure in the high-vacuum space is 1 to 2×10^{-8}, which is much lower than pressures normally achieved at 300° C in systems pumped with oil pumps.

Torus Development

Tests on the 1/6-size models of the Levitron torus showed that collapse pressure of these toruses is proportional to the 2.4 power of the thickness to the minor diameter ratio (t/d). For toruses of 4:1 aspect ratio, t/d of 6×10^{-3} gives 60 psi collapse pressure. This provides a safety factor of 4 at 1 atm.

Ultrahigh-Vacuum Aluminum Vessel

The 70-liter aluminum vessel was baked at 240° C for 24 h, and upon cooling developed a small leak. The leak was stopped by tightening the flange bolts. A base pressure of 8×10^{-10} torr was reached in 8 h. At the end of 1 day the pressure was 5×10^{-10} torr, and the base pressure finally reached was 1.1×10^{-10} torr—all uncorrected for x-ray current and read on a nude gauge. Stainless steel bolts in the main flange are being replaced by aluminum alloy to prevent relaxation of bolting pressure while cooling down from bake-out. No pressure bursts were seen at any time. Zeolite plus copper wool in liquid nitrogen is used as a backing pump. The specific outgassing rate of the baked aluminum surface was 8×10^{-13} torr-liters per sec cm^2 after 1 day and 2×10^{-13} after 35 days. Atomic species of the residual gas was determined by a mass spectrometer. This is done under conditions whereby the vessel is valved off from the pumping system and the pressure allowed to rise to 10^{-7} torr. The largest signals were masses 28, 15, and 14. The signal at mass 28 was about three times that at 14 or 15.

The molybdenum pump has been mounted between the liquid nitrogen trap and the Conoseal valve of this system, and awaits bake-out.

Aluminum foil gaskets are in routine use as the preferred seal for all high-vacuum development work and fabrications.

3 ELECTRICAL ENGINEERING DEVELOPMENT

Hugh W. Van Ness

Pyrotron

David R. Branum

Table Top

The experiment has been in operation all during the past six months with no major electronic-electrical failures.

A three-phase oscillator is under design for this experiment. A 2-Mc "breadboard" unit is now being used in the experiment.

An additional capacitor energy storage system of 150,000 joules has been designed for the Solatron experiment in this area. All major components are on order or will be ordered in July of this year.

Toy Top III S

The experiment has been in a continuous operating mode for the past six months.

There have been several capacitor failures in the 300,000-joule bank, which is made up from the old 7.5-μF General Electric capacitors.

There have been several ignitron switch failures. These ignitrons are in the pulse crowbar area of the above 300,000-joule bank, and fail when the high mechanical stresses on the tubes crack the anode seals.

2X Multistage Compression Experiment

The past six months have been devoted to construction of experimental facilities in Buildings 180 and 156.

In Building 180, a 1-MJ capacitor bank is 80% complete, and four 32-kJ "fast" capacitor banks, five 232-kJ "semifast" capacitor banks, and 100-channel source main pulse and trigger pulse capacitor banks are all completed.

A transmission line supporting and enclosing structure has been built between Buildings 156 and 180. A transmission line connecting to an 80% completed, 1.25-MJ capacitor bank section in Building 156 is now under construction. Eventually, the entire 10 MJ of capacitors presently in Building 156 will be made available to the experiment in Building 180.

For capacitor bank charging, nine supplies will be provided in Building 156. Of these, four that are rated 25 kV, 4 A each are 90% complete. The remaining five supplies, rated 25 kV, 6 A each, consist of three that are presently used for the Toy Top III experiment and two others that are 75% complete.

In addition to the capacitor banks, all other electronic needs of the experiment have been under construction. The control center in Building 180 is 90% complete and the main control circuits are under construction while the diagnostic cable runs are under design.

Pyrotron

G. Gordon North

Alice

During January and February the Alice machine was in nearly continuous operation. The diagnostic equipment rack facilities were doubled. A spectrum analyzer and other tuned rf receiver equipment were provided for monitoring ion cyclotron radiation in the confinement chamber. A method for continuously measuring the plasma potential over a 4-kV range with a 1-msec time resolution was successfully operated.

The P-3 washer stack ion source was successfully fired into the Alice confinement chamber by use of the recently designed auxiliary pulse forming network. This provided an increase in pulse length from 200 to 600μsec

The last week of February, two modular sections of the mirror field coils failed by shorting. The cause of these failures is not yet understood. The scheduled shutdown for modifications, to begin in March, thus began a week early. The machine remained down for repair and modification until May, when reassembly was begun. Magnetic field shielding was designed and installed around the "B" rack diagnostic area. The calutron-type ion source vacuum tank was replaced by one with a rearward beam tube extension to accommodate the future Piggy-Back ion source. The new ion source, which will operate independently of the present one, will not only increase the total injected beam intensity but also will permit injection at two different energies and with different types of particles.

Minor modifications were made to the 100-kV injector facility in Building 180 so that its electrical and vacuum systems could be used for the operation and development of the new Piggy-Back ion source. Experimental operation of the new source, with changes requiring day-to-day support, has been in progress since January.

The required equipment for the operation of a nude magnetron gauge and mass spectrometer, close-coupled to the mirror field confinement chamber, have been provided.

A Kenotron high-vacuum diode tube with a variable filament power supply and suitable metering has been built into a porta-rack for general use as a variable 50-kV 20-kW dummy load.

The J. C. Carter rotating-coil fluxmeter to be used in the calutron source field regulator system has been restored to satisfactory operation and is awaiting mounting on the machine.

A brief experimental study has been made of the requirements for operating ion gauge tubes of the Bayard-Alpert type in a magnetic field. With proper tube orientation and calibration data it appears that useful vacuum pressure readings could be made under these conditions. However, it is not possible to regulate emission with tubes in a magnetic field. Also, the filament power frequency should be at least 3 kc for intermittent operation in field strength up to 20 kG.

Cryogenics Coil Experiment

Effort during this period has been directed toward redesign of a new sodium coil. Little change will be required in the electrical system or diagnostics for this new coil. Therefore, only minor electronics effort has been supplied to meet the continuing needs of this program.

Pinch Program

Levitron Experiment

Until recently, the Levitron had been operating on a regular basis since the end of March. A number of capacitor bank failures occurred in this interval as a result of the longer, 5-msec pulse field rise times now being used.

To achieve longer rise times, the Z and θ windings and the capacitor banks were modified. These modifications were made in the early part of the year during a scheduled down time for general overhaul. Changes were also made in the units used to induction-heat the copper core and Inconel liner during vacuum bakeout.

Presently a new crowbar system is being installed on the high-voltage capacitor banks used to drive the Z and θ windings. In this change the large number of size A crowbar ignitrons now being used will be replaced with four size D ignitrons. The purpose is to reduce the probability of ignitron prefire, which has been the major cause of capacitor bank failure during longer-pulse field rise times. In addition, an automatic hi-pot system is being installed on these ignitron systems to further prevent the possibility of prefire.

Investigation of Energy Storage System

Limited tests were made on the Homopolar generator in the early part of this year. During these tests, pulse currents of 300,000 A were reached. Typical results gave a pulse duration of 0.1 sec with a rise time of less than 20 msec. Initial stored energy was 2 MJ.

To observe the abrupt decrease in shaft rpm of the Unipolar generator during the current pulse, a special tachometer was designed and put into service.

Beta Pinch Capacitor Bank

Construction of a new 150,000-kJ 20-kV capacitor bank for the Beta Pinch experimental area is now complete. The work on this bank was done by an outside contractor. Numerous inspections and checks on the bank indicate that the construction is satisfactory in all respects.

Operation of this bank will not begin until design and construction of the control facilities are completed. Although this bank was designed primarily for fast-pulse service, provisions were made to allow long-rise-time operation with only minor changes.

Astron

D. O. Kippenhan

The Astron concept is based on a stable, dense, rotating layer (E layer) of relativistic electrons contained by external solenoidal fields for the containment and heating of a plasma of deuterium and tritium. The resulting total field of the external magnetic coils and the self-field of the spinning "E" (electron) layer creates a region of closed magnetic field lines (magnetic bottle) in which a plasma of deuterium and tritium can be trapped, contained, and heated by collision to the temperature required for sustained thermonuclear reaction.

The construction work on the electron accelerator for the Astron machine was completed in February 1963. The construction consisted of procuring, installing, and testing approximately 500 cores, 500 core voltage-monitoring attenuators, 500,000 ft of coaxial load cables, 500 thyratrons, 500 thyratron switch chassis, 500 pulse shapers, 500,000 ft of coaxial pulse-forming network cable, 59 bias reset chassis, 59 group control chassis, 59 high-voltage disconnect cabinets and their associated resistors and control chassis, 4 command resonance charging supplies, 4 division control chassis, 4 bias reset control chassis, the triggering system for the 500 thyratrons, a cathode power supply, and all associated interconnecting, interlocking, and control functions.

The critical-path-method of program scheduling in the construction of this accelerator was extremely successful. It gave a complete analysis of the work progress and a good understanding of the implications of shifts in manpower and effort to accomplish a specific task. It was possible to keep work on schedule by understanding what needed more emphasis and then taking corrective action.

Successive accelerator sections were put into operation starting in October 1962, and the final section in February 1963. Since February, the accelerator has been operated with continued improvement of both operation and beam quality. From operations, various additions have been added or will be added to the accelerator. These include a central timing monitor system for the thyratrons, and the core monitor system for detecting prefires and prefire rates and core voltage flatness.

At this date the accelerator has produced a 170-A pulsed electron beam accelerated to an energy level of 4.2 MeV, with a pulse duration of 0.25 μsec at a pulse-repetition rate of 5 pulses per second.

A maintenance record system is being set up to collect information for statistical studies of component failures. The accelerator has approximately 10^5 electronic components, therefore data-processing techniques will be used for this record system. These statistical studies will permit the scheduling of preventive maintenance and aid in the redesign of marginal components.

The Astron reaction chamber consists of a vacuum liner surrounded by a single-layer solenoidal magnet and two inner solenoidal magnets, one cantilevered from each end. The center space between the ends of the cantilevered magnets is the region where the E layer and the magnetic bottle for containing the reacting plasma will be formed.

The outer magnet is wound with modular connections such that independent dc magnet power supplies can control the shape of the field so as to form the usual "mirror" configuration. Forty-nine 30-kW, sixteen 15-kW, and one 200-kW dc power supplies energize this outer magnet. These current-regulated power supplies have been specified and are now on order. The design of this installation is complete and the power cables are being installed. Delivery of the power supplies is expected before early fall.

The inner cantilevered magnet is mechanically wound with individual modular magnets in such a way that independent dc power supplies can control the shape of this aiding field. These cantilevered magnets are powered from 33 power supplies at 4 kW, 9 power supplies at 2.25 kW, 13 power supplies at 1 kW, and 17 power supplies at 250 W. The cost of these supplies was substantially reduced by a scheme utilizing a large unregulated nonadjustable power supply and obtaining fast response, regulation, filtering, and multiple outputs by transistor pulse-width modulation. These current-regulated power supplies have been designed and components ordered for assembly starting in July. The design of the installation is complete and the power cables are installed.

The intense electron beam from the induction accelerator is injected into the region between the outer magnet and the cantilevered magnet through a special inflector magnet. This allows the electron beam to pass through the outer return magnetic field unaffected and emerge in the inner field. The beam is canted enough to miss the inflector pipe on the first revolution. As the beam progresses down the region between the cantilevered magnet and the outer magnet it passes by deceleration resistors for rf mode rejection. Additional deceleration resistors, located at the point where the beam starts down the magnetic mirror gradient, cause energy loss that aids in trapping the E layer.

The helical path of the beam down the chamber is affected by the beam energy and the E-layer buildup is affected by the magnetic field shape and magnitude. This required that all the power supplies be programmable in various configurations, some as a function of injected beam energy and some as a function of E-layer buildup.

Switch Development

David B. Cummings

Ignitron Tests

The WX 4973 is a low-inductance stabilized ignitron made to our design by the Westinghouse Electric Corporation. It is similar to the WX 4564 reported last year. Further test results show even longer decay time without evidence of arc transfer to the wall. It was tested on the Table Top capacitor bank up to 12 kV with currents up to 3 kA with a decay time constant of about 230 msec. This is a charge of about 700 coulombs, which is substantially more than any tube yet reported. With the addition of a stress shield, higher voltages should be possible.

The WX 4973 was tested further to compare its voltage-drop decrease during a pulse to that of an open 5-inch switching ignitron (WX 4681). The

The tubes were used to discharge a 330-μF capacitor bank through a 1-ohm resistor at up to 6 kV. At this higher current, the voltage on the close-spaced WX 4973 dropped to the knee of its curve in about 10 μsec, compared with about 60 μsec for the more conventional tube. Also, the voltage drop was about 25% lower for the stabilized tube.

The tests of the special ignitors in the WX 4839 have been repeated by Westinghouse in the WX 5325. This ignitor is a sintered carbide ignitor on a threaded Kovar rod to give a radial electric field which cannot be shorted out by mercury wetting on the surface. Not having the ignitor relieved by a discharge to the ignitor support greatly increases the ignitor heating. Unfortunately, this broke the ignitor in the five tubes tested. It appears this approach will not work.

New Designs

Several years ago, 2-inch ignitrons having metallic electrostatic stress shields were built for LRL by the General Electric Company, National Electronics, Inc., and the Westinghouse Electric Corporation. The results were very erratic. It appears now that this was due to poor processing and other reasons. With the increasing need for 25-kV ignitrons, some of these ideas again appear attractive. This is confirmed by the British experience on high-voltage ignitrons. Requests for designs with a stress shield in a short, 4- to 5-inch-diameter ignitron brought two proposals. Both tubes will have 20 to 25 nH inductance, which is about the same as the 7703.

National Electronics, Inc. proposed the T-2295. It will be 4.25 in. in diameter by 7 in. high. The lower stress shield will be a flared spinning. The anode bolt will be machined to a matching contour to provide for a smooth field distribution at the anode seal. This stress shield design is similar to that of the A.E.I. BK 178.

The General Electric Company proposed the ZG 7239. It is a 5-in-diameter by 8-1/4-in-high tube. It will have a 4-in.-diameter glass seal and a massive 2.5-in. anode bolt. The stress shield is patterned after their GL 6228 pentode-high-voltage ignitron. It has both a lower and an upper shield without a flare at the gap between them. Both tubes will have two rectifier-type ignitors.

In addition, National Electronics is making for us an experimental 5-inch open ignitron (NL 1059, WX 4651, ZG 7207) with an electrostatic stress shield. Although it will have a high inductance, it should hold more than 20 kW and be mechanically interchangeable with its generic type.

Bumpy Torus Experiment

G. Gordon North

Design and installation of the electronic systems for the Bumpy Torus experiment are now complete. Although most of the mirror coils around the torus have not yet been installed, the dc cabling and power supplies are presently ready for connection to these coils.

At present, experimental operation of the injection section is under way. Operation to date has demonstrated that energetic beams of electrons can be injected into the mirror coil configuration.

Atomic Scattering and Cross-Section Measurements

David R. Branum

The cross-section experiments are being installed in their new building - 180 B.

Three electronic control rack areas have been installed. Two of the experiments are now operational and the third experiment will be installed in August of this year.

VII. TALKS AND PUBLICATIONS

<u>University of California Nuclear Engineering Department Seminar, Berkeley, March 25, 1963</u>

R. F. Post, LRL Mirror Machine Program.

<u>Meeting on Theoretical Aspects of Controlled Thermonuclear Fusion, Berkeley, April 8-9, 1963</u>

Terry Kammash and Warren Heckrotte, Stable Longitudinal Oscillations in Anisotropic Plasma (UCRL-7282-T Abst., Mar. 14, 1963; p. 2 of UCRL-10740, April 1, 1963).

Richard F. Post, Finite Orbit Effects at Low Plasma Density (UCRL-7295-T Abst., Mar. 22, 1963; p. 4 of UCRL-10740, April 1, 1963).

H. P. Furth, Variational Principle for Finite-Conductivity Hydromagnetic Stability (UCRL-7281-T Abst., March 14, 1963; p. 6 of UCRL-10740, April 1, 1963).

<u>APS 1963 Spring Meeting, Washington, D. C., April 22-25, 1963</u>

H. P. Furth, Variational Principle for Long-Wave, Finite-Resistivity Fluid Modes, Bull. Am. Phys. Soc. Ser. II <u>8</u>, 330 (1963) (UCRL-7228-T Abst., Feb. 5, 1963).

N. C. Christofilos, R. E. Hester, W. A. S. Lamb, D. D. Reagan, and R. E. Wright, Induction Accelerator for Electrons, Bull. Am. Phys. Soc. Ser. II <u>8</u>, 378 (1963) (UCRL-7220-T Abst., Feb. 4, 1963).

<u>Meeting of the Pacific Northwest Chapter of the American Vacuum Society, Seattle, Washington, May 4, 1963</u>

Norman Milleron, Dark Holes and Light Walls in Controlled Thermonuclear Research, invited paper.

<u>Meeting of the Northern California Vacuum Society, Berkeley, June 24, 1963</u>

Norman Milleron, Clean Vacuum Systems, invited paper.

<u>Meeting of the Southwest Vacuum Group, Los Angeles, June 26, 1963</u>

Norman Milleron, Calibration Stability and Pumping Efficiency, invited paper.

Publications

Annals of Physics

Laurence S. Hall, A Statistical Theory of Transport Phenomena, 20, 383 (1962) (UCRL-6751, Jan. 19, 1962).

Applied Optics

G. R. Spillman, W. S. Cooper III, and J. M. Wilcox, Nine-Channel Polychromator for Observation of Time-Dependent Spectral Line Profiles, 2, 205 (1963) (UCRL-9843 Rev., Jan. 22, 1962).

The Physics of Fluids

H. P. Furth, Prevalent Instability of Nonthermal Plasmas, 6, 48 (1963) (UCRL-6907, May 28, 1962).

G. Gibson, W. C. Jordan, and E. J. Lauer, Particle Behavior in a Static, Asymmetric, Magnetic Mirror Geometry, 6, 133 (1963) (UCRL-6856, March 29, 1962).

G. Gibson, W. C. Jordan, and E. J. Lauer, Particle Behavior in Static, Axially Symmetric, Magnetic Mirror and Cusp Geometries, 6, 116 (1963) (UCRL-6771, March 9, 1962).

Günter Ecker, Theory of the Fully Ionized Plasma Column with External Particle Production, 6, 290 (1963) (UCRL-10616, Feb. 1963).

Harold P. Furth, John Killeen, and Marshall N. Rosenbluth, Finite-Resistivity Instabilities of a Sheet Pinch, 6, 459 (1963).

Wulf B. Kunkel, William R. Baker, Alexander Bratenahl, and Klaus Halbach, Boundary Effects in Viscous Rotating Plasmas, 6, 699 (1963) (UCRL-10399 Rev., Jan. 10, 1963).

The Physical Review

M. H. Mittleman, Excitation of Atomic Hydrogen by Fast Protons, 129, 190 (1963) (UCRL-6808-T, March 5, 1962).

Gary A. Pearson and Wulf B. Kunkel, Electron Velocity Distribution in a Slightly Ionized Gas with Crossed Electric and Strong Magnetic Fields, 130, 864 (1963) (UCRL-10536, Nov. 12, 1962).

Physical Review Letters

John R. Hiskes, Inverted Cascades in Energetic Neutral Hydrogen Beams, 10, 102 (1963) (UCRL-7115 Rev. 2, Dec. 28, 1962).

C. C. Damm, J. H. Foote, A. H. Futch, and R. F. Post, Cooperative Oscillations in a High-Temperature Plasma Formed by Neutral Atom Injection, 10, 323 (1963) (UCRL-7250-T Feb. 21, 1963).

Robert H. McFarland, Cause of the Observed Polarization of Electron-Induced Radiation from Helium, 10, 397 (1963) (UCRL-7283, March 1, 1963).

Le Vide

L. L. Levenson, N. Milleron, and D. H. Davis, Molecular Flow Conductance, 18, 42 (1963) (UCRL-6253, Aug. 15, 1961).

This report was prepared as an account of Government sponsored work. Neither the United States, nor the Commission, nor any person acting on behalf of the Commission:

A. Makes any warranty or representation, expressed or implied, with respect to the accuracy, completeness, or usefulness of the information contained in this report, or that the use of any information, apparatus, method, or process disclosed in this report may not infringe privately owned rights; or

B. Assumes any liabilities with respect to the use of, or for damages resulting from the use of any information, apparatus, method, or process disclosed in this report.

As used in the above, "person acting on behalf of the Commission" includes any employee or contractor of the Commission, or employee of such contractor, to the extent that such employee or contractor of the Commission, or employee of such contractor prepares, disseminates, or provides access to, any information pursuant to his employment or contract with the Commission, or his employment with such contractor.